Vol. 03 No. 03 2025

RiESTech

JOURNAL
RECENT IN ENGINEERING SCIENCE AND TECHNOLOGY

MBI

E- ISSN : 2985-8321
P -ISSN : 2985-704X

Recent in Engineering Science and Technology (RiESTech)
PT MENCERDASKAN BANGSA INDONESIA (MBI)
Available online at: http://www.mbi-journals.com/index.php/riestech

E- ISSN : 2985-8321
P -ISSN : 2985-704X

Recent in Engineering Science and Technology (RiESTech)

Volume 3 No 3 July 2025

FOCUS AND SCOPE

RIESTECH

Recent in Engineering Science and Technology **(RiESTech):** I*SSN: 2985-704X (print), ISSN: 2985-8321 (online)* a peer-reviewed quarterly engineering journal, publishes theoretical and experimental high-quality papers to promote engineering and technology's theory and practice. In addition to peer-reviewed original research papers, the Editorial Board welcomes original research reports, state-of-the-art reviews, and communications in the broadly defined field of recent engineering science and technology. **RiESTech** covers topics contributing to a better understanding of engineering, material science, computer science, environmental science, and their applications. **RiESTech** is concerned with scientific research on mechanical and civil engineering, Electrical/Electronics and Computer Engineering, and Metallurgical and Materials Engineering with specific analytical techniques and/or computational methods.

The frequency of RiESTech publications is four times a year namely in January, April, July, and October. The scope of RiESTech includes a wide spectrum of subjects namely:

Mechanical and Civil Engineering (Automotive Technologies; Construction Materials; Design and Manufacturing; Dynamics and Control; Energy Generation, Utilization, Conversion, and Storage; Fluid Mechanics and Hydraulics; Heat and Mass Transfer; Micro-Nano Sciences; Renewable and Sustainable Energy Technologies; Robotics and Mechatronics; Solid Mechanics and Structure; Thermal Sciences)

Electrical/Electronics and Computer Engineering (Instrumentation; Coding, Cryptography, and Information Protection; Communications, Networks, Mobile Computing, and Distributed Systems; Compilers and Operating Systems; Parallel Processing, and Dependability; Computer Vision and Robotics; Control Theory; Electromagnetic Waves, Microwave Techniques and Antennas; Embedded Systems; Integrated Circuits, VLSI Design, Testing, and CAD; Microelectromechanical Systems; Microelectronics, and Electronic Devices and Circuits; Power, Energy and Energy Conversion Systems; Signal, Image, and Speech Processing; Machine Learning and Data Science)

E- ISSN : 2985-8321
P -ISSN : 2985-704X

Metallurgical and Materials Engineering (Advanced Materials Science; Ceramic and Inorganic Materials; Electronic-Magnetic Materials; Energy and Environment; Materials Characterization; Metallurgy Extractive; Polymers and Nanocomposites)

Environmental Science and Engineering (Waste Management, Climate Change, Zero Waste, Environmental Disaster Management, Circular Economy, Sustainable Development, Environmental Security, Environmental Management, Environmental Ecology, Conservation of Natural Resources And Environment, Environmental Impact Analysis, Planning and Environmental Administration, Environmental Health, Environmental Pollution, Environmental Accounting, and Environmental Information Systems)

Recent in Engineering Science and Technology (RiESTech)
PT MENCERDASKAN BANGSA INDONESIA (MBI)
Available online at: http://www.mbi-journals.com/index.php/riestech

E- ISSN : 2985-8321
P -ISSN : 2985-704X

Recent in Engineering Science and Technology

(RiESTech)

Volume 3 No 3 July 2025

Recent in Engineering Science and Technology (RiESTech)
PT MENCERDASKAN BANGSA INDONESIA (MBI)
Available online at: http://www.mbi-journals.com/index.php/riestech

E- ISSN : 2985-8321
P -ISSN : 2985-704X

Layout and Typesetting:

Imam Sapto Nugroho, Universitas Indonesia (Alumni), Indonesia
Kamil Raihan Permana, Universitas Indonesia, Indonesia
Raihan Trinanda Agsya, Politeknik Negeri Jakarta, Indonesia

PUBLISHER
PT MENCERDASKAN BANGSA INDONESIA (MBI)
Address : 4th Floor Gedung STC Senayan Room 31-34, Jl. Asia Afrika Pintu IX, Jakarta 10270, Indonesia.

Recent in Engineering Science and Technology (RiESTech)
PT MENCERDASKAN BANGSA INDONESIA (MBI)
Available online at: http://www.mbi-journals.com/index.php/riestech

E- ISSN : 2985-8321
P -ISSN : 2985-704X

Recent in Engineering Science and Technology (RiESTech)

Volume 3 No 3 July 2025

PREFACE

Journal RiESTech (p-ISSN: 2985-704X (print), e-ISSN: 2985-8321 (online); is a peer review journal published by PT Mencerdaskan Bangsa Indonesia. The RiESTech journal is published four times a year in January, April, July, and October. This journal provides direct open access to its content on the principle that making research freely available to the public supports a greater global exchange of knowledge within the engineering field. This journal aims to provide a place for academics, researchers, and practitioners to publish original research articles or review articles. The scope of articles published in this journal relates to various topics in the field of outcomes of research activities.

The RiESTech journal publishes papers strictly following the RiESTech guidelines and templates for manuscript preparation. All submitted manuscripts will go through a double-blind peer review process. The paper is read by members of the editor (according to the area of specialization) and will be screened by the Managing Editor to meet the criteria required for RiESTech publication. Manuscripts will be sent to two reviewers based on their historical experience in reviewing manuscripts or based on their areas of specialization. RiESTech has review forms to keep the same item reviewed by two reviewers. Then the editorial board makes a decision on the comments or suggestions of the reviewers.

Reviewers provide an assessment of originality, clarity of presentation, contribution to the field/science. This journal publishes research articles, review articles/literature reviews, case reports and concept/policy articles, in all fields of Computer Science, Informatics Engineering, Multimedia, Arts. The article to be published is an original work and has never been published. Incoming articles will be reviewed by the reviewer team.

The Editorial Board will try to continue to improve the quality of the journal so that it can become an important reference in the development of engineering sciences. The greatest appreciation and gratitude to Mitra Bestari along with members of the Editorial Board and all parties involved in the publication of this journal. Complete writing instructions are displayed on the portal of this journal.

Regards,

Chief Editor

Recent in Engineering Science and Technology (RiESTech)
PT MENCERDASKAN BANGSA INDONESIA (MBI)
Available online at: http://www.mbi-journals.com/index.php/riestech

E- ISSN : 2985-8321
P -ISSN : 2985-704X

Recent in Engineering Science and Technology (RiESTech)

Volume 3 No 3 July 2025

Contents

Articles

RiESTech
Recent in Engineering Science and Technology

MBI

Article

Wire Rope Sling Failure Analysis: Technical Root Causes, Investigation Methodology Critique, and Lessons for Lifting Safety and Organizational Learning

Ahmad Zaky [1,*], Yudha Pratesa [1] and Johny Wahyuadi Mudaryoto [1]

[1] Department of Metallurgical and Materials Engineering, Faculty of Engineering, Universitas Indonesia, Depok, West Java 16424, Indonesia
* Correspondence: ahmad.zaky41@ui.ac.id

Abstract: Wire rope slings are critical in heavy lifting operations, yet their failure remains a persistent safety concern. This paper presents a case study of a catastrophic sling rupture that occurred during a heavy lifting trial, despite the lift being within its rated capacity. A multi-faceted failure analysis identified hidden corrosion fatigue at the sling's ferrule and an unanticipated extreme overload condition as the primary technical root causes. Procedural and organizational factors—including inadequate risk assessment, deviation from critical lift protocols, and failure to act on prior lessons—also contributed to the incident. The contractor's investigation is critically reviewed against best-practice Root Cause Analysis guidelines, highlighting both strengths and gaps in its methodology. Key lessons to improve lifting safety are discussed, such as implementing rigorous inspection and retirement criteria for aging slings and ensuring comprehensive lift planning. Overall, the case underscores the importance of robust investigation practices and effective organizational learning to prevent similar failures in the future.

Keywords: Wire Rope; Lifting Slings; Corrosion Fatigue; Failure Analysis; Root Cause Analysis; Failure Investigation; Lifting Operations; Safety Culture; Organizational Learning; Accident Prevention

Citation:. Zaky, A., Pratesa, Y., Mudaryoto, J. W. (2025) Wire Rope Sling Failure Analysis: Technical Root Causes, Investigation Methodology Critique, and Lessons for Lifting Safety and Organizational Learning. Recent in Engineering Science and Technology, 3(03), 1–24. Retrieved from https://www.mbi-journals.com/index.php/riestech/article/view/111

Academic Editor: Vika Rizkia

Received: 14 May 2025
Accepted: 28 May 2025
Published: 31 July 2025

Publisher's Note: MBI stays neutral with regard to jurisdictional claims in published maps and institutional affiliations.

1. Introduction

Wire rope sling failures remain a persistent problem in heavy lifting operations, even when standard industry procedures and safety factors are applied. Such failures can have severe consequences for safety and operations [4]. In practice, steel wire ropes inevitably degrade over time through mechanisms like fatigue, wear, and corrosion, requiring diligent inspection and timely replacement to prevent accidents [1]. Nonetheless, recent case studies and incident reports show that sling failures continue to occur in cranes, hoists, and other heavy lift systems, indicating potential gaps in current maintenance and usage practices. Researchers have noted that human and organizational factors (e.g. operational errors or inadequate training) often contribute to these incidents alongside technical causes [4], compounding the challenge of prevention.

Engineering failure analysis of wire ropes have identified a range of mechanical failure modes behind sling accidents. Fatigue cracking is one of the most frequently reported causes; for example, a broken crane rope was examined and concluded that undetected fatigue cracks (associated with decarburization of the steel) grew over time due to poor

inspection practices [7]. Corrosion is another critical factor: corrosion pitting and rust can significantly weaken rope wires and shorten their service life, making fatigue failures more likely [8]. Wear and abrasion (both external and internal) also contribute to degradation – a cableway rope failure was initiated by excessive pressure on the rope, which caused slipping between inner and outer wire layers and led to strand breakage [3]. Likewise, overloading or abnormal loading conditions can precipitate sudden failure; Lateral pressure on a rope (e.g. sharp bending or crushing forces) drastically reduced its load-bearing capacity in a ropeway accident, resulting in fracture [6]. Often, multiple degradation mechanisms act in combination. Steel wire ropes are typically subject to several simultaneous damage processes (fatigue, corrosion, wear, etc.), which can lead to premature and unexpected rope breakage if not detected [5]. Indeed, field experience has recorded wire rope sling failures occurring well before the expected service life – for instance, slings designed for decades of use have sometimes failed in just a few years of operation [9]. These observations underscore the need to pinpoint why such failures occur despite following standard guidelines.

Given the diverse causes and the potential complexity of sling failures, a rigorous failure investigation is essential after any such incident. Best practices from the literature suggest that investigations should be comprehensive – integrating on-site field assessments, detailed fractographic and metallurgical examination of broken wires, mechanical testing, and stress analysis – to accurately determine root causes [4]. In practice, many scholarly case studies demonstrate the value of this approach. For example, a 12-ton overhead crane rope that snapped after only 53 days in service; through careful visual inspection, stereoscopic microscopy, SEM fractography, and hardness tests, it was discovered that localized plastic deformation and wear on individual wires had created stress concentrations that eventually led to a fatigue failure of the rope [2]. Similarly, corrosion effects must be factored into any root cause analysis – the fatigue tests on high-strength wires revealed that corrosion markedly steepens fatigue S–N curves and lowers the wire's endurance, indicating a much shorter life in corrosive environments [8]. Advances in analytical modelling are also aiding investigations: it was developed a share-splitting slip theoretical model for wire rope sling fatigue and validated it with experimental data and electron microscopy of fracture surfaces [9]. All of these studies highlight that only a systematic and critical investigative methodology can unravel the often multi-faceted reasons behind sling failures.

This paper focuses on a recent real-world incident in which a wire rope sling catastrophically failed during a heavy lifting trial. In the incident, a large module panel was being lifted and manoeuvred by a crane (via a pair of wire rope slings and shackles) when one of the slings suddenly parted under tension. Notably, the lift plan had followed standard procedures – the hardware was within its rated Working Load Limit (WLL) and an exclusion zone was enforced – yet the sling still failed unexpectedly. A contractor-led investigation was carried out to determine the cause of this sling failure. The objective of this paper is to critically review that investigation, using the incident's findings as a case study for analysis. The sling failure investigation and its conclusions will be examined in light of the best practices, standards, and investigative methodologies outlined in the literature. In particular, comparing the contractor's process and outcomes with those recommended by prior failure analyses (e.g.

thorough root cause analysis, consideration of all potential failure mechanisms, and technical forensic techniques as noted above). Through this review, this paper aims to identify any gaps or deviations in the investigative approach and to discuss how these may have influenced the understanding of the failure.

In summary, this Introduction has outlined the recurring issue of wire rope sling failures and the critical need for meticulous investigations when such failures occur. The following sections of the paper will present the details of the incident and the contractor's investigation findings, then provide a discussion comparing those findings with established knowledge. Ultimately, the goal is to extract key lessons learned from the case and to propose practical improvements for future incident investigations in heavy lifting operations, so that similar failures can be better prevented or appropriately analysed in the future.

2. Methodology

This study uses a qualitative case-study methodology to assess the investigation process of the wire rope sling failure. Observational data from the incident, including the steps taken during the investigation, were reviewed in detail. The analysis compares the contractor's methods and conclusions with established failure analysis practices, specifically examining whether the root causes were fully identified in alignment with findings from similar peer-reviewed case studies.

2.1 Data Collection and Review Approach

All available data from the contractor's investigation was first collected during presentation and information distribution through email correspondence, meeting and then examined. Key factual information was extracted, including the sequence of events leading up to the sling failure, the condition of the failed sling and associated hardware, and any analysis or tests the contractor performed (e.g. visual examinations, measurements, etc.). This information provided a baseline understanding of what the contractor did during their failure analysis. No additional experiments or field inspections were conducted in this review; instead, the contractor's own evidence (photos, fracture observations, load estimates, etc.) was used as the primary data set. Data from field (photos) and investigation (through interview to personnel whom involved) information sharing as source material to be evaluated rather than as formal results to be accepted at face value.

This case compiles various literatures from both academic journals and industrial standards. By reviewing these sources, it was compiled a set of expectations for a thorough sling failure investigation – for example, checking for signs of metal fatigue, corrosion, wear, overloading, material defects, and reviewing maintenance and inspection records. The literature review also highlighted typical root causes and contributing factors in sling failures that investigators have found in past cases (such as improper use, manufacturing flaws, or inadequate inspection regimes). This set of best practices from prior studies formed the criteria against which the contractor's investigation was evaluated.

2.2 Analytical Framework: Root Cause Analysis (RCA)

The evaluation centered on the principles of Root Cause Analysis (RCA). RCA is a systematic method used to drill down to the underlying causes of a failure by asking iterative "why" questions and examining evidence at each step. Rather than stopping at the obvious immediate cause of the sling failure (e.g. the sling breaking under load), RCA seeks to uncover deeper factors that allowed the failure to occur – for instance, *why* the sling failed at that load, *what* factors (material, design, usage, or organizational) contributed, and *how* similar failures could be prevented. In applying an RCA lens, we reviewed the contractor's investigation to see whether it had identified not just *how* the sling failed, but *why*. This meant checking if the contractor explored multiple facets of causation: the condition of the sling itself (e.g. any pre-existing damage or manufacturing defect), the loading scenario and rigging method, and organizational factors like procedures or training. They were looked for evidence that the failure sequence from the initial event back to potential root causes. For example, did they examine the fracture surface of the sling for tell-tale features of fatigue or overload? Did they consider whether the sling was suited for the load and configuration? Did they review if maintenance or inspection practices missed any warning signs? By systematically answering these questions, we gauged the depth of the contractor's root cause analysis.

It should be noted that various frameworks exist to analyse accidents and failures. One such technique is the Bowtie method, which graphically maps out the pathways from causes to the incident and identifies preventive and mitigating barriers. In the context of this study, the Bowtie approach is mentioned for awareness but was not employed in detail. The Bowtie diagram can be a useful visualization to ensure all potential causes and controls are considered; however, this paper prioritized the RCA approach as it directly focuses on cause-and-effect relationships and is well-suited for pinpointing technical failure origins. Thus, while the contractor's investigation might be visualized in a Bowtie format to check completeness, This paper review did not construct a full Bowtie diagram. Instead, it remained focused on qualitatively evaluating root causes as derived from the investigation.

2.3 Comparison with Published Failure Investigations

Using the information gathered from both the contractor's data input and the literature, we performed a comparative analysis. In practice, this meant evaluating each major aspect of the contractor's investigation against how expert investigations are described in case studies. For instance, if the contractor performed a physical examination of the broken sling, we compared the thoroughness of that examination to those in the literature: Did it include high-magnification fracture analysis or just a naked-eye inspection [2]? If the contractor concluded a certain cause, it need to be checked whether that cause aligns with known failure modes reported by other sling failure analysis. It was also noted whether the contractor identified any contributing factors beyond the immediate cause. Good investigations typically consider human and organizational factors; for example, it was discovered failure found that fatigue cracks had initiated at decarburized (weakened) spots on the wire, and that poor inspection practices allowed the deterioration to go unnoticed until failure [7]. This illustrates how a technical cause (metal fatigue from a material anomaly) and an organizational cause (inadequate inspection) can both be root causes of a failure. In another published sling failure

investigation, discovered a manufacturing quality issue: a hoisting rope was inadvertently made with mixed-strength wires, leading to uneven stress distribution and early wire fractures [10]. That case underscored the importance of verifying material compliance and quality control as part of determining why the rope failed.

By drawing on these examples from *Engineering Failure Analysis*, the methodology checks whether the contractor's investigation considered a similarly broad range of factors. Specifically, we assessed if the contractor inspected the failed sling for evidence of fatigue, wear, corrosion, or material defects in the manner experts recommend. We verified if they analysed the sling's load history and usage conditions to identify any misuse or overloading. We also examined whether the investigation reflected on procedural aspects (such as whether the sling was appropriate for the task and if proper pre-use inspections were done). Each of these elements from the contractor's work was compared to the best practices noted in the literature review. Where the contractor's report was silent on an aspect that literature deems important (for example, if no metallurgical analysis was mentioned, despite such analysis yielding critical insights in published case studies), it was flagged this as a potential gap in the investigation. Conversely, if the contractor's approach mirrored what published investigators have done – say, collecting broken sling samples and sending them for laboratory analysis – this was noted as a strength indicating alignment with established methods.

Throughout this review process, the guiding question was: Does the contractor's investigation adequately identify the root cause(s) of the sling failure, and is it as thorough as investigations documented in peer-reviewed case studies? By applying an RCA framework and benchmarking against published sling failure analysis, it needs to ensure that this evaluation is both systematic and grounded in proven engineering failure investigation techniques. This methodology allows the study to objectively support its overall aim, which is to gauge the quality and completeness of the contractor's sling failure investigation in light of known best practices and lessons learned from similar failure cases.

3. Case Description

3.1 Incident Overview and Background

A contractor-led investigation was conducted into the failure of a wire rope sling during a trial lifting operation. The incident occurred during a system integration test (SIT) of a subsea equipment foundation's hinged protection panel. This large steel panel (weighing approximately 19.3 metric tons) is attached to the foundation structure by hinges and is designed to open and close with a relatively small force applied via a single padeye (rated for an 8 metric ton working load). The SIT plan on the day of the incident was to verify the panel's operation by lifting it from horizontal (open) to vertical (closed) using a mobile crane. Prior to the lift, a safety exclusion zone was established around the panel, and all non-essential personnel were cleared from the area. A toolbox talk was held with the lifting team on the morning of the trial, emphasizing that the crane operator should stop the lift if the load exceeded 20 MT (as a precautionary limit given uncertainties in required force).

Equipment and Rigging Setup: The lifting was performed with a heavy crawler crane and a rigging arrangement of wire rope slings and shackles. The crane used was a 350 MT capacity lattice-boom crawler crane, positioned on firm ground at one side of the panel's hinge axis. The panel's dedicated padeye (8 MT WLL) was connected to the crane hook by a series of slings and shackles. Initially, a single 2.5″ wire rope sling was used to attach the crane to the panel. One end of sling was shackled to the panel's padeye (using a 25 MT bow shackle); the other end of the sling was connected to the crane's main hook via a large 250 MT shackle and two auxiliary wire rope sling legs (each 3.5″ diameter). This configuration is shown in Figure 1. The two 3.5″ sling legs formed a double-line connection from the crane hook to the junction with sling, providing additional reach and load capacity. All lifting gear had been inspected and load-tested in the months prior to the trial. Table 1 summarizes the key equipment and sling specifications for the lift.

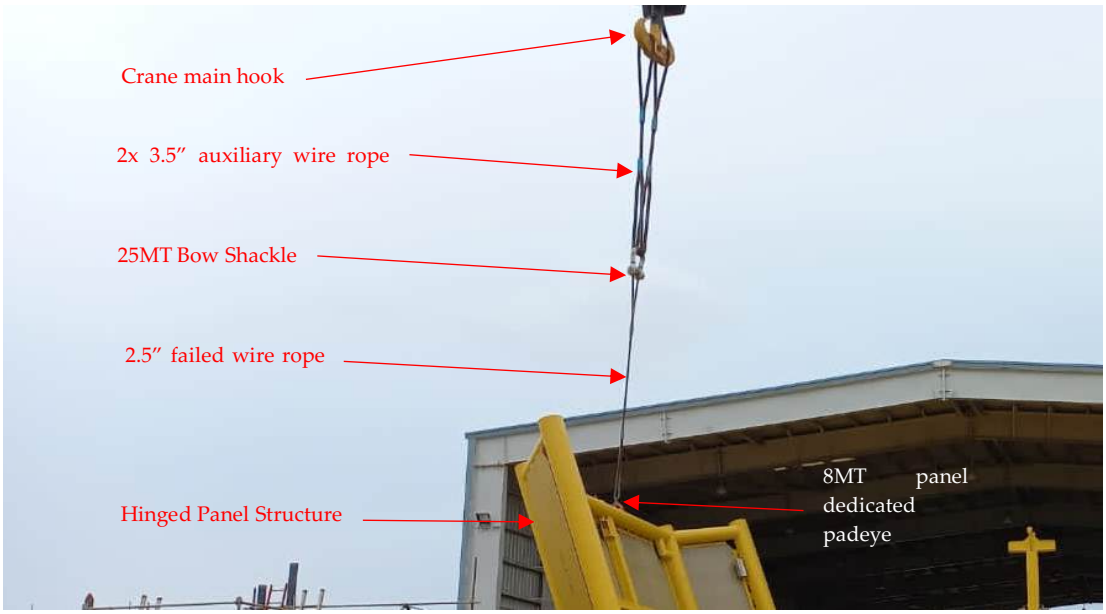

Figure 1. Initial rigging arrangement for the protection panel lift. The crane's hook (out of frame above) is connected via two 3.5″ wire rope sling legs and a large bow shackle to the single 2.5″ sling attached to the panel's lifting padeye. This setup was intended to pull the panel from horizontal toward vertical during the trial lift.

Table 1. Equipment and Sling Specifications (as used during the trial lift):

Item	Description / Specification
Crawler Crane	**350 MT SWL lattice-boom crane (mobile crawler), positioned ~40 m from panel hinge; main hook used for lift.**
Protection Panel	**~19.3 MT steel panel, hinged on subsea foundation; designed to require ~8 MT force via padeye to close. Padeye WLL 8 MT (single lifting point on panel).**

Item	Description / Specification
Primary Sling	**Wire rope sling, 2.5″ diameter × 15′ length. Rated SWL ~60 MT (≈54 tonnes) with minimum breaking load (MBL) 275 MT. Manufactured 2005 (17 years in service); last load test Jan 2022 to 69.1 MT.**
Auxiliary Slings	**2 × Wire rope slings, each 3.5″ × 20′. SWL 102 MT each. Used in double-line fashion between crane hook and primary sling. Manufactured 2009; last tested Jan 2022.**
Shackles	**250 MT bow shackle connecting auxiliary slings to crane hook; 25 MT bow shackle initially used at panel padeye (later replaced with 55 MT shackle for subsequent trials).**
Crane Instrumentation	**Load indicator in crane's cab (load cell system) and radius/angle sensors. Crane certification up to date (last inspection Sep 2021).**

3.2 Sequence of Events

Initial Lift Attempt: On the afternoon of April 7, 2022, the team proceeded with the first trial lift of the panel. The rigging was set as described, and the crane slowly took the slack and began lifting the free end of the panel off its supports. The panel was hoisted upward toward a vertical position while the crane boom was held relatively fixed. Almost immediately, the crane's load indicator showed a rapidly increasing load as the panel's weight shifted. The plan was to then slew the crane (swing the boom) to swing the panel shut. However, before the panel could fully close, the measured load exceeded the pre-set stop threshold. The crane operator announced a load of about 22 MT at a 42 m radius, surpassing the 20 MT limit given by the engineers, and the lift was halted. At this point the panel had been lifted into a near-vertical position but not closed. The first attempt was aborted due to the higher-than-expected force required – nearly three times the padeye's WLL – indicating that the panel was binding or resisting movement more than anticipated. The panel was carefully lowered back to its resting position without further incident.

Second Lift Attempt (Reposition and Travel Method): The engineering team paused to reconsider the approach. It was recognized that swinging the boom created a side-loading scenario on the sling and panel. For the second attempt, the crane was repositioned to face the panel more directly. The crane was moved (on its tracks) to be roughly in line with the panel's plane, so that the subsequent closing motion could be performed by tracking the crane forward (driving the crane) rather than swinging the boom. This aimed to pull the panel straight in, reducing side loads. The same sling was still used at this point, but the padeye shackle was upgraded to a 55 MT capacity shackle for a greater safety margin. Around 1:55 PM, the second trial commenced: the crane again lifted the panel up to vertical and then slowly travelled

forward, attempting to push the panel from vertical toward the closed position. Despite the new approach, the panel refused to fully rotate into place – friction at the hinges or misalignment was preventing closure. The forces in the sling again built up beyond safe limits, and the team aborted the second attempt as well. The panel remained held by the crane, partially open, but it was clear another strategy was needed. The load experienced in this attempt was significant (later data indicated the force was on the order of tens of tonnes), though the exact value was uncertain due to instrumentation issues described later. After lowering the panel back down again, the team convened to plan adjustments.

Third Lift Attempt (Final, Failure): For the third and final attempt, the rigging was further modified. Recognizing that the required force was much higher than expected, the crew replaced sling with a higher-capacity sling (2.5″ diameter, same sling was actually of that size – the report clarifies this sling's specs as 2.5″, 60 MT SWL) and ensured all shackles were adequately rated (55 MT at the padeye, 250 MT at the hook). The crane was also positioned as close as feasible to the structure to minimize the reach and angle. Shortly after 3:15 PM, the third trial began: the panel was lifted once more toward vertical, and the crane slowly tracked to push it toward the closed position. This time the panel moved slightly further, coming very near to aligning in the closed position. Without warning, the primary sling suddenly parted. The failure occurred when the panel was almost upright, under peak tension. The severed sling recoiled and the panel, now free, swung back down under gravity, slamming into its original open position on the supports. Figure 2 shows how the moments before and after sling failure.

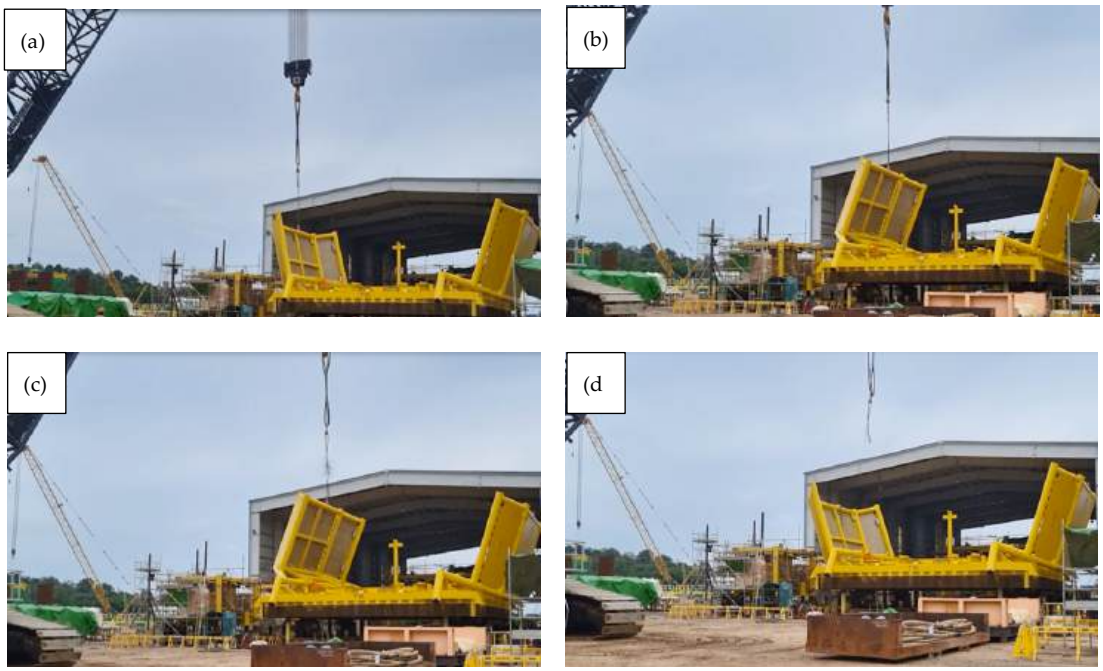

Figure 2. (a) Crane Rigging Attached To Panel At Open Position At Start Of SIT Trial Lifts. (b) Panel and Sling Inclination Prior to Parted. (c) Panel Position When Sling Parted. (d) Aftermath of the sling failure. The protection panel (right) is shown fallen back to its open position after the sling snapped.

Figure 3 shows how one frayed end of wire rope sling remains attached to the panel's padeye, and Figure 4 shows the other end recoiled toward the crane hook. Fortunately, all personnel were well outside the exclusion zone, and there were no injuries when the sling snapped and the 19-ton panel dropped. The two broken pieces of sling remained attached at each end — one piece still on the crane's hook and the other still secured to the panel's padeye. The crew immediately stopped all operations and secured the area. Within minutes, they lowered the crane hook to the ground, detached the remaining sling piece, and used a man-lift to recover the sling piece that was still on the panel. The incident was formally reported, and an investigation team was mobilized to examine the failure. The chronological of event is explained in Table 2 in timeline order.

Table 2. Event Timeline of the Incident: (Chronology on April 7, 2022)

Time	Event
06:30 AM	Pre-lift preparations: SIT engineer briefs rigging team on trial lift plan. Rigging crew (foreman as lifting supervisor, with three riggers) gathers equipment and sets up crane at test location. Toolbox Talk (TBT) conducted; "Stop lift if load >20 MT" instruction given. Safety checks and permits completed (HIT card filed).
~1:30 PM	First Trial: Crane attached to panel; panel lifted from horizontal toward vertical. Load quickly exceeds expected value (≈22 MT recorded). Lift aborted before fully closing panel. Panel lowered back safely. Team notes that required force is much higher than design 8 MT – indicating unexpected resistance.
~1:55 PM	Second Trial: Crane repositioned parallel to panel; attempt to close panel by tracking crane forward. Panel again lifted and pulled toward closed position. Panel still will not fully close; high force observed (lift aborted again). Decision made to use a larger sling and bring crane closer.
3:15 PM	Third Trial: Rigging upgraded (higher-capacity sling, larger shackle); crane moved closer. Panel lifted nearly closed using crane movement. Sling fails catastrophically at peak load. Panel drops back open. All work stopped immediately.
3:20 PM	Post-incident actions: Area barricaded and secured. Broken sling pieces retrieved. Incident reported to management. Investigation initiated the same day.

Figure 3. The wire rope sling parted near its end termination – one frayed end remains attached to the panel's padeye (yellow circled).

Figure 4. The other end recoiled toward the crane hook. The failure occurred at the sling's ferrule (socket) where the wire rope is swaged, later found to contain corroded wires.

3.3 Investigation Findings and Observations

A detailed examination of the failed sling and a review of the operations was conducted by the contractor's investigation team. The wire rope sling was found to have failed at the ferrule (the metal sleeve securing the eye at the sling's end). Close inspection revealed that the wire strands inside the ferrule were severely corroded. The break appeared to originate where the rope enters the ferrule, suggesting a classic hidden corrosion fatigue failure, which significantly reduced the sling's strength. The sling had been in service for 17 years; despite passing a load test three months prior (*see Figure 5*), it was likely had diminished load capacity due to internal deterioration that went undetected in routine visual inspections.

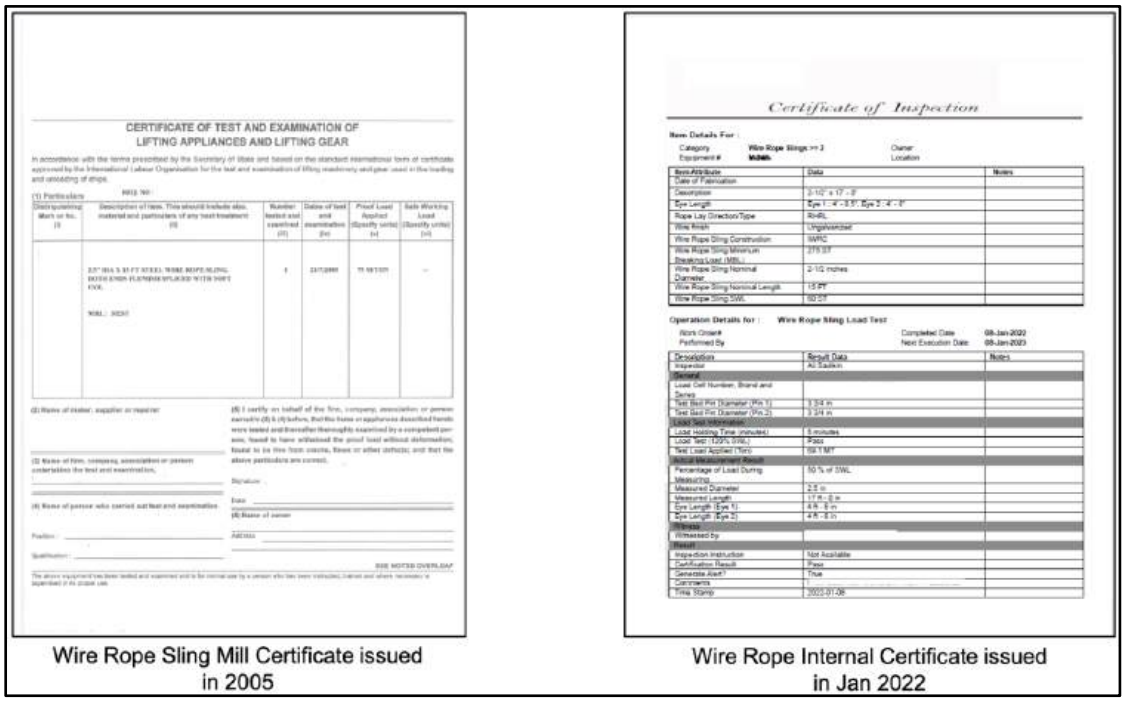

Figure 5. The sling had been in service for 17 years; despite passing a load test three months prior.

Apart from the metallurgical analysis of the sling, the investigation uncovered several contributing factors related to the planning and execution of the lift:

- Load greatly exceeded expectations: The force required to close the panel was far higher than the design intent (peak load estimated around 60 MT versus the 8 MT design load for the padeye). This was attributed to the method of lifting – using a single crane at one end of the panel introduced significant binding and side load on the panel's hinges, meaning the crane was effectively lifting much of the panel's weight and overcoming friction, rather than the panel swinging freely. The panel's weight estimation (≈19 MT) was accurate, but the method of applying force was not as envisioned in design, leading to a gross overload of the padeye and sling. Notably, a prior factory test had determined that using one crane on the padeye was not effective to close the panel – in that test, two cranes had been used to successfully close it – however, this lesson learned was not fully implemented in the planning of the SIT trial.
- Inadequate risk assessment and lift planning: The contractor's procedures classified this trial lift as a critical lift (due to the unusual rigging and high consequence of failure), which

would require a detailed risk assessment and specialized lift plan. However, the team on site treated it as a routine lift. No formal task risk assessment was conducted beyond the standard pre-job briefing. The decision to proceed with a single-sling, single-crane method, despite the known difficulties, represented a deviation from recommended practice without a proper management-of-change. The lack of a Critical Lift Plan and oversight meant that hazards like the padeye overload and sling stresses were not fully evaluated.

- Use of an aged sling without detecting internal damage: The failed sling had been maintained in the rigging inventory for many years. While it had proper certification documents and recent load test records, there was no age-based retirement criterion for slings in use – meaning an older sling could remain in service if it passed visual inspections and load tests. The investigation noted that the sling's storage conditions (often outdoors in a marine yard environment – *see Figure 6*) likely contributed to internal corrosion. The internal corrosion was not outwardly visible and was missed during inspections. This latent defect left the sling weaker than its rated capacity. When the sling experienced the high tension during the third trial, it failed below its original MBL, at the corroded section.

Figure 6. Sling outdoor storage condition

- Operational signals and Stop-Work: During the operations, the lifting team did register that the load was exceeding safe limits (as evidenced by the first abort at 22 MT). However, after re-rigging, when similar or higher loads were encountered, no one exercised Stop-

Work Authority to halt the job for a re-evaluation of the overall approach (beyond just upgrading the sling). The investigation highlighted that once the padeye's 8 MT limit was exceeded by a large margin, the operation should have been re-assessed from first principles. There was an over-reliance on simply using a bigger sling and crane, rather than addressing the fundamental issue of the method. Fortunately, the safety exclusion zone was maintained, which prevented any injuries when the sling ultimately failed.

Table 3. Key Findings from the Contractor's Investigation:

Key Finding	Details
Sling failure due to hidden corrosion	The wire rope sling failed at its ferrule, where internal corrosion of the wires was found. This corrosion significantly weakened the sling, causing it to part under a load well below its original breaking strength.
Actual load far above design capacity	The force required to close the panel (~60 MT) vastly exceeded the panel padeye's rating (8 MT) and the sling's intended safe load. The single-crane method induced high friction and side loads, effectively resulting in a severe overload of the rigging.
Lift misclassified as standard	The operation was treated as a standard lift instead of a critical lift, contrary to procedure. A detailed lift plan and risk assessment were not carried out, and a planned two-crane method (from earlier testing experience) was not used.
Deficient risk mitigation	When warning signs appeared (load readings over limit, earlier attempts aborted), the team did not stop and comprehensively reassess the plan. The Stop-Work Authority was not utilized despite clear indications of danger (padeye and sling overload).
Aged equipment and lack of criteria	The failed sling had been in service for 17 years. No specific retirement age criteria existed, and periodic inspections did not reveal its internal deterioration. Storage conditions and infrequent specialized audits may have contributed to its degraded state.
Equipment issues (secondary)	The crane's load monitoring system was found to have a faulty sensor, causing unreliable data. Although not a direct cause of the failure, this issue complicated the real-time assessment of the load and underlined the importance of robust equipment checks.

- Crane instrumentation and load readings: Post-incident analysis of the crane's onboard computer logs showed some inconsistent data. In fact, the crane's boom angle sensor was later found to be faulty, which called into question the precision of some recorded load values (the sensor error can affect how the load moment is calculated). A calibration check after the incident revealed the load cell was giving fluctuating readings at certain angles. Regardless of this instrumentation issue, the evidence of the physical overload (bending of the sling, the eventual break, etc.) confirmed that the forces were far beyond normal limits. The faulty sensor contributed to some confusion (for instance, the crane indicated ~60.3 MT at failure, a value which may or may not have been accurate), but it did not cause the incident – rather, it meant the operators did not have a perfectly reliable indication of actual load. The true load was likely extremely high, consistent with the sling failure.

In summary, the case involved a convergence of factors: an underestimation of the forces required, use of an inadequately inspected sling, and shortcomings in lift planning and hazard recognition. The contractor's investigation concluded that the sling parted primarily due to mechanical overload aggravated by internal corrosion. The incident underscores the need for rigorous critical lift planning, consideration of alternate methods (such as using multiple lift points or cranes for heavy hinged structures), proactive retirement of aging slings, and attentive execution with the willingness to halt work when conditions deviate from expectations. The findings from this case were to be used to improve lifting practices and prevent similar occurrences in the future.

Chapter 4: Critical Analysis

4.1 Application of RCA and Bowtie Methodology

The root cause analysis (RCA) methodology as explained in Chapter 2 is applied to evaluate the contractor's investigation of the wire rope sling failure. A cause-and-effect analysis was conducted, integrated with a Bowtie approach to map out both the contributing causes (threats) and the consequences of the sling failure event. Figure 6 illustrates a simplified Bowtie diagram for the sling failure, highlighting key causal factors on the left and potential outcomes on the right. This diagram places the *wire rope sling failure* as the central "top event," fed by multiple hypothesized causes such as *excessive load*, *wear/corrosion*, *improper rigging angle*, and *manufacturing/material defects*. These factors align with common failure causes identified in literature – for instance, excessive wear, corrosion, and overloading are frequently cited precursors to wire rope breakage [2]. On the right side, Figure 7 shows the likely consequences of a sling break (e.g. dropped load, equipment damage, injury), which underscore the high risk nature of such failures. The Bowtie also conceptually includes barrier controls: for example, *regular inspections* to catch corrosion or *adherence to load limits* to prevent overload. This integration of Bowtie analysis ensures that the evaluation not only considers why the sling failed (causes) but also whether adequate preventive barriers were in place or missing. By applying this methodology, we can systematically examine whether the contractor's investigation identified the same spectrum of causes and assessed the effectiveness of existing controls.

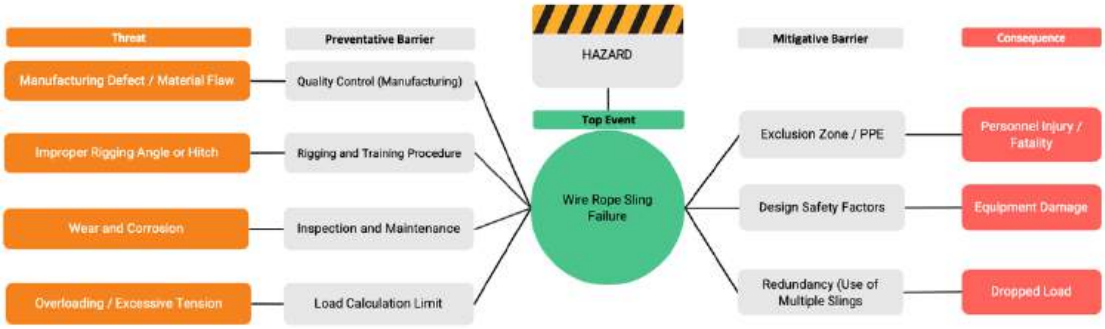

Figure 7. Simplified Bowtie diagram for the wire rope sling failure, showing key contributing causes (left side) and consequences (right side), along with examples of preventive and mitigative barriers (grey).

Using this RCA/Bowtie framework, the contractor's findings can be critically analyzed for completeness and depth. The Bowtie diagram helps visualize how each cause was addressed in the investigation. For instance, one hypothesized cause was wear and corrosion of the sling. Localized wear and plastic deformation can initiate stress concentrations leading to fatigue fracture in wire ropes [2]. The contractor through their presentation, did note corrosion near the sling's ferrule (end termination), suggesting they recognized a degradation mechanism. However, a rigorous RCA would probe further: *Was corrosion the primary contributor to failure, or did it simply exacerbate an overload condition?* Similarly, improper rigging or side loading (bending the sling at an angle) appears in the Bowtie as a potential cause. Side loading is known to dramatically increase stress on a sling and reduce its effective strength [11], yet the contractor's analysis should confirm if such off-axis loading occurred during the lift. In the incident, evidence shows the crane movement caused a side pull on the sling, increasing the tension beyond straight-line conditions. An effective RCA connects this operational factor to the failure: e.g. by noting that the sling experienced a higher load due to geometry, consistent with modelling studies on bending effects. Another threat in Figure 6 is *excessive load* relative to the sling's safe working limit. The contractor's data (crane log indications and the weight of the panel being lifted) strongly suggest that the sling was overloaded – possibly far beyond the pad eye's 8 MT design load – which would directly cause failure if true. Bowtie analysis encourages verifying whether safeguards against overload were present (such as load calculations or real-time load monitoring) and if they failed. In this case, the crane's load cell readings were unreliable due to a sensor fault, meaning a key preventive barrier (accurate load feedback) was compromised. Overall, the methodology helps ensure each causal pathway is considered and that the contractor's investigation is measured against a comprehensive map of potential causes and missed barriers.

4.2 Assessment of the Contractor's Investigation in Relation to Established Best Practices

Having mapped out expected causes and controls, we now evaluate the contractor's investigation using criteria derived from peer-reviewed case studies on wire rope failures. Table 4 summarizes this evaluation, comparing the investigation's scope and findings against industry best practices [2][7][10]. Key areas of evaluation include the completeness of failure

analysis, correct identification of failure mode and root cause, and the procedural rigor of the investigative approach.

- Failure Mode Identification: The contractor's report indicates the sling "parted at the ferrule with signs of wire corrosion." This suggests a failure mode potentially involving corrosion-assisted breakage, but it remains unclear if the break was due to gradual fatigue or an instantaneous overload. Peer-reviewed investigations stress the importance of determining the failure mode via fractographic and metallurgical analysis [14][7]. For example, fatigue fractures initiated by decarburized micro-cracks in a failed crane rope, using microscopic examination [7]. In the contractor's case, no mention of detailed fracture surface examination or wire break morphology was made; thus, the precise failure mode was left somewhat ambiguous (the report lists "undetermined corrosion" as a factor). This is a partial gap – while the presence of corrosion was noted (a clue toward possible fatigue or stress corrosion cracking), a conclusive determination (e.g. overload versus fatigue failure) was not documented. Without techniques like scanning electron microscopy [2], the investigation may have missed distinguishing whether corrosion caused a brittle stress-corrosion failure at the ferrule or simply weakened the sling which then snapped in overload.
- Root Cause Identification: The contractor did identify numerous contributing factors, extending beyond the broken sling itself. Notably, they recognized latent organizational issues – for instance, the lack of a defined retirement age for slings (the failed sling was ~17 years old with no replacement criteria) and shortcomings in risk assessment (treating a complex lift as a routine operation). These align with best practices in RCA, which call for probing into not just *what* failed, but *why* the conditions for failure were present. The investigation enumerated causes ranging from procedural errors (inadequate hazard assessment, bypassing of management-of-change processes) to environmental factors (outdoor storage leading to corrosion) and human factors (decision to proceed with one-crane method despite a previous two-crane failure). This breadth shows commendable scope and mirrors the multi-factor approach seen in case studies. For example, a manufacturing lapse (mixing of wire grades) as the root cause of a rope's premature failure [10]. Similarly, the contractor's analysis did not stop at the broken sling's condition; it dug into *why* an old, possibly degraded sling was still in use, and *why* the operation overstressed it. In terms of root cause identification, the investigation meets the standard by uncovering systemic issues (e.g. lack of critical lift planning, inadequate maintenance policies) that set the stage for the sling's failure. One area for improvement is clearer prioritization of these causes – the report listed seven "COMET factors" but did not explicitly label any single factor as *the* root cause. A more explicit linking of the chain (for instance: improper risk assessment led to use of one crane and an old sling, which led to overload and failure) would improve clarity.
- Analytical Rigor and Evidence: A strong failure investigation relies on thorough evidence collection (visual inspection, nondestructive examination, laboratory testing) [14]. The contractor's team performed a visual examination (noting corrosion at the ferrule) and reviewed load test records and crane logs. However, there is no indication of metallurgical analysis of the failed sling segment (such as sectioning the ferrule to inspect internal

corrosion, or microscopic examination of broken wire ends). By contrast, published case analyses usually include such examinations – for example, stereoscopic fractography and microhardness tests were used to correlate failure features with operational conditions [2]. Without similar tests, the contractor's conclusion about corrosion remains qualitative. The investigation could be considered incomplete in forensic analysis: it did not quantify the extent of internal corrosion or confirm if the mode of failure was ductile overload or fatigue. This is a notable miss, because a laboratory analysis might have revealed, say, a fatigue beach mark pattern or a brittle fracture surface, altering the emphasis of the root cause. On a positive note, the investigation did incorporate operational data (crane computer logs, test history), which is in line with comprehensive analysis – it recognized that the *operational context* (load magnitude, side-loading due to crane movement, etc.) was critical to the failure. In summary, the evidence gathering was sufficient to identify obvious factors but fell short of the depth seen in peer-reviewed failure analyses.

- Procedural Rigor: The methodology followed by the contractor shows elements of a formal RCA. The use of a timeline of events, a list of contributing factors (labelled as latent issues and direct causes), and a set of corrective actions indicates a structured approach. This mirrors standard investigative processes and even the Bowtie paradigm, wherein hazards (e.g. an 8 MT pad eye being used in a high-load scenario) are linked to threats (causes) and controls (or lack thereof). The investigation could have benefitted from explicitly using an RCA tool (such as a fault tree or fishbone diagram) to visualize cause-effect linkages for clarity, but the content implies these linkages in narrative form. Importantly, the investigation considered human and organizational factors – a hallmark of rigorous analysis. For instance, it identified that the team knowingly exceeded the pad eye's limit without a proper MOC (Management of Change) approval, and that lessons learned from a factory test (FAT) were not implemented. By acknowledging these, the contractor's team demonstrated a systems-thinking approach consistent with modern accident analysis models. One minor critique is the lack of external peer review or reference to standards in the report – the analysis was internal, and there is no mention of consulting wire rope failure standards or guidelines (for example, ISO or ASTM standards for sling inspection, or published criteria for retirement). Incorporating such benchmarks (e.g. citing that no internal wire breaks were acceptable per ISO standards, or that 17 years far exceeds typical sling service life in marine environments) would strengthen the authority of the conclusions. Nonetheless, the overall procedural rigor was strong, addressing multiple facets and producing actionable recommendations.

Table 4. Summary on how the contractor's investigation compares to key criteria drawn from the literature.

Evaluation Criterion	Assessment of Contractor's Investigation
Failure Analysis Completeness	*Partial.* Visual examination and operational data were assessed, but limited forensic analysis of the failed sling was performed. No metallurgical tests or detailed fractography were reported, whereas case studies recommend such analysis for conclusive results [2].
Failure Mode Identification	*Partial.* Corrosion at the failure point was observed, but it was uncertain if failure was by overload or fatigue. The investigation lacked definitive evidence (e.g. microscope fractography) to classify the failure mode, unlike peer analyses that clearly distinguish fatigue vs. overload [7].
Root Cause Depth	*High.* The investigation went beyond the immediate cause to identify multiple underlying causes (procedural failures, lack of maintenance policies, environmental factors). This systems approach meets best-practice standards, as seen in comprehensive case reviews [10].
Procedural Rigor in Analysis	*High.* A structured RCA-like process was evident (timeline of events, cause factor list, actions). Human, technical, and organizational factors were all considered. The thoroughness in identifying latent issues (e.g. training and audit deficiencies) reflects a robust methodology.
Adherence to Best-Practice Criteria	*Moderate.* The investigation addressed major factors and provided recommendations, but it did not reference external standards or criteria for wire rope condition (e.g. discard criteria, design factors). It also lacked independent expert review. Aligning findings with industry standards (for instance, criteria for retirement due to age/corrosion) would further validate the conclusions.

In summary, the contractor's investigation was broad in scope and identified key contributors to the sling failure, matching well with the multifaceted causes reported in literature for similar cases. The inclusion of factors like inadequate risk assessment and sling age/corrosion shows an understanding that accidents arise from multiple failings, not just a single point of hardware failure. This aligns with peer-reviewed case studies where investigators found combined causes (e.g. material defects plus operational overload) behind wire rope failures [7][2]. The main shortcomings of the investigation lie in the depth of technical failure analysis – specifically, the lack of detailed metallurgical examination – and in fully

documenting adherence to criteria (no explicit citation of standards, and uncertainty in failure mode determination). These gaps could be filled by a more rigorous application of the RCA methodology: for example, performing a laboratory failure analysis to conclusively determine how the sling broke, and using a Bowtie diagram or fault tree to ensure all possible causes and missed barriers are accounted for and communicated clearly. Overall, however, the investigation's findings are consistent with known failure modes of wire rope slings and provide a solid basis for the preventive actions recommended.

Chapter 5: Discussion

5.1 Alignment with Best Practices and Literature on Sling Failures

The contractor's investigation findings largely align with known failure mechanisms for wire rope slings, while also revealing some gaps compared to best practices. The analysis determined that the sling failure was precipitated by in-service deterioration – specifically internal corrosion at the ferrule and accumulated wear due to long service and poor storage. This accords with the broader literature on wire rope failures, which emphasizes that progressive damage like wear, corrosion, and localized deformation can create stress concentrations leading to fatigue fractures [2]. Even under normal operations, small-scale wear and plastic deformation in ropes will amplify local stresses and eventually trigger sudden fatigue failure [2]. The failed sling in this case, having been in service since 2005, exhibited exactly such hidden degradation (corrosion in the termination) that was not apparent in routine inspections or a recent load test. This finding is consistent with failure analysis of a crane rope, where undetected defects combined with cyclic loading led to fatigue cracking; they concluded that fatigue, exacerbated by inadequate inspection, was a primary cause of rope rupture [7]. In this incident, the fact that the sling passed a load test only weeks before failure yet still broke underscores the challenge of detecting internal flaws – subtle defects (like decarburization cracks in steel wires) can escape notice and initiate failure [7]. The contractor's identification of internal corrosion as a root cause shows an awareness of these failure modes and reflects an alignment with best practices in failure investigation, which call for looking beyond obvious external damage.

Notably, the investigation did not find evidence of manufacturing or design defects in the sling, focusing instead on deterioration and operational factors. This is an important distinction from some cases in the literature where the root cause traced back to material or manufacturing issues. For instance, a wire rope failure that was ultimately caused by a manufacturing error: the rope was built with a mix of low- and high-strength wires, contrary to specifications, leading to uneven stress distribution and premature wire breaks [10]. In the present case, the sling had been certified to the correct capacity and had a long service history, suggesting no such intrinsic defect. The failure therefore diverges from such scenario, and instead aligns more with wear-and-tear induced failures [2], emphasizing the role of service conditions rather than manufacturing quality. That said, the contractor's plan to send the broken sling for third-party laboratory analysis indicates a commendable thoroughness. Engaging in metallurgical failure analysis (as done in published studies [2]) could confirm the micro-mechanisms of failure and

ensure no contributing factor (such as an undetected material anomaly) is overlooked. This step goes beyond many routine investigations and shows an effort to meet the rigor seen in scholarly analysis of sling failures.

Overall, the technical conclusions of the contractor's investigation are well-grounded in established knowledge. The determination that *inadequate maintenance and inspection regimes* allowed a deteriorated sling to remain in use is strongly supported by prior studies. As one best-practice guideline notes, wire ropes must be removed from service before damage (wear, corrosion, broken wires) accumulates to a critical level [7]. In this incident, the absence of an age-based retirement criterion for slings – the sling was 17 years old – was a clear lapse. The investigation acknowledged this by pointing out the lack of a procedure for age-based rejection and recommending that slings older than 10 years be retired. This corrective action resonates with the preventative focus advocated in literature: discard criteria should consider not only visible damage but also time-related degradation [7]. In sum, the investigation's findings (internal corrosion, side-loading during the lift, insufficient pre-job planning, etc.) align with known causes of sling failure, and the areas where it diverged from ideal practice (e.g. the need for more proactive inspection standards) were recognized and addressed through recommended actions.

5.2 Implications for Investigation Quality and Organizational Learning

Beyond the technical cause, this case carries broader implications for improving incident investigations and fostering organizational learning in lifting operations. One positive aspect is the investigation's comprehensive approach in identifying not just the immediate cause of the sling failure, but also underlying organizational and process weaknesses. The analysis went on to examine why the situation arose – uncovering issues like improper lift planning, failure to heed prior test lessons, and gaps in safety procedures (such as the lack of a defined "critical lift" protocol and lapse in applying Management of Change when the plan deviated). By tracing contributing factors through management and communication lapses, the inquiry reflects a systems-thinking approach that is often championed in safety literature. This is in contrast to more superficial investigations that focus only on operator error or hardware failure. Indeed, recent research on incident investigations has warned that focusing solely on "sharp-end" factors (frontline mistakes or isolated technical faults) tends to yield weak corrective actions that don't prevent recurrences [13]. In this incident, the contractor's team avoided that pitfall: they looked at latent organizational conditions – such as procedure deficiencies and cultural aspects (e.g. reluctance to exercise Stop-Work Authority) – and issued recommendations to address these deeper issues. This aligns with best-practice models of learning from incidents, which stress that true improvement comes from addressing systemic weaknesses and not just replacing the broken part or blaming personnel [13].

However, the case also highlights challenges in translating lessons into practice, an area where organizational learning must be strengthened. It was noted that a similar lifting attempt during Factory Acceptance Testing (FAT) had failed, and lessons learned (LL) were circulated, yet the project team proceeded with essentially the same approach that led to the sling failure.

This lapse indicates a breakdown in cross-project learning and knowledge transfer. Research in accident prevention emphasizes that recurring incidents with the same root causes are a sign that organizations are not effectively learning from past mistakes [13]. Recurring accidents were attributed to companies addressing surface-level problems while deeper issues persisted, and often failing to implement or follow up on recommended remedial measures [13]. This case follows this pattern: despite prior warning from the FAT, the knowledge was not institutionalized into planning or procedures, resulting in a repeated failure. The key implication is that organizations involved in lifting operations need more robust mechanisms for capturing and applying lessons learned. Simply holding post-incident meetings or disseminating a memo is not enough; there must be a systematic integration of those lessons into revised standards, training, and decision-making for future lifts.

Improving the quality of investigations plays a pivotal role in this learning cycle. The thoroughness of this particular investigation – which produced a detailed cause analysis and a multifaceted action plan – sets a high benchmark. It demonstrates how a well-conducted investigation can directly feed into organizational improvement. For instance, the action plan from this inquiry included tangible changes: new engineering controls (e.g. requiring dual cranes or revised rigging methods for similar lifts), procedural updates (implementing a critical lift registry and stricter sling retirement criteria), enhanced training (counselling the team on stop-work authority and refreshing the Management of Change process), and even a *Just Culture* review to ensure accountability is balanced with learning. Such breadth of remedial actions is indicative of a learning-oriented investigation outcome, as it addresses technical fixes and process/cultural reforms. This approach is precisely what the literature advocates for high-hazard industries – learning from incidents should trigger both immediate fixes and deeper organizational changes to reduce risk long-term [13].

Going forward, lifting operations can benefit from the lessons of this case by institutionalizing higher investigation standards and learning practices. First, organizations should ensure that any significant near-miss or equipment failure (like a sling snap) is analysed with the same rigor as a high-consequence accident, potentially involving third-party experts when needed to get to root causes. Second, the feedback loop from investigation to action needs to be swift and effective: as this case shows, having a clear timeline and responsibility for each recommended action (ranging from technical audits to procedure revisions) is critical. Finally, there should be an emphasis on knowledge sharing – both within the organization and across the industry. The recurrence of a preventable failure mode is far less likely when companies treat every incident as a learning opportunity and proactively update their practices. By comparing investigation findings with established best practices (as we did here using peer-reviewed studies) and by committing to continual improvement, lifting operations can significantly enhance their safety performance. In essence, the contractor's investigation – with its mix of aligned findings and candid exposure of procedural gaps – serves as a catalyst for organizational learning. It reinforces that thorough incident investigations are not just post-mortems of failure, but a cornerstone of *prevention*, enabling evidence-based improvements in equipment maintenance, risk assessment, and safety culture for future operations.

6. Recommendations

Based on the investigation findings, the following concise recommendations are proposed, targeting both the contractor involved in the incident and the wider lifting operations community:

- Enhance Sling Inspection and Maintenance: Enforce a rigorous inspection program with daily pre-use checks by a competent person. Damaged slings, such as those with broken wires or corrosion, should be immediately removed from service. Following established discard criteria ensures worn slings are retired before failure.
- Proactive Replacement of Aged or Damaged Slings: Implement a policy to retire slings after a reasonable service life or harsh use, even if they pass inspections. Research shows that wire ropes can wear out quickly under heavy use, and past failures highlight the need for proactive removal. Maintain detailed sling records to guide timely replacements.
- Improve Lift Planning and Risk Assessment: Strengthen procedures for planning complex lifts, classifying high-risk operations as critical lifts. Incorporate lessons from prior tests and ensure operations stay within equipment limits, adjusting rigging strategies when necessary. Hazard analyses should specifically consider the planned lift manoeuvre.
- Use Proper Sling Configuration to Minimize Stress: Ensure slings are used in configurations that prevent excessive bending or improper loading. Verify that rigging hardware meets recommended diameter ratios and angle restrictions to avoid internal wear. By adhering to design parameters, contractors can reduce the risk of sling failure.
- Reinforce Standards Compliance Across Industry: Ensure strict adherence to wire rope sling standards and regulations by all stakeholders. Require evidence of compliance, such as inspection logs and sling certifications, to promote a safety culture. Emphasizing these standards helps maintain sling integrity and ensures safe usage across all projects. This approach reduces the risk of accidents caused by degraded slings.
- Disseminate Lessons and Training on Failure Mechanisms: Actively share lessons learned from failure case studies to enhance collective knowledge. Incorporate real-world examples, such as undetected fatigue cracks and corrosion, into training programs for rigging inspectors and engineers. This will help identify critical warning signs and prevent catastrophic sling failure. Industry conferences and safety publications should circulate this information to promote proactive safety measures.
- Continuous Improvement of Equipment and Practices: Encourage the development and use of advanced inspection techniques, like non-destructive testing (NDT), especially for slings in critical service. Update industry guidelines to address issues revealed by failure incidents, such as defining more conservative safe life limits for slings. Promote a strong safety management system, including hazard identification and "stop-work" authority, to halt operations if abnormal conditions arise. These improvements will reduce sling failures and enhance lifting safety.

7. Conclusion

The investigation into the wire rope sling failure revealed that both technical and organizational factors contributed to the incident. The immediate cause was the sling's rupture due to undetected internal corrosion, which was exacerbated by overloading during a non-standard lift. Root Cause Analysis (RCA) identified two primary issues: the sling's severe internal corrosion, which routine inspections failed to detect, and procedural failures, including inadequate lift planning and a lack of safety oversight. These oversights highlighted gaps in risk management and communication.

The findings prompted corrective actions, including stricter sling inspection and retirement policies, better adherence to lift planning and load limits, and improved communication of lessons learned across the team. These measures are aimed at preventing similar failures and fostering a more proactive safety culture. Ultimately, the investigation served as a catalyst for improvement, with the application of RCA leading to enhanced practices and standards to improve the safety and reliability of future lifting operations.

References

1. Chaplin, C. R. (1995). Failure mechanisms in wire ropes. *Engineering Failure Analysis, 2*(1), 45–57.
2. Guerra-Fuentes, L., Torres-López, M., Hernández-Rodríguez, M. A. L., & García-Sánchez, E. (2020). Failure analysis of steel wire rope used in overhead crane system. *Engineering Failure Analysis, 118,* 104893.
3. Mapelli, C., & Barella, S. (2009). Failure analysis of a cableway rope. *Engineering Failure Analysis, 16,* 1666–1673.
4. Márquez, A. A., Venturino, P., & Otegui, J. L. (2014). Common root causes in recent failures of cranes. *Engineering Failure Analysis, 39,* 55–64.
5. Mouradi, H., El Barkany, A., & El Biyaali, A. (2018). Steel wire ropes failure analysis: Experimental study. *Engineering Failure Analysis, 91,* 234–242.
6. Piskoty, G., Affolter, C., Sauder, M., Nambiar, M., & Weisse, B. (2017). Failure analysis of a ropeway accident focusing on the wire rope's fracture load under lateral pressure. *Engineering Failure Analysis, 82,* 648–656.
7. Torkar, M., & Arzenšek, B. (2002). Failure of crane wire rope. *Engineering Failure Analysis, 9*(2), 227–233.
8. Xue, S., Shen, R., Chen, W., & Miao, R. (2020). Corrosion fatigue failure analysis and service life prediction of high strength steel wire. *Engineering Failure Analysis, 110,* 104440.
9. Xue, S., Shen, R., Shao, M., Chen, W., & Miao, R. (2019). Fatigue failure analysis of steel wire rope sling based on share-splitting slip theory. *Engineering Failure Analysis, 105,* 1189–1200.
10. Peterka, P., Krešák, J., Kropuch, S., Fedorko, G., Molnar, V., Vojtko, Marek. (2014). Failure analysis of hoisting steel wire rope. *Engineering Failure Analysis, 45,* 96-105.
11. Ivanov, H. I., Ermolaeva, N. S., Breukels, J., & de Jong, B. C. (2020). Effect of bending on steel wire rope sling breaking load: Modelling and experimental insights. *Engineering Failure Analysis, 116,* 104742.
12. Chang, X., Peng, Y., Zhu, Z., Gong, X., Yu, Z., Mi, Z., & Xu, C. (2019). Breaking failure analysis and finite element simulation of wear-out winding hoist wire rope. *Engineering Failure Analysis, 95,* 1–17.

13. Joe-Asare, T., & Stemn, E. (2024). Improving remedial measures from incident investigations: A study across Ghanaian mines. *Safety and Health at Work, 15*(1), 24–32.
14. Miller, B. A. (2000). FAILURE ANALYSIS of Wire Rope. *Advanced Materials & Processes*, *157*(5), 43.
15. American Society of Mechanical Engineers (ASME). (2018). *ASME B30.9-2018: Slings*. New York, NY: ASME.
16. International Organization for Standardization (ISO). (2018). *Cranes — Wire ropes — Care and maintenance, inspection and discard (ISO 4309:2017)*. Geneva, Switzerland: ISO.
17. Occupational Safety and Health Administration (OSHA). (2015). *Guidance on safe sling use*. Washington, DC: U.S. Department of Labor.

RiESTech
Recent in Engineering Science and Technology

MBI

Article

Green Corrosion Inhibition of API 5L Grade B Steel Using Myrmecodia Pendans and Piper Crocatum Extracts in 3.5% NaCl

Rani Kusumawardani [1], Agus Budiono [1], Johny W. Soedarsono [1], Yudha Pratesa [1,*]

[1] Department of Metallurgical and Materials Engineering, Universitas Indonesia, Depok 16424
* Correspondence: yudhapratesa@ui.ac.id

Abstract: Method to prevent the corrosion during pipeline hydrotest using seawater is generally by the addition of inorganic inhibitor containing corrosion inhibitor agent, oxygen scavenger and biocide, so that require to find out the alternative eco-friendly materials with better performance. The main objective of this study is to investigate the efficiency of the use of mixture of extract of *Myrmecodia pendans* and *Piper crocatum* as an alternative of eco-friendly inhibitor for reducing the use of inorganic inhibitors for corrosion protection of steel material API 5L Grade B in 3.5% NaCl. The corrosion inhibition ability of natural ingredient extraction are investigated by using tafel polarization test and EIS and verified by weight loss test. The content of the active compounds in natural ingredient extraction along with adsorption compound on metal surfaces and inhibition mechanism are investigated by EIS, FTIR and adsorption isotherm model. In the mixed green inhibitor concentration of 2 ml *Myrmecodia pendans* and 1 ml *Piper crocatum* is resulted in approximately 73.66% inhibitor efficiency while concentration of 1 ml chemical cocktail and 2 ml green inhibitor are significantly reduce the corrosion rate from 0.42 mm/year to be 0.03 mm/year with approximately 93.15% inhibitor efficiency. The green inhibitor affected the cathodic as well as the anodic polarization curves which were known as mixed corrosion inhibitor type. The adsorption of compounds contained in the *Myrmecodia pendans* and *Piper crocatum* on a metal surface are occur spontaneously follows the Langmuir adsorption isotherm. The findings of this study demonstrate that the use of a mixed green inhibitors delivers high corrosion protection efficiency and markedly decreases dependence on synthetic inhibitors.

Keywords: Green Corrosion Inhibitor; Mixed Inhibitor; *Myrmecodia pendans*; *Piper crocatum*; Polarization

Citation: Kusumawardani, R., Budiono, A., Soedarsono, J. W., Pratesa, Y. (2025). Green Corrosion Inhibition of API 5L Grade B Steel Using Myrmecodia Pendans and Piper Crocatum Extracts in 3.5% NaCl. Recent in Engineering Science and Technology 3(03), 25–39. Retrieved from https://www.mbi-journals.com/index.php/riestech/article/view/112

Academic Editor: Noor Hidayati

Received: 24 May 2025
Accepted: 12 June 2025
Published: 31 July 2025

Publisher's Note: MBI stays neutral with regard to jurisdictional claims in published maps and institutional affiliations.

1. Introduction

Oil and gas industry faces many corrosion problems at various stages, including exploration of oil wells, transport fluid from the well or the processing, storage and refinery operations in the onshore and offshore[1]. In oil and gas pipelines system, initial corrosion can be triggered by seawater during pre-commissioning and hydrotest where the seawater are used for pressure testing. In addition to the corrosion due to the environment with salt (NaCl) and dissolved oxygen, anaerobic conditions (without oxygen) can trigger the activation of the types of bacteria such as Sulphate Reducing Bacteria (SRB) which can initiate other corrosion processes i.e Microbial Induced Corrosion (MIC) that is local corrosion with a relatively high corrosion rate[2]. Among the various methods to avoid or prevent damage or degradation of the metal surface,

corrosion inhibitor is one of the best methods for corrosion protection and one of the most useful in oil and gas industry[3]. Currently, this method are still survive caused low cost and practical method[3,4]. Treated seawater with anorganik inhibitor commonly used during pre-commisioning process of subsea pipelines which chemical inhibitor basically are toxic and difficult to decompose by environmental so that it is essential to develop alternative corrosion inhibitors as known as green inhibitor which are environmentally acceptable, economical and renewable[6]. Several study of green corrosion inhibitor development based on natural product such us *Myrmecodia pendans*[6][7][8], Green tea and *Piper Betle*[9], Purple Sweet Potato[10], *Pluchea indica* (L.)[11], and other natural plants.

Most studies focus on using a single natural product as a corrosion inhibitor to control corrosion [6][10][11]. However, this approach may not achieve the expected technical and economic efficiency. Using a mixture of natural products can be an alternative to improve the efficiency of green inhibitors through synergistic effects [12][13]. Additionally, combining natural and chemical products can reduce the use of chemical inhibitors [15]. In general, the protection mechanism is ions or molecules adsorption on the surface of the metal which can create barriers inhibitor (film forming) to inhibit the electrochemical reactions (anodic and cathodic) so as to inhibit the corrosion process[16].

Myrmecodia pendans contains several antioxidant compounds such as saponins, tannins, Phenolic, flavonoids, alkaloids, Triterpenoid, steroids and glycosides[17] which phenolic compounds be regarded as a powerful antioxidant for their ability to donate hydrogen or electrons and form the basis of stable transition[15]. The chemical structure of the main antioxidant phenolic constituents in the myrmecodia pendans is shown in Fig. 1. In the process of corrosion inhibition, flavonoid compounds able to inhibit with the ability of flavonoids to be heterocyclic compounds[11]. In *Piper crocatum* plants, showed positive results contain phenolic compounds, flavonoids, terpenoids and steroid compounds[18]. In betel leaf essential oil contains a variety of bioactive phenolic compounds present in significant quantities and have to antimicrobial properties[19]. Cytotoxic chemical structure of the terpenoids and steroids constituents in Piper crocatum is shown in Fig. 2. In general, inhibitor derived from the extract of organic compounds will work to inhibit corrosion by forming a hydrophobic layer on the metal surface[20]. Hydrophobic layer formed by adsorption of molecules contained in the inhibitor with antioxidant compounds. Antioxidant compounds contained in the *Myrmecodia pendans* and *Piper crocatum* are predicted to inhibit the corrosion process and metal surface with adsorption mechanism that will form the inhibition layer. In other research that uses Pyridine-based inhibitors in CO_2 environments showed R_{ct} increases (up to 1760 $\Omega \cdot cm^2$) and C_{dl} reductions, attributed to N-heteroatom adsorption, indicating a thicker protective layer[21].

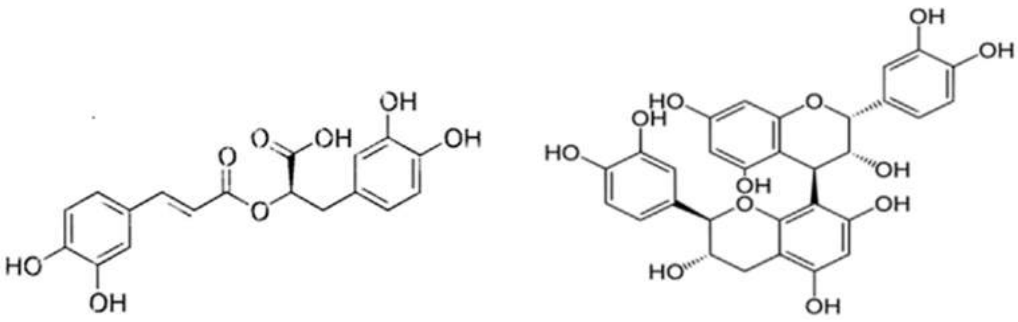

(**a**) (**b**)

Figure 1. The chemical structure of the main antioxidant phenolic constituents of *Myrmecodia pendan*s (a) rosmarinic acid and (b) procyanidin B1[18]

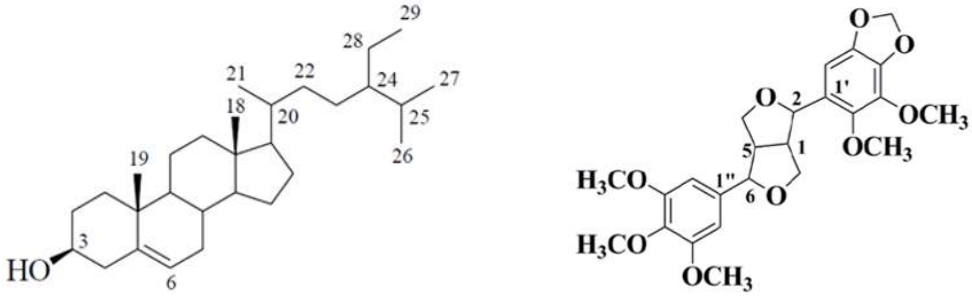

(**a**) (**b**)

Figure 2. Cytotoxic chemical structure of the terpenoids and steroids constituents of *Piper crocatum* (a) β-sitosterol dan (b). 2-(5′,6′-dimethoxy-3′,4′-methylene dioxyphenyl)-6-(3″,4″,5″-trimethoxyphenyl)-3,7-dioxabicyclo[3,3,0] octane[22]

2. Materials and Experiment Methods

2.1. Sample Preparation

The specimen used was carbon steel API 5L Grade B standard taken from part of offshore topside piping wellhead platform. The size of 15 mm x 15 mm x 6.4 mm specimen was formed from 152,4 mm diameter steel pipe with ±30 mm length and 40 schedule pipe thickness (± 7.1 mm thick) for mounting of linear polarization and EIS tests while size of 30 mm x 20 mm x 6.4 mm are used for weight loss test. The sample surface is polished with 1000 grit silicon carbide paper to get a smooth surface and flat. The chemical composition of carbon steel material samples are presented in Table 1.

Table 1. The chemical composition of API 5L Gr. B carbon steel material samples

	C (%)	**Si (%)**	**S (%)**	**P (%)**	**Mn (%)**	**Cr (%)**	**Mo (%)**
API 5L Grade B	0.203	0.352	0.005	0.016	0.887	0.124	0.026
	Ni (%)	**Ti (%)**	**Cu (%)**	**Nb (%)**	**V (%)**	**Al (%)**	**Fe (%)**
	0.104	0.003	0.165	≤0.002	≤0.002	0.042	Balance

The laboratory tests were conducted to determine and investigate the corrosion behavior of carbon steel material API 5L Grade B samples that immersed in 3.5 % NaCl solution. Laboratory testing was performed without and with the addition of green inhibitors and the use of single and mixed inhibitor with a chemical inhibitor mixture at room temperature and atmospheric pressure.

2.2. Fourier Transform Infrared (FTIR)

Fourier transform infrared (FTIR) test was performed to characterize the functional groups of active compounds from green inhibitor extracts. Linear polarization test was carried out to obtain the corrosion potential and current density data as the basis to calculate the effectiveness of natural ingredients extract as an green inhibitor and verified by weight loss test. While the mechanism of inhibition was investigated by electrochemical impedance spectroscopy (EIS) testing and calculation of the adsorption isotherm models. The flow diagram of the overall experiment process from preparation until conclusion and reporting are as shown in Fig. 3.

2.3. Inhibitor Extract

Based on Pradityana study[6], the most effective of *Myrmecodia pendans* inhibitors are at 500 ppm concentration so that in this study, the similar concentration was adopted. The results of extract natural inhibitor will be diluted with 1:10 ratio to facilitate mixing[23]. Mixed and single extract natural inhibitor will be added into 3.5% NaCl solution as green inhibitor at 200 ml volume with 1.5% v/v concentration therefore obtained 1.5ml/1000ml (1500 ppmv) concentration with assumption that 1.5 ml will produce 0.5 grams of dry weight inhibitor which is equivalent to 0.5gr/1000ml (500 ppmw).

2.4. Corrosion Test

Linier polarization testing is carried using three electrode circuit (conventional three-electrode cell assembly) that is graphite as the counter electrode (CE), Ag/AgCl as reference electrode, and samples of carbon steel API 5L Grade B as working electrode in 3.5% NaCl solution. The 200 ml cell system equipped with copper cables mounting on carbon steel sample as working electrode. Polarization tests are carried out on cathodic potential range of -0.3 mV to the anodic potential of +0.2 mV (vs Ag/AgCl) with potential corrosion in the scan rate of 0.1 mV/s. Measurements were performed for single or mixed green inhibitor as well as mixed with a chemical inhibitor cocktail type.

The mechanism of corrosion occurred on the sample steel material API 5L Grade B are investigated by electrochemical impedance spectroscopy (EIS) testing. A basic method of EIS testing are based on response of the circuit to the AC voltage as a function of frequency. Electrochemical impedance measurements is performed on potensiostatic condition using the same potentiostat instrument for linier polarization testing. Sinusoidal wave voltage (AC) with the low amplitude of 10 mV is superimposed on the open circuit corrosion stable potential. Value of real impedance (Z ') and the imaginary impedance (Z'')

are measured at various frequencies in the range of 10 MHz to 0.1 Hz. Nyquist plot of the real impedance (Z') value and the imaginary impedance (Z'') value will be generated from EIS testing.

Weight loss testing was conducted to verify the linear polarization and eis testing. Duration of immersion was conducted for 32 days and 10 hours with adjustments to the actual conditions in the field as a subsea pipeline hydrotest fluid. Samples for weight loss testing were made with a hole for a tying rope with a diameter of 3 mm. After immersion the samples was weighed and the average weight loss value was calculated.

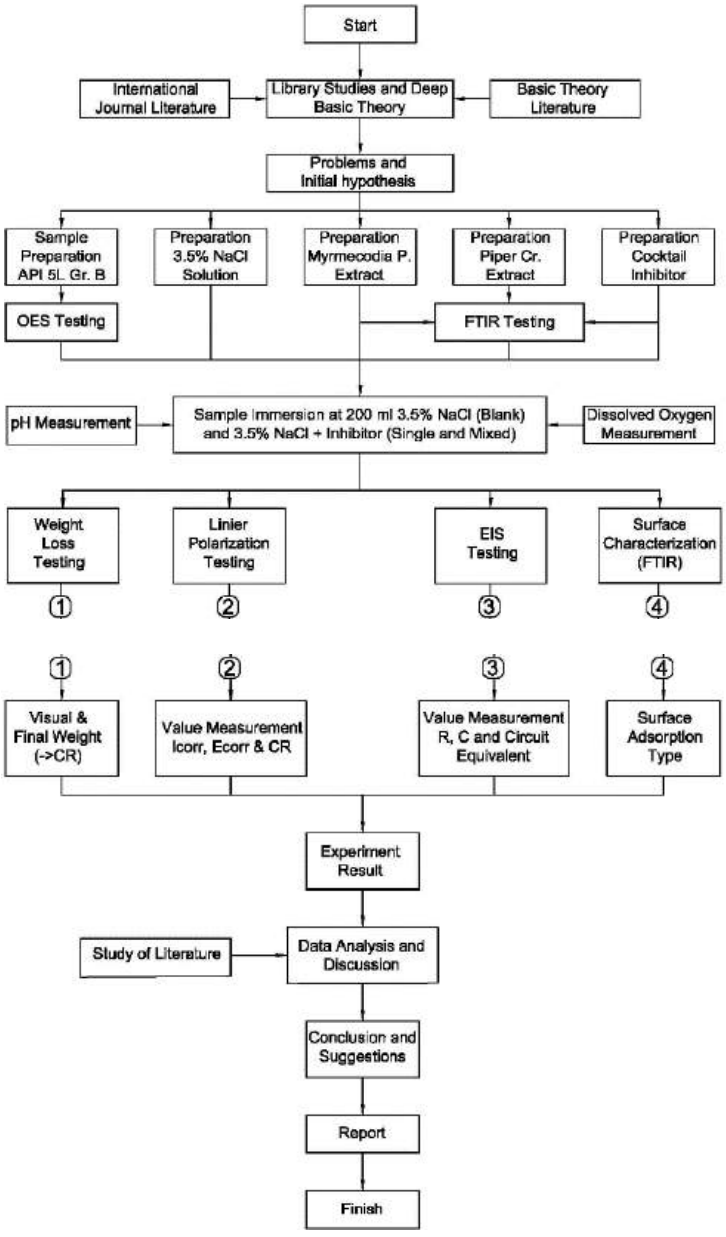

Figure 3. Experimental flow diagram

3. Results and Discussion

3.1. Inhibitor Solution

3.1.1. Fourier Transform Infrared (FTIR)

From the pH measurement results on 3.5% NaCl solution can be observed that the use of green inhibitor would increase the level of acidity with pH values decreased. Refer to pourbaix diagram on iron can be observed that the acidity reduction of the environment will shift the stability curve towards corrosive region (uniform corrosion) which will increase the possibility of corrosion[24], however this behaviour can be compensated by inhibitor effects from green inhibitor extracts with increase polarization resistance on steel surfaces and reduce the corrosion rate as shown in Fig.5-7 and Table 2.

Refer to interpretation result of FTIR testing for green inhibitor and carbon steel samples on a 3.5% solution, there are identified some top of wavenumber which showing the absorption spectrum of functional groups that detected adsorbed on the metal surface where peak wavenumbers are identified similar between two types of this natural inhibitor as well as functional group of chemical inhibitor cocktail as shown in Fig.4. *Myrmecodia pendans* and *Piper crocatum* extracts contain phenolic-type hydroxyl groups[17] that are able to form hydrogen bonds with water (O-H stretch) which helps the adsorption process on metal surfaces. In *Piper crocatum* extract, there are oily alkene hydrocarbon groups (nonpolar) so that the solubility of red betel in a 3.5% NaCl solution is lower than that of *Myrmecodia pendans* so that it has a repellent (hydrophobic) property on metal surfaces with C-H stretch groups. Nonpolar alkene groups (e.g., C=C and C-H stretches) form a hydrophobic layer on metal surfaces, limiting direct contact with water and chloride ions[25][26]. These two characteristics synergize in the process of inhibiting metal surfaces by forming a protective layer/film forming (barrier). This barrier inhibits electrochemical corrosion by repelling polar electrolytes like NaCl[27]. This aligns with studies on plant extracts like *Azadirachta indica* and *Psidium guajava*, where similar functional groups improved inhibition efficiency[28].

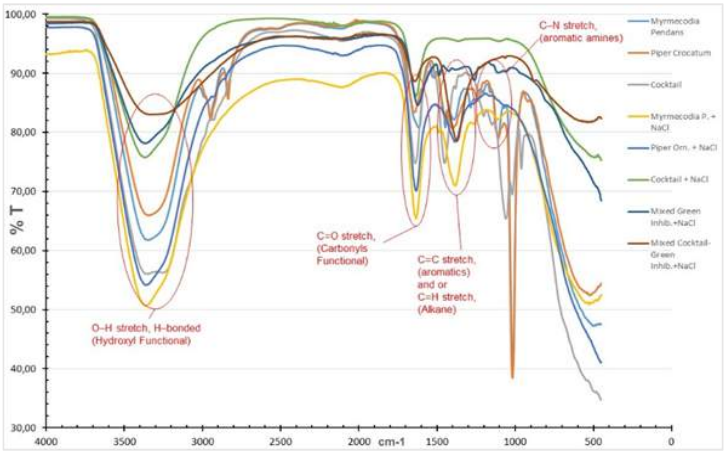

Figure 4. Graph of FTIR result for all variation inhibitor (Extract Inhbitor + Sample and Mixed Inhibitor + Sample)

3.2. Corrosion Test

3.2.1. Potentyodinamic Polarization (PDP)

From the linier polarization result in 3.5% NaCl solution without addition of inhibitor and with addition of a chemical inhibitor and natural extracts will obtain polarization curve as shown in Fig. 5, while the addition of mixed inhibitor of *Myrmecodia pendans* and *Piper crocatum* on some variation of mixing ratio will obtain polarization curve as shown in Fig. 6. In addition of cocktail inhibitor and green inhibitor on some variation of mixing ratio will obtain polarization curve as shown in Fig. 7. The electrochemical parameters of the linier polarization test such as the corrosion current density (i_{corr}), corrosion potential (E_{corr}), Tafel slope (β_a & β_c), and the corrosion rate (CR) based on post processing results of Fig. 5-7 are as shown in Table 2.

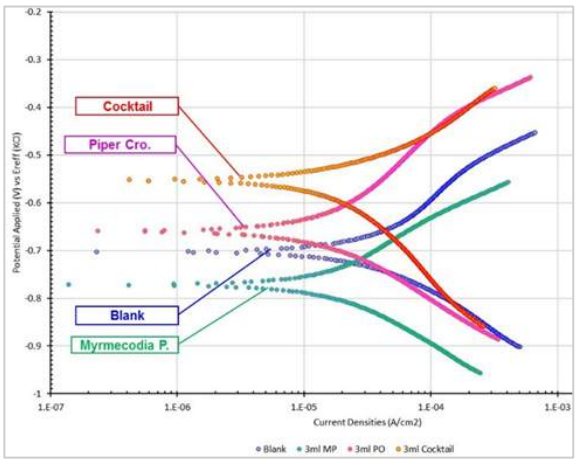

Figure 5. Polarization curve for 3.5% NaCl solution without inhibitor and with pure cocktail inhibitor and green inhibitor

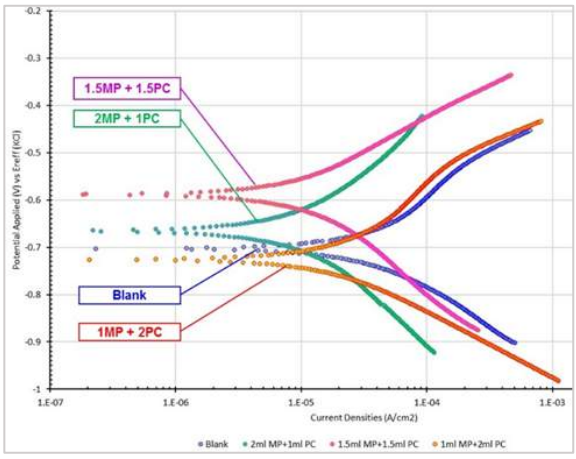

Figure 6. Polarization curve for 3.5% NaCl solution with mixed inhibitor *Myrmecodia pendans* and *Piper crocatum* at various mixed ratio

The results of polarization measurements as shown in Fig. 5-7 and Table 2 indicate that there was an effect of inhibition by natural inhibitors *Myrmecodia pendans* and *Piper*

crocatum as well as cocktails inhibitor along with the mixture on low carbon steel corrosion in 3.5% NaCl environmental. The reduction of corrosion rate is characterized by impairment of current densities from 36.13 μA.cm^{-2} (CR = 0.42 mm/year) to the value of 13.59 μA.cm^{-2} (CR = 0.16 mm/year) with addition of *Myrmecodia P.* inhibitor. The current densities to be 9.52 μA.cm^{-2} (CR = 0.11 mm/year) in addition of mixed green inhibitor and 2.47 μA.cm^{-2} (CR = 0.03 mm/year) in the addition of mixed green inhibitor and a cocktail inhibitor. The maximum efficiency of 93.15% is achieved by mixed cocktail and green inhibitor with mixing ratio of 1 ml cocktail and 2 ml of green inhibitor. It is characterized by increasing polarization resistance from Rp = 578.65 Ω in the blanks without inhibitor to R_p = 5535.20 Ω on mixed green and chocktail inhibitor. Both anodic (βa) and cathodic (βc) Tafel slopes shifted, confirming mixed inhibition type. For example, βa increased from 173.86 mV/dec (blank) to 243.86 mV/dec with mixed inhibitors[29]. Efficiency and increased polarization resistance can be affected by compounds of both natural materials extracts and cocktail inhibitor were approximately equal to so that complementarity each other as shown by functional groups of FTIR results in Fig. 3.

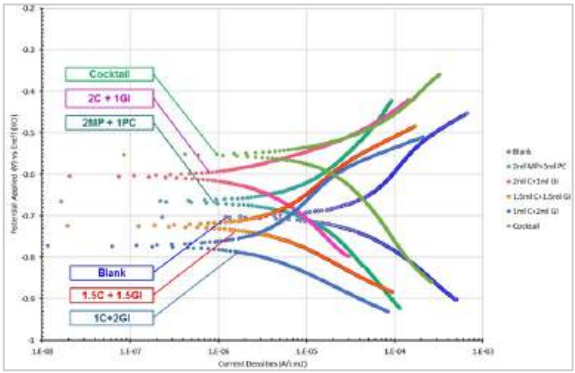

Figure 7. Polarization curve for 3.5% NaCl solution with mixed cocktail inhibitor and green inhibitor (*Myrmecodia pendans* and *Piper crocatum*) at various mixed ratio.

Table 2. The electrochemical parameters of the linier polarization on 3.5% NaCl solution with addition of inhibitor and mixed at various mixing ratio

No	Inhibitor Type and Concentration (%v/v)	E_{corr} (mV)	I_{corr} (μA.cm^{-2})	Rp (Ω)	β_a (mV.dec^{-1})	β_b (mV.dec^{-1})	C_R (mm/year)	Efficiency η (%)
Group 1- Without Inhibitor and With Pure Chemical and Green Inhibitor								
1	3.5% NaCl (Blank)	-702.75	36.13	578.65	173.86	244.98	0.42	0
2	3 ml MP	-769.35	13.59	1149.00	161.12	143.02	0.16	62.39
3	3 ml PC	-665.01	15.09	1880.30	167.43	156.12	0.18	58.24
4	3 ml Cocktail	-559.03	15.54	1080.80	128.03	225.62	0.18	57.00

Group 2 – Mixed Inhibitor Between *Myrmecodia pendans* and *Piper crocatum* at Various Ratio								
1	2 ml MP + 1 ml PC	-659.68	9.52	2501.80	243.86	220.46	0.11	73.66
2	1.5 ml MP + 1.5 ml PC	-569.35	10.34	2440.20	234.33	146.32	0.12	71.37
3	1 ml MP + 2 ml PC	-724.76	13.08	1412.00	129.55	150.12	0.16	63.80
Group 3 – Mixed Inhibitor Between Cocktail and Green Inhibitor at Various Ratio								
1	2 ml C + 1 ml GI	-629.63	4.11	3960.00	131.40	198.63	0.05	88.64
2	1.5 ml C + 1.5 ml GI	-725.04	3.48	4162.50	114.76	167.74	0.04	90.38
3	1 ml C + 2 ml GI	-776.03	2.47	5535.20	185.11	102.03	0.03	93.15

3.2.2. Electrochemical Impedance Spectroscopy (EIS)

Electrochemical impedance spectroscopy (EIS) testing was conducted to identify the mechanism of inhibition on Sodium chloride corrosion (sea water corrosion) and surface phenomena that occur at the interface metal / electrolyte due to the effect of inhbitor addition. The EIS test results are displayed in the Nyquist plots on 3.5% NaCl solution without inhibitor addition and with addition of a pure chemical and natural extracts inhibitor as shown in Fig. 8 while the addition of mixed inhibitor of *Myrmecodia pendans* and *Piper crocatum*. Extract on various mixing ratio will generate Nyquist plot as shown in Fig. 9. In addition of mixed cocktail inhibitor and green inhibitor on various mixing ratio will generate Nyquist plot as shown in Fig.10.

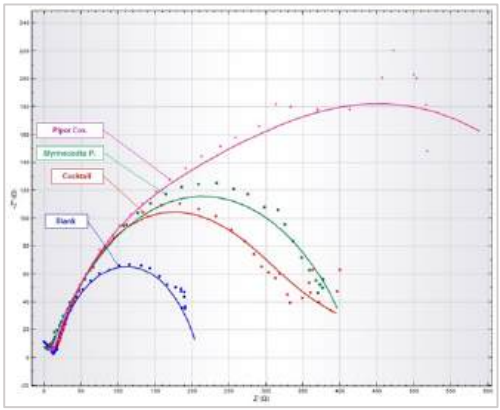

Figure 8. Nyquist plot of 3.5% NaCl solution without inhibitor and with pure cocktail inhibitor and green inhibitor

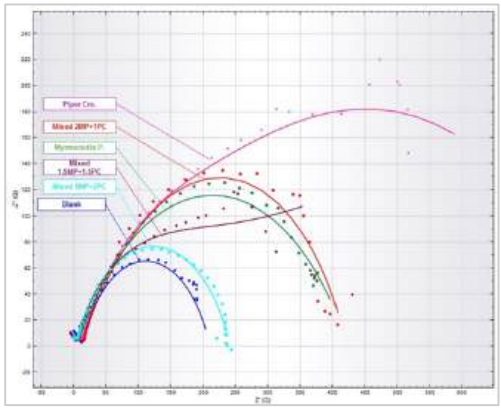

Figure 9. Nyquist plot of 3.5% NaCl solution with mixed inhibitor *Myrmecodia pendans* and *Piper crocatum* on various mixing ratio

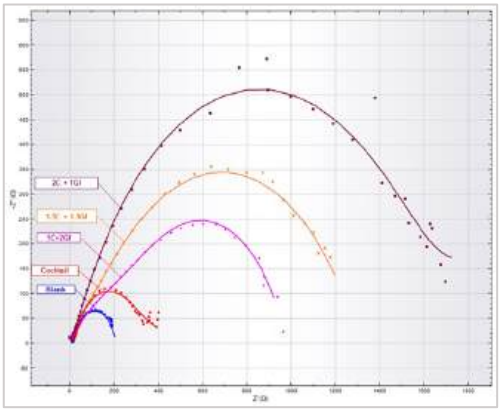

Figure 10. Nyquist plot of 3.5% NaCl solution with mixed cocktail inhibitor dan green inhibitor (*Myrmecodia pendans and Piper crocatum*) on various mixing ratio

Table 3. Parameters of EIS on 3.5% NaCl solution without and with addition of inhibitor on various mixing ratio

No	Inhibitor Type and Concentration (%v/v)	R_{ct} ($\Omega.cm^2$)	C_{dl} ($\mu.Fcm^{-2}$)	Efficiency η (%)
Group 1- Without Inhibitor and With Pure Chemical and Green Inhibitor				
1	3.5% NaCl (Blank)	200.95	2498.50	-
2	3 ml MP	427.25	848.91	52.97
3	3 ml PC	775.23	2777.10	74.08
4	3 ml Cocktail	333.43	221.80	39.73
Group 2 – Mixed Inhibitor Between *Myrmecodia pendans* and *Piper crocatum* at Various Mixing Ratio				
1	2 ml MP + 1 ml PC (Mixed GI #1)	422.05	913.68	52.39
2	1.5 ml MP + 1.5 ml PC (Mixed GI #2)	317.9	923.99	36.79
3	1 ml MP + 2 ml PC (Mixed GI #3)	239.00	430.75	15.92
Group 3 – Mixed Inhibitor Between Cocktail and Green Inhibitor at Various Mixing Ratio				
1	2 ml C + 1 ml GI (Mixed #1)	1760.10	74.00	88.58
2	1.5 ml C + 1.5 ml G1 (Mixed #2)	1149.40	885.84	82.52
3	1 ml C + 2 ml GI (Mixed #3)	1543.00	731.50	86.98

The parameters of impedance and polarization resistance (R_{ct}), double layer capacitance (C_{dl}) and inhibition efficiency (EI%) results from EIS testing without addition of inhibitor and with addition of inhibitors can be given as shown in Table 3. EIS measurements as shown in Fig. 8-10 and Table 3 shows that with addition of inhibitor, the overall impedance have experienced a significant improvement that can be attributed to Warburg impedance however capacitive impedance due to control mechanism of charge transfer can be attributed to the overall impedance. C_{dl} decreased from 2498.5 $\mu F/cm^2$ (blank) to 731.5 $\mu F/cm^2$, suggesting a thicker protective layer[30]. From the measurement

data results, the corrosion rate and efficiency shown better results with the use of mixed inhibitor. The corrosion rate is significantly decreased and efficiency is increased in the use of mixed inhibitors between green inhibitor and cocktail inhibitor.

3.2.3. Weight Loss

The laboratory test have been verified by weight loss test as shown in Table 4. After 32 days, the corrosion rate decreased from 0.2676 mm/year (blank) to 0.0661 mm/year (75.3% efficiency) with mixed inhibitors. Weight loss results correlated with EIS and polarization, confirming inhibitor stability over time. The same result with palm oil leaves extract achieved 83.7% efficiency in NaCl via weight loss[31]. From the experiment result, a mixture of extract of *Myrmecodia pendans* and *Piper crocatum* are effective for use as an alternative environment friendly corrosion inhibitor for corrosion protection of API 5L steel material in NaCl environment.

Table 4. Data and analysis of weight loss test result for 778 hours (32 days 10 hours)

No	Description of Sample	Surface Area (cm^2)	Weight Before Immersion (gram)	Weight After Immersion (gram)	C_R (mm/year)	Efficiency η (%)
Group 1- Without Inhibitor and With Pure Chemical and Green Inhibitor						
1	3.5% NaCl (Blank)	16.9462	26.5424	26.2258	0.2676	-
2	3 ml MP	16.6641	26.1157	26.0258	0.0773	71.12
3	3 ml PC	14.1838	20.8232	20.7558	0.0681	74.57
4	3 ml Cocktail	16.0851	22.5272	22.4615	0.0585	78.14
Group 2 – Mixed Inhibitor Between *Myrmecodia pendans* and *Piper crocatum* at Various Ratio						
1	2 ml MP + 1 ml PC	13.0446	18.3399	18.2841	0.0613	77.10
2	1.5 ml MP + 1.5 ml PC	14.7224	22.6386	22.5736	0.0632	76.37
3	1 ml MP + 2 ml PC	13.9873	20.4600	20.3930	0.0686	74.36
Group 3 – Mixed Inhibitor Between Cocktail and Green Inhibitor at Various Mixing Ratio						
1	2 ml C + 1 ml GI	17.5872	27.3906	27.2855	0.0856	68.01
2	1.5 ml C + 1.5 ml GI	14.3430	21.1877	21.1096	0.0780	70.85
3	1 ml C + 2 ml GI	15.5796	23.3890	23.3171	0.0661	75.30

3.3. Adsorption Isotherm

In Table 5 shows the calculation of adsorption isotherm model Langmuir and four adsorption isotherm models of Temkin, Frumkin, Bockris-Swinkels, and virial Parson[29]. The modeling of adsorption isotherm mode Langmuir are generate the greatest average value of correlation coefficient (degree of conformity), with a value ≥ 0.95. Langmuir isotherm models is assume that organic molecules adsorbed as a monolayer on a metal surface without any interaction with other organic molecules adsorbed[32] and the organic molecules adsorbed on only one site[33]. The same result with Chitosan-Schiff base inhibitors followed Langmuir adsorption ($R^2 = 0.99$) on steel in NaCl[34]. Therefore, the inhibitor molecule from mixed inhibitor of chemical and natural inhibitor of *Myrmecodia pendans* and *Piper crocatum* can be predicted to adsorption on metal surfaces by forming a single inhibition layer (monolayer).

Table 5. Correlation coefficient value (R^2) for the fifth adsorption isotherm mode

No	Inhibitor Type and Concentration (%v/v)	Degree of Conformity Value, Correlation Coefficient (R^2)				
		Langmuir Isoterm	Temkin Isoterm	Frumkin Isoterm	Bockris-Swinkels Isoterm	Virial Parson Isoterm
1	Mixed Green Inhibitor	0.9899	0.7523	0.9111	0.9111	0.7523
2	Mixture of Green Inhibitor and Chemical Coctail Inhibitor	0.9748	0.3227	0.8521	0.5387	0.3227
Average Value (R^2)		0.9824	0.5375	0.8816	0.7249	0.5375

4. Conclusions

In this study, mixture of *Myrmecodia pendans* and *Piper crocatum* as green inhibitor on chemical cocktails inhibitor has been aligns with the study objective's by confirming that the green inhibitor is effevtice as a corrosion inhibitor. Analysis of the findings of several tests resulted in the following conclusions:

1. Functional groups of phenolic and flavonoid compounds are dominate the composition of *Myrmecodia pendans* and phenolic compounds in *Piper crocatum* extract as an antioxidant compounds that contribute to inhibit corrosion of the carbon steel material.
2. Corrosion inhibitor from a mixture of *Myrmecodia pendans* and *Piper crocatum* extract are works as mixed corrosion inhibitor type which reduce the cathodic and anodic current density in the 3.5% NaCl environment. This mixed corrosion inhibitors can

reduce the corrosion rate of 0.42 mm/year to 0.03 mm/year with an efficiency of 93.15% based on linear polarization testing and 86.98% based on EIS testing.

3. Addition of corrosion inhibitor will be physically adsorbed on the metal surface following Langmuir isotherm mode. The formation of inhibition layer on the metal surface will be dominant to control the transfer charge or diffusion so that it will inhibit the corrosion process which be affected by the mixing ratio.

Addition of green inhibitor on chemical inhibitor of cocktail type will increase the efficiency of corrosion protection of steel materials based on test measurement which it is significantly increase the efficiency of a pure chemical inhibitors with added green inhibitor.

References

1. D.A. Jones, N.D. Greene, Electrochemical Measurement of Low Corrosion Rates, Corrosion. 22 (1966) 198–205. https://doi.org/10.5006/0010-9312-22.7.198.
2. J.S. Lee, R.I. Ray, B.J. Little, E.J. Lemieux, Evaluation of deoxygenation as a corrosion control measure for ballast tanks, Corrosion. 61 (2005) 1173–1188. https://doi.org/10.5006/1.3278153.
3. R. Riastuti, G. Mashanafie, V. Rizkia, A. Maksum, S. Prifiharni, A. Kaban, G. Priyotomo, J. Soedarsono, Effect Of Syzygium Cumini Leaf Extract As A Green Corrosion Inhibitor On Api 5l Carbon Steel In 1M HCl, Eastern-European J. Enterp. Technol. 6 (2022) 30–41. https://doi.org/10.15587/1729-4061.2022.267232.
4. A. Groysman, Anti - Corrosion Management , Environment and Quality at the Oil Refining Industry, (n.d.) 1–18.
5. R.W. Revie, Uhlig's Corrosion Handbook Third Edition, Copyright © 2011 John Wiley & Sons, Inc., 2011. https://doi.org/10.1002/9780470872864.
6. A. Pradityana, S. Sulistijono, A. Shahab, Effectiveness of Myrmecodia Pendans extract as eco-friendly corrosion inhibitor for material API 5L grade B in 3,5% NaCl solution, Adv. Mater. Res. 789 (2013) 484–491. https://doi.org/10.4028/www.scientific.net/AMR.789.484.
7. A. Pradityana, Sulistijono, D.A. Shahab, Application of myrmecodia pendans extract as a green corrosion inhibitor for mild steel in 3.5% NaCl solution, Appl. Mech. Mater. 493 (2014) 684–690. https://doi.org/10.4028/www.scientific.net/AMM.493.684.
8. A. Pradityana, S. Sulistijono, A. Shahab, The Influence of Adding Bio Inhibitor Sarang Semut *(Myrmecodia pendans)* to Carbon Steel API 5L Grade B in Solution of HCl 1 M, Adv. Mater. Res. 1123 (2015) 187–191. https://doi.org/10.4028/www.scientific.net/amr.1123.187.
9. A. Rustandi, J.W. Soedarsono, B. Suharno, The use of mixture of piper betle and green tea as a green corrosion inhibitor for API X-52 steel in aerated 3.5 % NaCl solution at various rotation rates, Adv. Mater. Res. 383–390 (2012) 5418–5425. https://doi.org/10.4028/www.scientific.net/AMR.383-390.5418.
10. Ayende, A. Rustandi, J.W. Soedarsono, D. Priadi, Sulistijono, D.N. Suprapta, G. Priyotomo, R. Bakri, Effects of Purple Sweet Potato Extract Addition in Ascorbic Acid Inhibitor to Corrosion Rate of API 5L Steel in 3.5%NaCl Environment, Appl. Mech. Mater. 709 (2014) 384–389. https://doi.org/10.4028/www.scientific.net/amm.709.384.

11. R.I. Pramana, R. Kusumastuti, J.W. Soedarsono, A. Rustandi, Corrosion inhibition of low carbon steel by Pluchea indica less in 3.5% NaCL solution, Adv. Mater. Res. 785–786 (2013) 20–24. https://doi.org/10.4028/www.scientific.net/AMR.785-786.20.
12. F. Valensky, Efek Sinergistik Dari Triazine Dan Kalium Iodida Pada Inhibitor Korosi Baja Karbon Dalam Larutan 0,5M HCl, (2014).
13. X. Li, S. Deng, H. Fu, X. Xie, Synergistic inhibition effects of bamboo leaf extract/major components and iodide ion on the corrosion of steel in H3PO4 solution, Corros. Sci. 78 (2014) 29–42. https://doi.org/10.1016/j.corsci.2013.08.025.
14. U.M. Eduok, S.A. Umoren, A.P. Udoh, Synergistic inhibition effects between leaves and stem extracts of Sida acuta and iodide ion for mild steel corrosion in 1M H 2SO 4 solutions, Arab. J. Chem. 5 (2012) 325–337. https://doi.org/10.1016/j.arabjc.2010.09.006.
15. A.M. Engida, N.S. Kasim, Y.A. Tsigie, S. Ismadji, L.H. Huynh, Y.H. Ju, Extraction, identification and quantitative HPLC analysis of flavonoids from sarang semut (Myrmecodia pendan), Ind. Crops Prod. 41 (2013) 392–396. https://doi.org/10.1016/j.indcrop.2012.04.043.
16. A.Y. Musa, A.A.H. Kadhum, A.B. Muhamad, Corrosion inhibitor film forming in aerated and deaerated solutions, Int. J. Electrochem. Sci. 5 (2010) 1911–1921. https://doi.org/10.1016/s1452-3981(23)15394-6.
17. J. Sudiono, C. Oka, P. Trisfilha, The Scientific Base of Myrmecodia pendans as Herbal Remedies, Br. J. Med. Med. Res. 8 (2015) 230–237. https://doi.org/10.9734/bjmmr/2015/17465.
18. Emrizal, A. Fernando, R. Yuliandari, K. Rullah, N.R. Indrayani, A. Susanty, R. Yerti, F. Ahmad, H.M. Sirat, D. Arbain, Cytotoxic Activities of Fractions and Two Isolated Compounds from Sirih Merah (Indonesian red betel), Piper Crocatum Ruiz & Pav., Procedia Chem. 13 (2014) 79–84. https://doi.org/10.1016/j.proche.2014.12.009.
19. S. Basak, P. Guha, Modelling the effect of essential oil of betel leaf (Piper betle L.) on germination, growth, and apparent lag time of Penicillium expansum on semi-synthetic media, Int. J. Food Microbiol. 215 (2015) 171–178. https://doi.org/10.1016/j.ijfoodmicro.2015.09.019.
20. A.P. Popoola, A.O. Alao, O. Sanni, Sustainable and Green Approach for Api 5L Pipeline Steel Acidic Corrosion Inhibition Using Agro-Industrial Waste: Experimental and Theoretical, Metals (Basel). 13 (2023). https://doi.org/10.3390/met13071155.
21. M.A. Yudistira, L. Mora, D. Friskila, Effect of Addition of Pyridine-Based Corrosion Inhibitors on Corrosion Behaviors of Carbon Steel in a Co 2 -Containing Environment, Test Eng. Manag. 83 (2020) 23315–23326.
22. A.M. Engida, S. Faika, B.T. Nguyen-Thi, Y.H. Ju, Analysis of major antioxidants from extracts of Myrmecodia pendans by UV/visible spectrophotometer, liquid chromatography/tandem mass spectrometry, and high-performance liquid chromatography/UV techniques, J. Food Drug Anal. 23 (2015) 303–309. https://doi.org/10.1016/j.jfda.2014.07.005.
23. T.N. Rohmannudin, S. Sulistijono, M. Adiyaksa, M.A.M. Chusururi, Study of Organic Substance (Myrmecodia pendans) Extraction Using Soxhletation Method as an Organic Inhibitor, IPTEK J. Proc. Ser. 0 (2018) 65. https://doi.org/10.12962/j23546026.y2018i4.3848.
24. M. Ash, I. Ash, Handbook of Corrosion inhibitors, 2000. https://linkinghub.elsevier.com/retrieve/pii/S0026057600834455.
25. S. Tarigan, I. Nababan, S. Sarli, Bioscientia Medicina : Journal of Biomedicine & Translational

Research Red Betel Leaf (Piper crocatum) Extract : A Potential Natural Alternative for Controlling Streptococcus mutans in the Oral Cavity, (n.d.) 7553–7565.

26. S. Bilgiç, Plant extracts as corrosion inhibitors against copper corrosion – An overview, Int. J. Corros. Scale Inhib. 12 (2023) 1224–1260. https://doi.org/10.17675/2305-6894-2023-12-3-24.
27. T. Siswina, M. Miranti Rustama, D. Sumiarsa, D. Kurnia, Phytochemical profiling of Piper crocatum and its antifungal activity as Lanosterol 14 alpha demethylase CYP51 inhibitor: a review, F1000Research. 11 (2022) 1–26. https://doi.org/10.12688/f1000research.125645.1.
28. M. Chigondo, F. Chigondo, Recent Natural Corrosion Inhibitors for Mild Steel: An Overview, J. Chem. 2016 (2016). https://doi.org/10.1155/2016/6208937.
29. R. Naghizade, G.S. Sajadi, A.K. Mashizi, Z. Golshani, M. Amiri, S.M.A. Hosseini, Investigation of mild steel corrosion inhibition in acidic media by Viola extract based on bulk and nanometer size, Sci. Rep. 14 (2024) 1–18. https://doi.org/10.1038/s41598-024-66434-x.
30. M. Pourmohseni, A. Rashidi, M. Karimkhani, Preparation of corrosion inhibitor from natural plant for mild stil immersed in an acidic environmental: experimental and theoretical study, Sci. Rep. 14 (2024) 1–15. https://doi.org/10.1038/s41598-024-58637-z.
31. N.I.H. Salleh, A. Abdullah, Corrosion inhibition of carbon steel using palm oil leaves extract, Indones. J. Chem. 19 (2019) 747–752. https://doi.org/10.22146/ijc.39707.
32. T. Jebakumar Immanuel Edison, M.G. Sethuraman, Electrochemical Investigation on Adsorption of Fluconazole at Mild Steel/HCl Acid Interface as Corrosion Inhibitor, ISRN Electrochem. 2013 (2013) 1–8. https://doi.org/10.1155/2013/256086.
33. M. Behpour, S.M. Ghoreishi, M. Khayatkashani, N. Soltani, Green approach to corrosion inhibition of mild steel in two acidic solutions by the extract of Punica granatum peel and main constituents, Mater. Chem. Phys. 131 (2012) 621–633. https://doi.org/10.1016/j.matchemphys.2011.10.027.
34. M.A. Ahmed, S. Amin, A.A. Mohamed, Current and emerging trends of inorganic, organic and eco-friendly corrosion inhibitors, RSC Adv. 14 (2024) 31877–31920. https://doi.org/10.1039/d4ra05662k.

RiESTech
Recent in Engineering Science and Technology

MBI

Article

The Remanufacturing of Track Rollers Requires The Application of A Hardfacing Technique, Which is Achieved by Combining Buttering with 309LMo Gas Metal Arc Welding (GMAW) and The TiC-O Flux-core Arc Welding (FCAW) Process.

Addin Aristotika [1,*], Winarto Winarto [1,*], Sabandi Ismadi [1], Eddy S. Siradj [1], Muhammad Anis [1]

[1] Department of Metallurgical and Materials Engineering, Universitas Indonesia, Depok 16424, Indonesia
* Correspondence: add.in412@gmail.com; winarto.msc@ui.ac.id

Abstract: The operation of the track rollers is dependent on the frictional forces between the rollers and the track. Furthermore, the presence of moisture-laden sand and mud in the surrounding environment accelerates the corrosion process, leading to a synergistic effect on abrasion wear. The production of new rollers is a highly energy-intensive process, resulting in the emission of significant quantities of carbon dioxide. The main objective of this research was to develop a process for remanufacturing track rollers by integrating hardfacing methods, specifically, combining buttering with gas-metal-arc welding (GMAW) that utilizes 309LMo and flux-core arc welding (FCAW) employing TiC-O. During the GMAW process, currents of 180 A, 220 A, and 260 A were applied at the same time as wire with a diameter of 1.2 mm, whereas the FCAW process involved using currents of 200 A, 250 A, and 300 A in conjunction with a wire with a diameter of 1.6 mm. An evaluation was conducted through mechanical tests and metallurgical analysis to determine the effect of the variable current on the physical and mechanical properties of the hardfill layer. Mechanical tests using the Rockwell method and metallurgical analysis via morphological observation were conducted to assess the performance of the remanufactured track roller. The outcomes revealed that as the current increase in GMAW/FCAW welding, the hardfacing layer became increasingly stiffer, but this effect was offset by the failure of the hardfacing interface to bond correctly, as shown by its insufficient fusion and the formation of cracks and holes that penetrated into the base metal. This study highlights the importance of welding parameters to achieve a balance between hardness in the base and weld metals, diffusion, and the quality of the bond between the two, as a practical and cost-efficient method for the remanufacturing industry.

Keywords: Remanufacturing; Track Rollers; Hardfacing; Buttering; 309LMo; GMAW; FCAW

Citation: Aristotika, A., Winarto, Ismadi, S., Siradj, E. S., Anis, M. (2025). The Remanufacturing of Track Rollers Requires The Application of A Hardfacing Technique, Which is Achieved by Combining Buttering with 309LMo Gas Metal Arc Welding (GMAW) and The TiC-O Flux-core Arc Welding (FCAW) Process. Recent in Engineering Science and Technology 3(03), 40–53. Retrieved from https://www.mbi-journals.com/index.php/riestech/article/view/117

Academic Editor: Noor Hidayati

Received: 10 June 2025
Accepted: 5 July 2025
Published: 31 July 2025

Publisher's Note: MBI stays neutral with regard to jurisdictional claims in published maps and institutional affiliations.

1. Introduction

The track rollers function by applying frictional forces between the roller and the track, thereby inducing wear and thinning of the component. In areas where bulldozers operate in the middle of wet sand and mud, the rollers are susceptible to corrosion. This, in turn, will result in a synergistic effect on abrasion wear. It has been demonstrated that this corrosion cannot be mitigated through the process of hardening the steel. Other surface treatments on the roller, such as carburizing and nitriding, or more conventional methods, are

not cost-effective and insufficient for highly wear-prone and corrosive environments encountered during roller use [1]. Substituting expensive materials like high-alloy steels or other cutting-edge materials is impractical because it significantly increases costs without a matching improvement in performance. Consequently, these materials cannot be considered efficient solutions. The disposal of worn rollers and subsequent manufacturing of new rollers require substantial investment in time and financial resources. The production of new rollers is a highly energy-intensive process, resulting in significant carbon dioxide emissions. As a result, the industry has widely adopted overlay welding or hardfacing techniques to extend the service life of worn components and reduce the wear of machine parts [2]. Plasma transfer arc welding, gas metal arc welding, gas tungsten arc welding, shielded metal arc welding, flux-core arc welding, and submerged arc welding are employed for hardfacing [3].

The primary goal of hardfacing is to reduce wear by applying a hard, abrasion-resistant coating to a component's surface via welding or a comparable process. Hard metal compounds, which combine carbide and metal, are used to increase the lifespan of machine components [4]. The accumulation of wear-resistant deposits on the metal surface increases the service life of the material. The hardfacing process involves the incorporation of metal–alloy powders into the material surface. The hardfaced metal parts become hard and exhibit increased wear resistance. The use of wear-resistant coatings requires the process of carburization to be carried out. On the other hand, previous studies have found that the oxidation of wear-resistant coatings during subsequent carburizing processes can have a negative impact on their ability to withstand wear [1]. Although the primary function of hardfacing is to restore worn components to a state of functionality, hardfacing is also employed in new-component pre-use applications. Hardfacing materials can extend their lifespan, providing additional benefits, such as increased operational efficiency, decreased need for replacement parts, and the use of less expensive base metals, ultimately resulting in moderate costs [3].

The welding process employed in this study was the FCAW method. Flux-core arc welding, or FCAW, is highly versatile and widely used due to its user-friendly nature, high current density, and ability to deposit significant amounts of weld metal by using multiple wires simultaneously. This is a significant benefit in the manufacturing sector, particularly because of the capacity to restore worn components [5]. FCAW has been identified as a particularly suitable process for overlay manufacturing because of its high productivity and deposition rate [2]. FCAW has been shown to be a superior method to other techniques due to its notable advantages, which include ease of controlling process variables, high-quality results, achieving deep penetration, yielding a smooth finish, accommodating thicker parts, and preventing contamination from the environment [6]. A significant advantage of the FCAW process is that once the initial operational phase has been completed, the operator skills required are substantially less complex than those required for manual processes. The employment of advanced technology in FCAW is the reason for the process's capacity for automatic operation, thereby enhancing its productivity.

The FCAW process has been found to produce carbides that significantly enhance the base metal's properties, such as mechanical strength, where a harder weld metal correlates with increased wear resistance, as well as corrosion and creep resistance [7].

The track roller that is the subject of this study is composed of a material known as SMnCrMoB435H. This material is classified as a medium-carbon steel, and it finds application as a tool steel. This material is produced through a continuous cooling process known as sinter hardening, which results in the formation of a bainitic microstructure within the steel. The presence of manganese and chromium (both of which have a high affinity for oxygen) and Mo will increase the hardenability of the steel. These elements have been shown to promote the formation of hard phases such as bainite and martensite [8]. The formation of both phases is also facilitated by the formation of borides. Furthermore, borides exhibit high hardness properties and good wear resistance [9]. Nickel is often replaced by manganese, which has proven to be up to four times more effective than nickel and also significantly more affordable, as noted by Sulowski in 2008 [10], thereby enhancing hardness.

This research aims to clarify the effects of hardfacing on PT X track roller components, specifically those arc-welded with flux-core technology, in terms of hardness distribution and their influence on previous problems in an effort to establish the key parameters required for achieving high-quality welding outcomes.

2. Materials and Experiment Methods

The specimen employed in this study was SMnCrMoB435H steel with dimensions of 220 millimeters in diameter and 50 millimeters in thickness. The welding process employed 309LMo stainless steel electrodes with a diameter of 1.2 mm for gas metal arc welding (GMAW) and the hardfaced TIC-O electrodes with a diameter of 1.6 mm for flux-core arc welding (FCAW). The samples were cleaned using a wire brush. The SMnCrMoB435H steel plate was welded using a combination of the GMAW and FCAW methods at constant voltage and speed. The variable currents used in both welding processes were 180/200 A, 220/250 A, and 260/300 A. These currents are referred to as samples A, B, and C, respectively.

Following the welding process, the samples were subjected to observation and evaluation procedures. Visual observation is required to ensure that the thickness of the hardfacing layer meets the minimum requirements for the track-rollers component. A scanning electron microscope (SEM) was used to perform sample observations to determine its microstructure. Energy-dispersive x-ray spectroscopy (EDS) was used for layer composition testing. Hardness testing is a type of mechanical test performed using the Vickers method with a load of 150 kg and a dwell time of 15 seconds.

3. Results and Discussion

3.1. Visual Observation

The thickness of the welding output was measured during the observation. Measurements were performed by determining the minimum and maximum thickness of each sample. The weld thickness was measured using a thickness gauge.

The findings of a welding thickness measurement study are detailed in Table 1 which contains the lists of the weld thicknesses at each variation in the welding current. The largest weld thickness (3.5 cm) was obtained for sample A. The maximum thickness of samples B and C was 3 cm. The maximum thickness of the three samples remained relatively consistent, primarily due to the welding current staying within the specified range outlined in the technical documentation for the welding wire. The minimum thickness of the hardfacing layer, as per the manufacturing requirements, must be 1.1 cm. According to visual observation, the resulting thickness fell within the range of 2.5 to 3.0 cm. The thickness complies with the manufacturing requirements. The excess thickness is intended to facilitate further manufacturing processes such as machining.

Table 1. The thickness measurement of the welding outcome.

Sample Code	Thickness (cm)	
	Min.	Max.
A	2.5	3.5
B	2.5	3
C	2.5	3

3.2. Scanning Electron Microscope (SEM) Analysis

A SEM analysis was performed to examine the bond interfaces (fusion lines) both between the hardfacing layer and the base metal and the phases produced during the welding process. As shown in Figure 1, sample A exhibits a clear and continuous transition between the hardfacing layer and the base material. There was no significant porosity or cracking, indicating good metallurgical bonding. The formation of elongated formations that penetrate the base material suggests sufficient diffusion and bonding. The microstructure exhibits good welding parameters with optimized interlocks and minimal mixing effects.

In sample A (Figure 1), the phase likely formed in the hardfacing layer is probably martensite, as evidenced by the needle-like and smooth morphology. This phase is formed by rapid cooling after the welding process. This finding aligns with the results of the EDS test conducted on sample A, which revealed the composition of the Fe-Cr-Ni-Mo hard coating. The possible phases of the base metals include pearlite and ferrite. Additionally, the presence of bainite or partial martensite at the interface is a possibility, owing to the heat effect of welding.

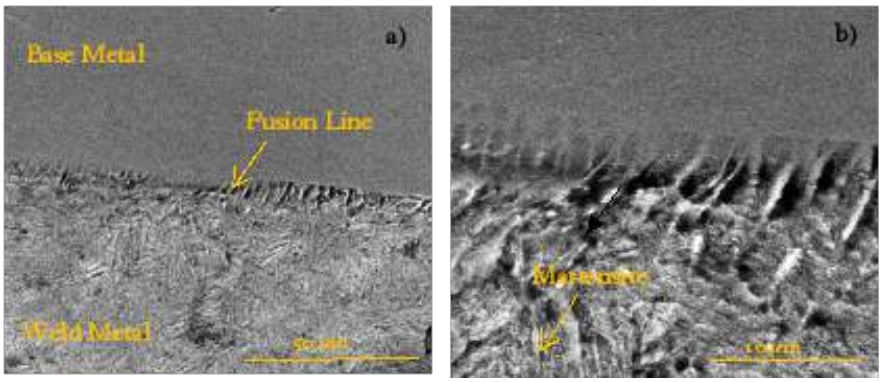

Figure 1. The interface bonding microstructure of sample A (180/200 A)

In sample B, as illustrated in figure 2, the interface layer exhibits substantial defects, including cracks and voids that extend into the base metal. The presence of these defects indicates a weakened interfacial bond (fusion line), which can result in premature failure under mechanical loading. The rough interface layer is a result of high heat input caused by the increased current, leading to excessive dilution of the welding wire, which in turn compromises the overall bond integrity[11].

As illustrated in Figure 2, the phase formed in the hardfacing layer of sample B is martensite, as evidenced by its needle-like and smooth morphology. This phase is quenched by rapid cooling after the welding process. The possible phases of the base metals include pearlite and ferrite. Additionally, the presence of bainite or partial martensite at the interface is a possibility, owing to the heat effect of welding.

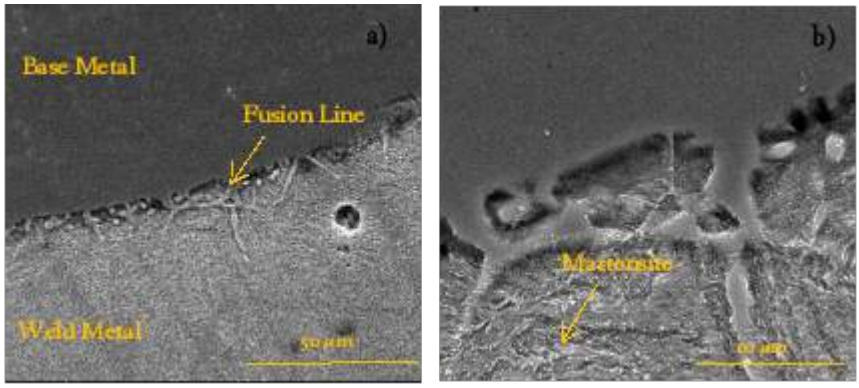

Figure 2. Interface bonding microstructure of sample B (220/250 A)

In sample C (Figure 3, the interfacial layer shows moderate bonding quality, with some areas showing interdiffusion but also visible cracks and porosity. The formation of irregular dendritic structures indicates that high heat input altered the integrity of the microstructure [12]. The presence of micro-cracks can be attributed to two factors: thermal expansion mismatch and the effect of over melting of the welding wire too quickly. Results from the Vickers test show that although the hardness distribution is still relatively high, potential performance degradation and long-term failure can arise from defects in the interface layer. Similar to samples A and B, sample C in Figure 3 also shows the formation of the martensite phase in the hardfacing layer. With regard to the base metal is likely

pearlite, ferrite, and potentially partial martensite. The presence of chromium and molybdenum carbide was detected, and these elements contributed to enhancing both strength and ductility. The presence of chromium, manganese, and iron in the base metal is also supported by the results of the EDS test carried out on sample C.

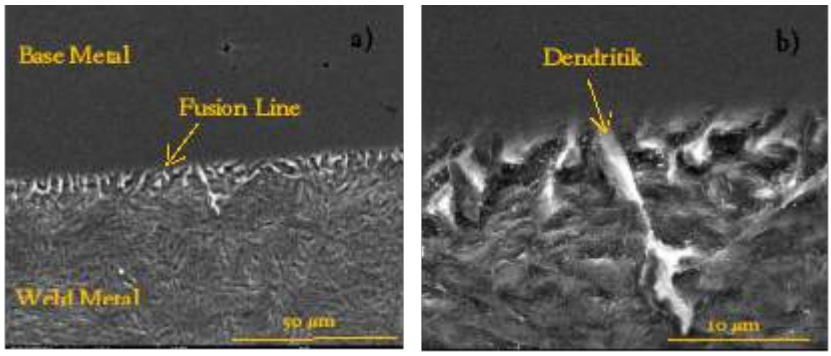

Figure 3. Interface bonding microstructure of sample C (260/300 A)

The microstructural observations were consistent with the hardness values obtained from the Vickers test results (see Table 2). As demonstrated by the microstructure, Sample A exhibited the most uniform and well-bonded interface layer. This particular sample showed a balanced distribution of hardness, with readings spanning from 195 to 233 HV. In contrast, sample B, which displayed visible imperfections, had higher hardness values (216 - 235 HV) but a non-uniform interface bonding layer. As illustrated in Figure 1, sample C, which exhibited the most substantial welding current, exhibited moderate hardness (230 – 223 HV). The microstructural analysis showed discrepancies in the interface layer, which implies a lack of fusion occurred. The presence of cracks in samples B and C indicates that increasing the welding current can cause excessive heat input, thermal stress, and structural defects, reducing the overall strength of the interface [13]. The analysis of sample A reveals a microstructure that strikes a balance between the mechanical properties and the presence of a robust interface layer, indicating optimization. This observation indicates that samples exhibiting such characteristics are probably optimal for the given study parameters.

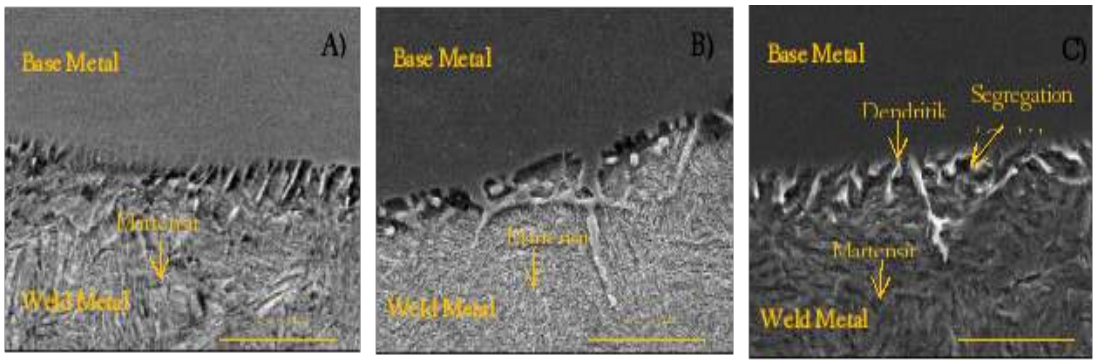

Figure 4. Microstructure comparison of samples A (180/200 A), B (220/250 A), and C (260/300 A)

3.3. Energy-dispersive X-ray Spectroscopy (EDS) Analysis

The EDS data for sample A (Figure 5) shows that the Fe-Cr-Ni-Mo hard coating composition is consistent with the chromoly steel base material and the wear-resistant coating. The presence of chromium and molybdenum has been pinpointed as a key factor in carbide formation, which in turn contributes to increased hardness. In addition, nickel (Ni) plays a crucial role in ensuring toughness [14].

The EDS test results analysis revealed that Sample A's hardfacing layer was made up of either low-alloy steel or mild steel, which was confirmed by the presence of iron (~97%) with small amounts of manganese and chromium. The absence of substantial concentrations of chromium and molybdenum in the hardfacing layer results in its deficient natural hardness and wear resistance.

Figure 7 shows the EDS test results for the base metal part of sample B. The base metal part of sample B had higher concentrations of chromium (18.82 wt.%) and nickel (12.51 wt.%) than sample A (16.49 wt.% Cr and 10.64 wt.% Ni). This led to enhanced wear resistance, toughness, and corrosion resistance. The slight increase in Mn in sample B also contributed to the improvement in the mechanical properties. This improvement is evident in the Vickers hardness test results, where the hardness test results of sample B are higher (216 HV) than those of sample A (195 HV). These results show that sample B may outperform sample A for applications requiring high wear resistance and impact toughness. However, the microstructure analysis results show that the interface layer of sample A is superior to that of sample B (it has no defects and is fused).

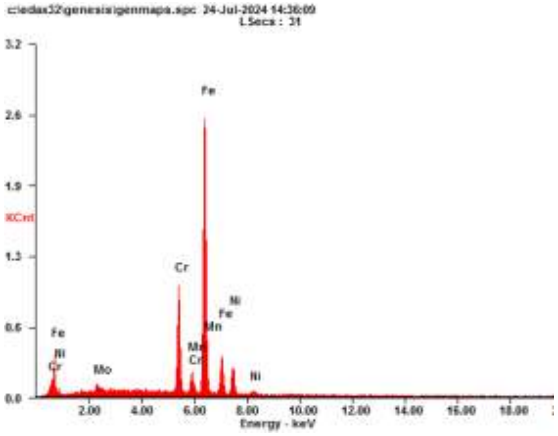

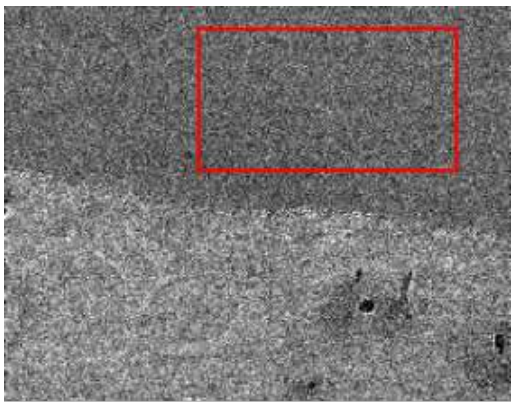

Element	*wt.%*	*at.%*
MoL	02.09	01.22
CrK	16.49	17.74
MnK	01.74	01.77
FeK	69.04	69.14
NiK	10.64	10.13
Matrix	Correction	ZAF

Figure 5. EDS results for base metal sample A (180/200 A)

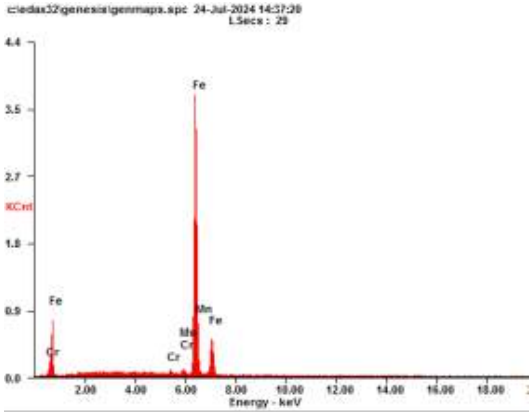

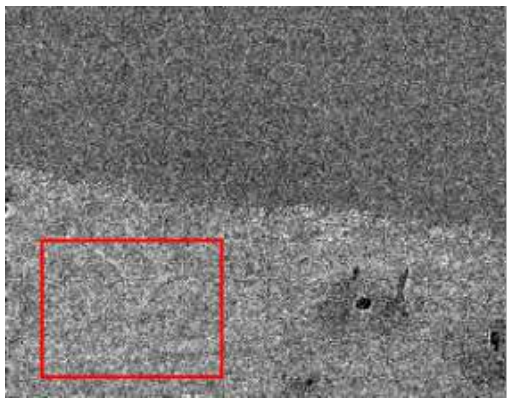

Element	*wt.%*	*at.%*
CrK	01.00	01.08
MnK	01.70	01.72
FeK	97.30	97.20
Matrix	Correc-tion	ZAF

Figure 6. EDS **results** on the hardfacing layer of sample A (180/200 A)

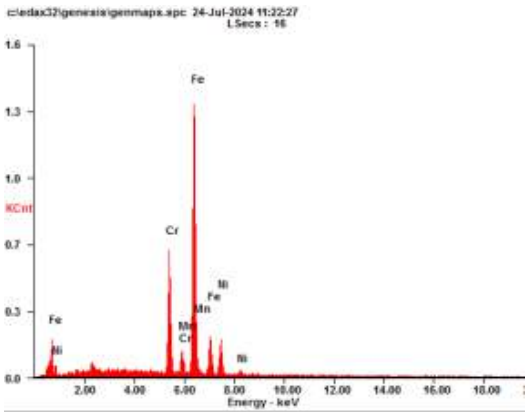

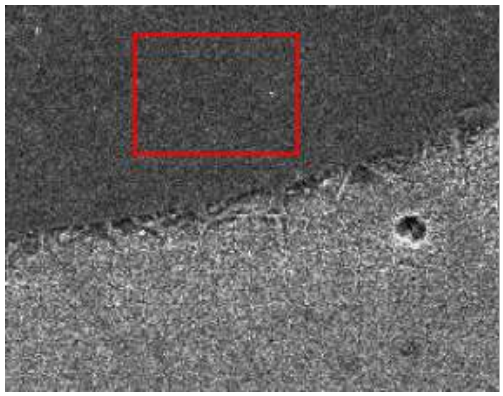

Element	*wt.%*	*at.%*
CrK	18.82	20.05
MnK	02.20	02.21
FeK	66.48	65.94
NiK	12.51	11.80
Matrix	Correc-tion	ZAF

Figure 7. EDS results for base metal sample B (220/250 A)

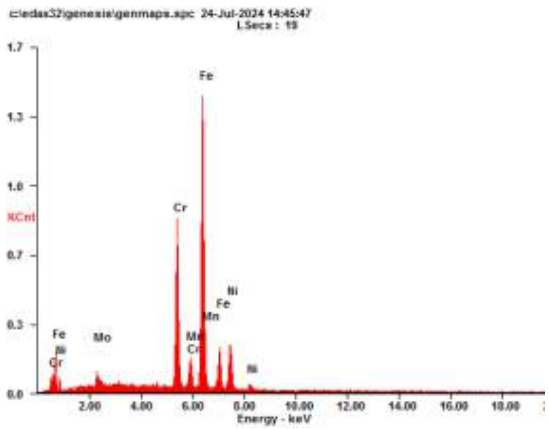

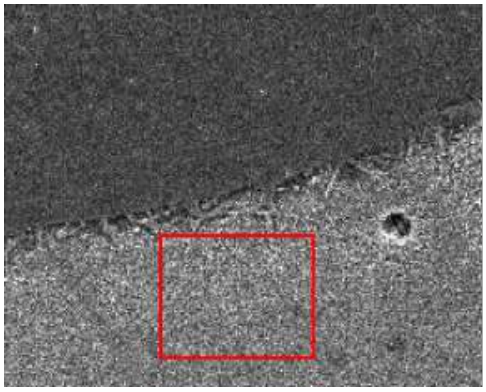

Element	*wt.%*	*at.%*
CrK	01.13	01.21
MnK	01.85	01.88
FeK	97.02	96.91
Matrix	Correc-tion	ZAF

Figure 8. EDS results on hardfacing layer B (220/250 A)

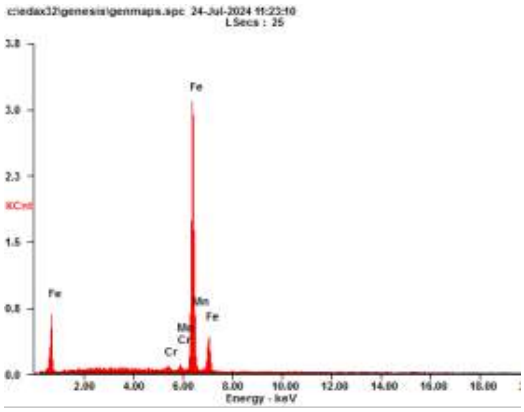

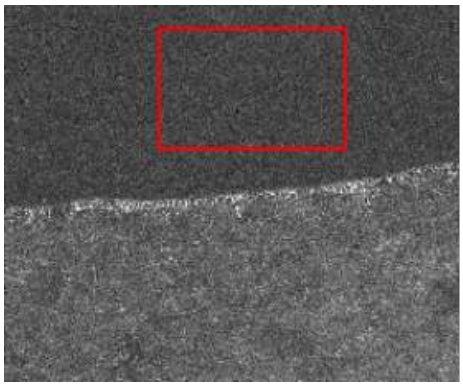

Element	*wt.%*	*at.%*
MoL	03.24	01.89
CrK	22.40	24.15
MnK	01.92	01.96
FeK	57.49	57.72
NiK	14.94	14.27
Matrix	Correc-tion	ZAF

Figure 9. EDS results for base-metal sample C (260/300 A)

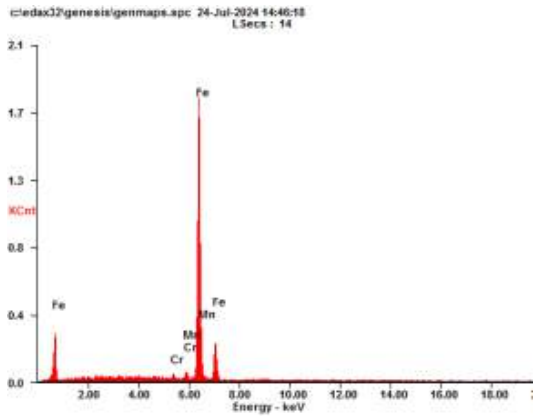

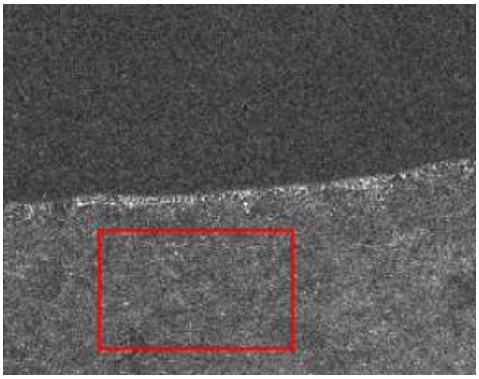

Element	*Wt.%*	*At.%*
CrK	00.97	01.04
MnK	02.21	02.24
FeK	96.82	96.72
Matrix	Correc-tion	ZAF

Figure 10. EDS results on hardfacing layer sample C (260/300 A)

The EDS test results for sample B's hardfacing layer (Figure 8) reveal that this layer is identical to that in sample A, comprising low alloy steel with very small amounts of Cr and Mn, rendering it vulnerable to wear and corrosion [15].

The EDS test results for the base metal of sample C (Figure 9) indicated the presence of Cr, Ni, Mo, Mn, and Fe elements. The test results for the hardfacing layer in sample C, as shown in Figure 10, are comparable to those of samples A and B, both of which had a hardfacing layer consisting mainly of iron-based steel with low chromium (Cr) and moderate manganese (Mn) content. This is consistent with the established specifications for hardfacing welding wire. The base metal part exhibits a substantial enhancement in resistance to wear and corrosion, which is attributable to its elevated concentrations of Cr, Ni, and Mo.

3.4. Hardness Test Analysis

The primary goal of hardness testing is to determine the variations in hardness within the weld area and the surrounding regions, which may be affected by the welding process, including the area influenced by heat and the base metal itself. The outcomes of the hardness test are presented in Table 2. The hardness value was determined in five distinct regions: the hardfacing layer area (areas I and II) and the base metal area (areas III, IV, and V). As shown in Table 2, the hardfacing layer exhibits a lower degree of hardness than the base metal. Conversely, in the domain of welding, it is anticipated that the hardness produced in the hardfacing layer is expected to exceed that of the base metal [16].

Table 2. Hardness test results of the hardfacing layer are expressed in HV.

Sample Code	Welding Current (A)	Hardness Value of the Tracing Area (HV)						
		Hardfacing			Base Metal			
		I	II	Average	III	IV	V	Average
A	180/200	194	196	195	238	233	227	233
B	220/250	216	216	216	237	239	230	235
C	260/300	229	232	230	225	222	222	223

In addition to examining the hardness distribution, hardness testing was conducted to determine the effect of increasing the current during the welding process. The hardness values (HV) of hardfacing and base metal are shown in Figure 11, with three unique welding current variations: 180/200 A for sample A, 220/250 A for sample B, and 260/300 A for sample C.

As demonstrated in Tabel 2, sample A exhibited the lowest surface-layer hardness (195 HV). Research has indicated that at lower currents, the layer formed may not undergo sufficient heat or significant dissolution, resulting in a relatively less rigid structure [15]. Sample B exhibited a high-hardness layer (216 HV), this observation signifies that the application of the welding current is adequate for promoting superior heat, resulting in a more refined microstructure. This, in turn, led to the enhancement of wear resistance. As indicated by the higher hardness value (230 HV) of sample C produced an increased hardness layer compared to sample B. The welding process-generated heat energy is also a contributing factor to the enhanced material melting and the strengthened bond between particles within the hardfacing layer. Increased heat input results in the formation of refined microstructure grains. The refined microstructure contains more grain boundaries, which hinder the movement of dislocations, ultimately resulting in increased material hardness [15].

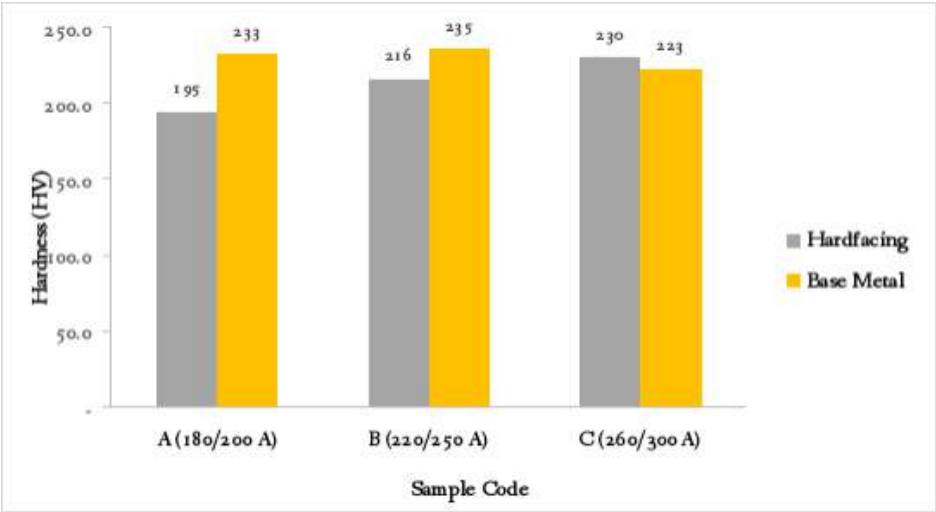

Figure 11. Effect of welding parameters on coating hardness

In the case of base metals, the effect of increasing the current on the hardness is not significant. The Vickers test results demonstrated that Sample A (233 HV) yielded the highest base metal hardness, indicating the least softening of the heat-affected zone (HAZ). An increase in the welding current resulted in a slight rise in the base metal hardness of Sample B, as indicated by an increase of 235 HV. This phenomenon can be attributed to the broader heat input exerting its influence on the HAZ. The increased heat resulted in a greater degree of austenitization of the base metal. During the rapid cooling process, when the cooling rate remains high, martensite formation is enhanced. In sample C, an increase in the welding current decreased the base metal hardness (230 HV). This indicates that an increase in the heat input can reduce the cooling efficiency, particularly in cases where the thermal mass is substantial. Slow cooling will form ferrite and pearlite phases, reducing the hardness.

Higher welding currents generally increases hardfacing hardness up to a point. Research findings suggest that the hardness of samples A, B, and C are associated with higher thermal energy levels, which are produced by higher currents, resulting in a faster fusion process and a stronger metallic bond between layers [17]. Following the welding process, the surface layer cools rapidly, resulting in the formation of denser microstructures, specifically martensite and hard phases featuring carbides or intermetallic, which emerge as a consequence of the high thermal condition during welding. The metal's hardness diminished slightly as the welding current increased, mainly due to thermal effects, which probably softened the microstructure within the heat-affected zone. The hardness of sample C (220/250 A) showed the best balance, achieving hardness (230 HV) while maintaining balance with the base metal (223 HV). Unfortunately, sample C did not exhibit a good interface layer, as observed under a microscope. Among the examined samples, sample C had an appropriate hardness value for the hardfacing layer, meeting the expected manufacturing requirements of at least 230 HV.

4. Conclusions

The process of hardfacing the SMnCrMoB435H material using mixed-metal arc welding (GMAW)/flux-core arc welding (FCAW) to the hardness profile was examined. It was observed that as the current increased in the MIG/FCAW welding, the hardfacing layer became harder. However, this is not supported by the interface bond, which does not appear to be fused. Cracks and holes that propagate to the base metal are also present.

FCAW welding of the track roller dimensions has a substantial impact on the microstructure of SMnCrMoB435H steel, which is subjected to GMAW-FCAW welding. The thickness of the hardfacing layer was found to be a minimum of 2.5 centimeters, which exceeds the targeted thickness of 1.1 centimeters.

In this study, the influence of welding current on the interfacial quality and mechanical performance of hardfacing layers was investigated. Sample A (180/200 A) exhibited optimal interface quality, as indicated by the uniform interface bonding and the absence

of significant defects. Conversely, Samples B and C exhibited signs of cracking and porosity, indicating that elevated current levels resulted in excessive heat input, leading to undesirable structural degradation. Furthermore, the hardness of the hardfacing layer reached 230 HV in sample C, which is in accordance with the targeted hardness specification. It is imperative to optimize welding parameters to achieve a balance between hardness, diffusion, and interface bonding quality to enhance durability in industrial applications.

Author Contributions: "Conceptualization, W.W.; methodology, W.W., A.A., S.I.; formal analysis, W., A.A., S.I; writing—original draft preparation, A.A.; writing—review and editing, W.A., E.S., M.A.; visualization, A.A.; supervision, W.W., E.S., M.A.; All authors have read and agreed to the published version of the manuscript."

Funding: This study received no specific funding from government, commercial, or non-profit organizations.

Acknowledgments: The authors would like to acknowledge the testing laboratory of the Center for Materials Processing and Failure Analysis, Universitas Indonesia, Depok, Indonesia, for its support and facilities. Appreciation is also extended to the Laboratory in Area Science and Technology B.J. Habibie, National Research and Innovation Agency (BRIN), Serpong, for valuable assistance and access to its research infrastructure.

Conflicts of Interest: The authors declare no conflict of interest.

References

1. T. D. Wodrich, Reinhard Jordan, and Alois Kroll, "Track chain link and undercarriage track roller having a metallurgically bonded coating," US 7,657,990 B2, 2006 Accessed: Dec. 11, 2024. [Online]. Available: https://patentimages.storage.googleapis.com/9d/11/c0/e2c6191f4b9e01/US7657990.pdf
2. P. F. Mendez *et al.*, "Welding processes for wear resistant overlays," *J Manuf Process*, vol. 16, no. 1, pp. 4–25, 2014, doi: https://doi.org/10.1016/j.jmapro.2013.06.011.
3. D. Tandon, H. Li, Z. Pan, D. Yu, and W. Pang, "A Review on Hardfacing, Process Variables, Challenges, and Future Works," *Metals (Basel)*, vol. 13, no. 9, 2023, doi: 10.3390/met13091512.
4. S. N. I. M. V. G. I. F. and D. L. O. Neikov, *Handbook of Non-Ferrous Metal Powders*. Elsevier, 2019. doi: 10.1016/C2014-0-03938-X.
5. A. Patnaik, S. Biswas, and S. S. Mahapatra, "An evolutionary approach to parameter optimisation of submerged arc welding in the hardfacing process," *International Journal of Manufacturing Research*, vol. 2, no. 4, p. 462, 2007, doi: 10.1504/IJMR.2007.015089.
6. A. Rehal and J. S. Randhawa, "Submerged Arc Welding Fluxes-A Review," *International Journal of Science and Research*, 2014, doi: 10.21275/02014158.
7. B. Gülenç and N. Kahraman, "Wear behaviour of bulldozer rollers welded using a submerged arc welding process," *Mater Des*, vol. 24, no. 7, pp. 537–542, Oct. 2003, doi: 10.1016/S0261-3069(03)00082-7.
8. M. Sulowski and A. Cias, "Microstructure and properties of Cr-Mn structural steels sintered in a microatmosphere," *Proceedings of the World Powder Metallurgy Congress and Exhibition, World PM 2010*, vol.

3, Dec. 2010.

9. L. L. Silveira, A. G. M. Pukasiewicz, G. B. de Souza, P. Soares, and R. D. Torres, "Effects of boron concentration on the microstructure, mechanical and tribological properties of powder-pack borided AISI 4140 steel," 2022. [Online]. Available: https://api.semanticscholar.org/CorpusID:246570209
10. M. Sulowski, "DILATOMETRIC INVESTIGATION OF Fe-Mn-Cr-Mo PM STEELS WITH DIFFERENT CARBON CONCENTRATIONS," 2008.
11. B. Derbiszewski, A. Obraniak, A. Rylski, K. Siczek, and M. Wozniak, "Studies on the Quality of Joints and Phenomena Therein for Welded Automotive Components Made of Aluminum Alloy—A Review," May 01, 2024, *Multidisciplinary Digital Publishing Institute (MDPI)*. doi: 10.3390/coatings14050601.
12. Niraj Kumar, Chandan Pandey, and Prakash Kumar, "Dissimilar Welding of Inconel Alloys With Austenitic Stainless-Steel: A Review," *J. Pressure Vessel Technol.*, vol. 145, no. 1, p. 011506, Feb. 2023.
13. Y. Q. Liu, D. Yu, Y. Zhang, J. P. Zhou, D. Q. Sun, and H. M. Li, "Research advances on weldability of Mg alloy and other metals worldwide in recent 20 years," Jul. 01, 2023, *Elsevier Editora Ltda*. doi: 10.1016/j.jmrt.2023.06.184.
14. H. Oktadinata, W. Winarto, D. Priadi, E. S. Siradj, and A. S. Baskoro, "Impact toughness characteristics of sm570-tmc steel joint using welding wire containing 0.4% nickel at different level of heat input," in *Key Engineering Materials*, Trans Tech Publications Ltd, 2020, pp. 117–124. doi: 10.4028/www.scientific.net/KEM.867.117.
15. S. Kou, "WELDING METALLURGY SECOND EDITION," 2003. [Online]. Available: www.copyright.com.
16. W. Winarto, M. Anis, and T. P. Hertanto, "Mechanical Properties and Microstructure of Welded Dissimilar Metals Using Buttering & Non-Buttering Layer," *Adv Mat Res*, vol. 0, pp. 341–346, Sep. 2013, doi: 10.4028/www.scientific.net/amr.0.341.
17. by Winarto and D. Priadi, "Effect of Preheating and Buttering on Cracking Susceptibility and Wear Resistance of Hardfaced HSLA Steel Deposit *," *Yosetsu Gakkai Ronbunshu/Quarterly Journal of the Japan Welding Society*, vol. 31, no. 4, pp. 202–205, 2013.

RiESTech
Recent in Engineering Science and Technology

MBI

Article

CLIMATE CHANGE IN INDONESIA: GREEN STEEL*

Nicholas Standish [1*]

[1] Emeritus Professor University of Wollongong, Northfields Ave Wollongong, NSW 2522, Australia
* Correspondence: mst97899@gmail.com

Abstract: Most studies of Indonesian Green House Gas (GHG) emission deal with land, forestry, electricity and construction, and exclude iron and steelmaking as such, which emits a sizeable 2.75t CO_2equivalent/ton of steel. This paper focuses on GHG emissions of Indonesian iron and steel industry, now existing and under construction - and that projected to 2060. It gives actual steps of how to start reducing the industry's GHG immediately using charcoal and employ ordinary people in environmental plantations and help poor people in towns and villages to earn some money by buying wood cuttings from them and processing it in distillation plants. It considers Indonesian ways and culture. There is no modelling of any process and activity, so everything can be checked from first principles or by reference to the source. One contentious conclusion is that to reduce the steel industry's GHG to near zero, it is imperative to use nuclear energy. Its use in Indonesia has been committed to by President Prabowo at the G20 Summit in Brazil in November 2024 and its actual start with 29 reactors was announced the following month (December 2024). This elicited immediate protests with a slogan of: "Indonesia bukan Chernobyl". A useful response by the government could be: Kami sangat setuju. Kami juga orang Indonesia. Sebab itu kita akan membangun reaktor gas Mitsubishi karena sama sekali reaktor tsb tidak mungkin meleleh seperti reaktor Chernobyl.

Keywords: Indonesia, green steel, direct reduction, plantations, biomass, nuclear power.

---

*Although there is no standardised universal definition of near-zero emissions, the International Energy Agency has defined it as 0.40 tonnes of CO_2e per tonne of crude steel for 100 per cent ore-based production (no scrap). For comparison, the average amount of CO_2 produced per ton of steel in 2020 was 1.89 metric tons, according to the World Steel Association

Citation: Standish, N. (2025). CLIMATE CHANGE IN INDONESIA: GREEN STEEL. Recent in Engineering Science and Technology 3(03), 54–68. Retrieved from https://www.mbi-journals.com/index.php/riestech/article/view/116

Academic Editor: Vika Rizkia

Received: 5 June 2025
Accepted: 22 July 2025
Published: 31 July 2025

Publisher's Note: MBI stays neutral with regard to jurisdictional claims in published maps and institutional affiliations.

1. Introduction

At the G20 Summit in Brazil in November last year (2024), President Prabowo emphasized Indonesia's commitment to achieving net-zero emissions by 2050 (later corrected by others to Jokowi's 2060 net-zero emissions). President Prabowo outlined an ambitious strategy to build 75 Gigawatts (GW) of renewable energy, including geothermal, wind, and solar, along with 5 GW of nuclear power. The real plan is to gradually reduce coal dependency, rather than immediately shut down coal plants.

Patunru and Resosudarmo (2024), in a detailed and well documented paper, show that in Indonesia, land use and forestry is by far the largest Green House Gas (GHG) emission source at 950 million tonnes per year (mty) of CO_2e (CO_2equivalent), electricity and heat as second (350mty CO_2e) and manufacture and construction as fifth (150mty CO_2e). Iron and steelmaking, as such, are not mentioned, so this paper may be viewed as new information. It is noted that Agriculture, Forestry, and Other Land Use, (AFOLU), unlike in Indonesia, is not the largest GHG emissions contributor globally, but second largest,

after electricity and heat production. The sector accounts for around 23% of global GHG emissions, Rocha et al (2021).

Blast Furnace-Basic Oxygen Furnace (BF- BOF) steelmaking route emits 2.75t CO_2e/ton of steel and Electric Arc Furnace (EAF) emits 1.71t CO_2/ton of steel, Kullman, (2023). Therefore, at today's Indonesian BF-BOF steelmaking of 9mty and the same of EAF steelmaking, Indonesia produces 24.8mty CO_2e, and 15.3mty CO_2 from EAF, making a total of 40.1mty CO_2e. Indonesia is on track to reach 45mty of steel by 2035, IISIA (2022) and on a 50-50 basis produce 100.4mty CO_2e, – a big enough proportion of the total emission to make sizeable difference.

Indonesian developments show backtracking to the traditional BF-BOF route, compared with two neighbouring countries which show significantly higher EAF investment compared to Indonesia's 1.7mt, Vietnam of 17.2mt and the Philippines of 12.8mt, or both over 10-fold, daCosta (2024).

Once all Indonesian iron and steel projects are completed, national capacity will increase by 125% for steelmaking and 55% for ironmaking. Out of the 24.5mt steel-making capacity in the pipeline, 22.8mt are using BOF, contradicting net zero commitments, and, as noted above only 1.7mt are using EAF. Meanwhile, from the 5.8mt of ironmaking expansion in construction now, all use BF, daCosta (2024). To achieve zero CO_2 by 2060, steelmaking – especially the BF-BOF route, being a very big emitter of CO_2, needs to be "greened" as quickly as possible, and completely so by 2060. In this "greening" activity, hydrogen plays a dominant role.

There are three commonly distinguished hydrogens: Green, Blue and Grey. Green produces no CO_2, Blue is made by steam reforming of natural gas with CO_2 capture, and Grey is produced in the same way, but without the CO_2 capture. Unit costs are the highest for the green hydrogen and lowest for the grey one. This paper examines how it can be done under actual Indonesian conditions, culture and social habits. The examination is based on basic fundamentals of theory in the Appendix, and the author's practical experience of 50 years, including 15 years in PT Krakatau Steel, Cilegon Plant.

2. IRONMAKING

Analysis of ironmaking processes used in various parts of the world show that currently (2024) there are just two main processes, Blast Furnace (BF) and Direct Reduction Iron (DRI). BF ironmaking is generally followed by BOF, and DRI is followed by EAF – thereafter, refining, casting and rolling to make coils, plates, billets and other steel products are identical in both cases.

The current world production of steel is nearly 2 billion tonnes per year, equating to some 1. 7 billion tonnes per year of iron. The BF-BOS route accounts for about 75% of that – the rest, mainly by shaft DRI reactors of which Midrex reactors are the most numerous.

Blast furnace sizes these days range from 2mty (million tonnes per year) to a few of 5mty. So, to just compete, any "green iron" reactor has to be in the same size class. Of all currently operated DRI reactors, the shaft reactors have a proven record over many years – and size-wise only Midrex Megamod, at 2.5mty is by far the biggest. It is noted that a fluidised bed reactor that has operated in Korea on an industrial basis is the Posco's FINEX, with 2mty of DRI.

Indonesia currently produces about 18mty of steel, of which about half uses molten iron from blast furnaces, Kullman (2023), so if Midrex Megamods are chosen, then four would be sufficient.

As already noted, the use of green hydrogen for DRI production, followed by green EAF melting, is now being strongly promoted in many countries.

Except for small amounts for special uses, there are as yet (2024) no tonnage hydrogen producing plants as such, in Indonesia, but PT PLN has combined with PT HDF, with the aim to produce hydrogen using water electrolysis, for power generation in Pulau Seribu to replace a 500 MVA diesel plant, SAMATOR (2024).

Also, in November 2022, PT Gunung Raja Paksi (GRP) and Australia's Fortescue Future Industries (FFI) signed an MOU to investigate the use of green hydrogen to help decarbonize GRP's steelmaking factories. According to The Jakarta Post of November 6, 2023, the company aims to replace natural gas with hydrogen sourced from FFI.

There has been a follow-up to this of a $60m loan from the International Finance Corporation (IFC) last year (2024) that also includes exploring different financing options to support GRP's decision to entirely decommission the company's newly built but never operated blast furnace, IFC (2024).

If this decision to decommission a newly built blast furnace is to help reduce GHG emission – and not as by Krakatau Steel, because as its then Dirut, Silmy Karim said its BF is uneconomic, Karim (2022), then Indonesians should be optimistic of reaching zero carbon by 2060.

As the blast furnace produces big amounts of molten iron in a short time, it needs to be replaced with something as productive, but very much greener, that is, with much less CO_2 emission but about as economic. Let's also keep in mind here that the only true economics is the totality of Run Of Mine (ROM) ore cost, grade processing, agglomeration, reduction, melting, refining, casting and hot rolling to end-products of Hot Rolled (HR) coils, plates, and such like.

So, we can now make a conclusion that barring a large economic superiority and accelerated start of Posco's HyRex hydrogen fluidised bed reactor, Indonesian green steel production will follow the DRI – EAF, or DRI – ESF route using Midrex (Megamod) reactor and as much green hydrogen as the LeChatelier's principle and the economics allow. .

ESF stands for Electric Smelting Furnace – a very recent project by BHP and others, designed to use the more plentiful lower grade iron ores of Pilbara, WA. Unlike EAF, ESF operates continuously producing molten (pig)iron, which is then processed as currently, namely, refined in BOF, cast into billets and slabs and rolled to produce products for sale. It has been tested in New Zealand and in December 2024 a 40,000 tpy pilot plant was about to be built in Western Australia. Its GHG emission has not been indicated by BHP, or by others.

Next, we have to decide on how this DRI-EAF route may be carried out in Indonesia economically and safely in practice with minimum compromises. Unfortunately, there are immediate problems.

Indonesia is a big country. One problem associated with this and identified by Pak Thohir in BUMN News 12/12/24, is: "Indonesia merupakan negara yang besar, sehingga masalah transportasi yang harus diperbaiki bukan hanya angkutan udara.

Another problem is, as of September 2024, 93 of the country's 201 coal plants supply energy to sectors like mining and smelting. While critical for industrial growth, these plants contribute significantly to emissions, complicating Indonesia's path to greener energy, Bimo (2024).

Out of these, 33 plants in Central, South, and Southeast Sulawesi power Chinese-owned nickel smelters, fuelling a key part of the global electric vehicle battery supply chain. This underscores China's strategic involvement in Indonesia's nickel processing sector, leveraging coal power to drive industrial operations, Bimo (2024). These power facilities are indispensable for processing nickel ore but rely on coal and therefore, as above, add significantly to GHG emissions.

Coupled with this is a note that "Adding 75 GW of renewable energy by 2040 will only generate fossil-free electricity for about 35% of projected national electricity demand.

To meet President Prabowo's vision, Indonesia must more than double this target", Tachev (2024).

Indonesia's internationally agreed Nationally Determined Contribution (NDC) and Control of Carbon Emissions in Development (CCED), regulations serve as the legal framework for domestic carbon pricing regulations intended to help Indonesia meet the climate targets to reduce greenhouse gas emissions and adapt to climate change. Indonesia's NDC includes targets to reduce emissions by 31.89% unconditionally and 43.2% conditionally by 2030, UNDP (2022). The NDC also includes targets to restore 2 million hectares of peatlands and rehabilitate 12 million hectares of degraded lands. NOTE: Carbon emission targets with decimal points are always interesting!

Other problems are: Developing green steel can take five to six years just to get official permission, driven by lengthy approval and planning processes. Long lead times and regulatory uncertainty can deter investment in energy projects.

The status of the Indonesia's iron and steel industry in the last few years is, paradoxically, – a jump from a 17th exporter in 2019 to world's 4th biggest in 2023 and also an importer of about the same amount, USDC (2023).

This makes decarbonizing the Indonesian steel industry even more important because steel exports to the European Union will be charged "carbon tariff" via Carbon Border Adjustment Mechanism (CBAM), effective next year (2026), if the suppliers cannot prove that the steel is "green". This will have a negative effect on the exports of the Indonesian steel industry. For this reason, the steel industry needs to undergo transformation to a GHG emission-free industry.

Farid Wijaya of IESR, explained that decarbonization for the steel industry will bring prospects for economic growth, although currently (2024) there are still quite a lot of challenges. There are also national laws and rules and international ones to which Indonesia is a signatory, that have a bearing on Indonesia's march to zero carbon by 2050/60.

CSR (Corporate Social Responsibility) is mandatory as mandated under Company Law and GR 47/2012, any company must implement CSR to comply with Indonesia's prevailing laws and regulations.

Mandatory Carbon Reporting is the law in 40 countries across the World. AASB S2 Climate-related Financial Disclosures and metrics and targets, including information about scenario analysis and Scope 1, Scope 2 and Scope 3 greenhouse gas emissions, where:

- Scope 1: Direct emissions from sources owned or controlled by the company.
- Scope 2: Indirect emissions from the purchase and use of energy, such as electricity, steam, heating, and cooling.
- Scope 3: All other indirect emissions that occur in the company's value chain, including both upstream and downstream emissions.

However, IFRS (International Financial Reporting Standards) Sustainability Disclosure Standard IFRS S2 Climate-related Disclosures issued by International Sustainability Standards Board (ISSB) is important, as non-compliance with IFRS standards can create barriers to cross-border capital movements, making it challenging to attract international investors or secure business credit. Indonesia is preparing to join IFRS S2.

Related to the economic issues in Indonesia is the observation that Indonesia's economy grapples with challenges like dependence on natural resource exports, infrastructure gaps, regional disparities, and a need for skilled labour. Corruption, complex regulations, environmental issues, and income inequality also impede growth, Triatmanto and Bawono (2023).

To sum up. Currently, the domestic steel production capacity is 27mty (million tonnes per year) and is increasing, and on track to reach over 45 million by 2035 and

planned to be 207mty by 2060 with associated carbon emission if nothing is done, of an eye-watering 600mtCO_2, Fathurrahmi and Wardhana (2024).

Clearly this is unacceptable, and the industry must decarbonize to reach the zero carbon by 2060.

There are already many good rules, steps and lists of activities that would normally be included in such projects, such as the World Economic Forum's, Energy Transition, giving a framework built around four key solutions to help reduce carbon emissions in industrial clusters. They are: 1. Systemic efficiency and circularity; 2. Direct electrification and renewable heat; 3. Hydrogen, and 4. Carbon capture, utilization and storage (CCUS). Please note that hydrogen is a key solution, too.

We will not repeat them here, but instead propose decarbonizing steps for iron and steel industry in Indonesia considering Indonesian culture and traditions and typical Indonesian ways of doing things – recognising, as noted by Patunru and Resosudarmo (2024), that "a uniform national policy may not work universally across regions".

The EAF way of steel production is the green steel way, if – and only if, the electricity for melting, casting and rolling to make steel products, eg coils, sections and bars, comes from GHG-free sources.

INDONESIAN IRON AND STEEL INDUSTRY

Indonesia has nearly 50 years of experience producing DRI, melting it in EAFs, casting and rolling – starting as Krakatau Steel in 1976 with a simple HyL1 batch process plant and ending with the high-technology, high pressure HyL3 process. For many years, the reducing gas was made by nickel catalysed steam reformed natural gas, but recently this was replaced by the "zero reformer" process, in which the heated natural gas, injected into the reactor where its in-situ reforming is catalysed by the freshly reduced iron.

Because Midrex reactors operate at ambient pressure, efficient in-situ reforming is still being investigated. This means it still needs external reforming of natural gas.

For economic reasons current Midrex practice is to do it with recycled top gas water and CO_2, even though the reaction is endothermic. However, if plentiful oxygen is readily available – which would be its case as a by-product of water electrolysis of making reduction hydrogen – it will be a big plus because oxygen reforming of CH_4 is exothermic,

$$CH_4 + \tfrac{1}{2}O_2 \rightarrow CO + 2H_2 + \text{heat}$$

Oxygen reforming requires a smaller reactor vessel. Exothermic also means that we will not need as much energy in preheating the reduction gas before it is injected into the reactor.

It is noted that in 1995, the partial combustion technology according to the above equation was incorporated in the HYL3 plant in PT Krakatau Steel, by injecting O_2 at the transfer line between the reducing gas heater and the inlet of the reduction reactor. This scheme allowed an important increase in the reducing gas temperature, as well as in-situ reforming. This decreased the reformed gas consumption by around 25 % and increased the productivity of the shaft furnace. In 1998 the total natural gas feed and O_2 injection to the shaft furnace led to the 'HYL self-reforming scheme', where the reformed gas make-up was reduced to zero.

As was said earlier; to reduce our carbon footprint, we must use "chemical hydrogen". Of course, if it is economical to have hydrogen for energy also, we can use it there, too.

Hydrogen is assumed to be produced through electrolysis using low emissions energy.

Until low carbon hydrogen is readily available, DRI shaft furnaces, like HyL and Midrex can use natural gas as a transition pathway.

Typical reformed gas into the reactor is: H_2 – 70%, CO – 15%, CO_2 – 10%, CH_4 – 5%, and the exit gas is: H_2 – 40%, H_2O – 20%, CO – 20%, CO_2 – 15%, CH_4 – 4%, N_2 – 1%.

H_2O and CO_2 in the exit gas are scrubbed away and about 2/3rd of H_2 and CO are recycled as reducing gas and the rest used as the heat source for gas preheating. Currently, H_2O and CO_2 are partially recycled, and the rest of CO_2 is sold.

The production of green DRI formally requires replacing the reformed gas with 100% green hydrogen. This will produce carbon free DRI, aligned with the first requirement of theory of making iron, but against the practical experience of DRI operators and EAF steelmakers.

Reasons for having carbon in DRI are: 1) pure iron DRI is pyrophoric and having carbon in it, usually as a cementite (Fe_3C) surface, will prevent spontaneous fire of DRI; 2) melting in EAFs needs foamy slag to reduce consumption of expensive graphite electrodes and wall refractories, and, of course, making high carbon steel; 3) If CO is also added to the DRI bed, the resulting exothermic reactions provide extra energy to counter endothermic reactions.

It should be said that EAF steelmakers would like to use DRI with about 4%C. In my view, to ensure all of the above 1) – 3), DRI carbon should be around 2%.

EAF gases contain significant amounts of chemical and sensible heat that is currently not recovered because of the batch or periodic nature of the process. On average, the gases contain about 20%CO and 5%H_2, as well as various amounts of CO_2, O_2 and N_2, depending on the practice used. Additionally, there is always steam formed from the water-cooling parts of the EAF.

In green steel making, recovering anything useful that can reduce the use of fresh material, is most important, so EAF's sensible heat and CO and H_2 gases will be recovered.

It is possible to design the DRI process for a zero-make-up water requirement mainly because water is a by-product of the reduction reaction ($FeO + H_2 = Fe + H_2O$) and is condensed and removed from the gas stream. As a consequence, with the adoption of a closed-circuit water system based on the use of water heat exchangers instead of conventional cooling towers, there may be no need for fresh make-up water and actually a small stream of water may be left available.

As to using much H_2, Midrex has reported that it has experience using various reducing gases with $H_2/CO = 0.5$ to 3.5 in commercial plants and using reducing gas with $H_2/CO = 4.2$, in a pilot plant.

3. RESULTS AND DISCUSSION

It has been demonstrated that to reduce Indonesia's Green House Gas (GHG) emission, it is worthwhile reducing it as such in the steel industry, as well as to avoid the steel exports from having tariff applied if the steel is not "green".

Because Indonesian steel industry has many years of experience of producing about 2mty of DRI pellets in a shaft reactor and melting it in EAFs in Krakatau Steel Plant in Cilegon and melting about another 10mty of scrap in EAFs in many other plants in Indonesia, there is no need to start with a pilot plant – instead, go directly to full size. Except for tonnage hydrogen, all other parts already have government regulations.

The Ministry ESDM has been in the process (2024) of drafting regulations on incentives and tax relief to green hydrogen developers, aiming to speed up the growth of the country's green hydrogen industry. In addition, the government is also evaluating a national hydrogen strategy expected to reduce fossil fuel usage, Dokso (2024). Actually, the government has just (May, 2025) launched the National Hydrogen and Ammonia Roadmap (RHAN) 2025–2060 as a derivative of the national hydrogen strategy. According to the Minister of Energy and Mineral Resources Bahlil Lahadalia the roadmap should be an opening signal to create a market and attract investment.

Whilst waiting for the implementation of the above RHAN roadmap and actual production of hydrogen, Indonesia can start building shaft furnaces of Midrex size, and companies with blast furnaces can start investigating the economics of altering them into DRI reactors – and if tonnage hydrogen is still not available, reforming natural gas and using it in the reactor, AND not allowing any CO_2 to escape, thereby ensuring production of "green" DRI.

What is envisaged is a single national charcoal industry consisting of biomass/wood processing plants and three wood supplying parts: 1. Plantations designed by a team of environmental scientists, arborists, forest scientists, agronomists, town planners AND Rural Fire Service (RFS) modelled on Australian RFS and its Volunteer part – all importantly under one minister! Maybe Transmigration and its Patriot Scholarship programs (22 Oktober 2024 Antara Press) could also participate; 2. City and town councils' horticultural departments; 3. Corner drop-off places where ordinary people can bring bundles of wood to sell.

In plantations the workers will live in town planners' villages built for the purpose, presumably with schools (SD and maybe SMP), shops, Puskesmas, fire stations and kantor desa. Depending on the plantation design team's advice, after the initial mechanical planting of millions of appropriate trees, workers will use only cangkul and manual handling to do the rest, like clear the weeds and prune the branches to send to the nearest distillation plant. It is of interest to note Setiawan and Iswati's (2019) research finding that receiving a PROPER Award "have affected positive and significant impacts carbon emissions in the plantation industries."

City and town councils have many parks and trees on roads and streets that need pruning all year round. The clippings and cuttings that before were burned, will now be taken to a central store via a weighbridge, for sorting and compressing and transported to the nearest distillation plant.

In corner drop-off places ordinary people will bring wood on motorbikes; when sufficient volume is collected it is transported to local storage centres; when sufficient volume is collected there, it is transported to the nearest biomass distillation plant. These drop-off places will have weighing balances and "one-way-in" designed wood receivers from which no wood can be stolen and resold. To prevent people saturating the wood and leaves with water to increase the weight to sell it and get more money, will be told "we don't buy wet wood, go back home, dry it in the sun and then come back". There will also be CCTV to watch that no money is pocketed by the drop-off government wood buyers. Naturally, the town council workers may bring some of the council clippings to sell in spite of each truck being weighed there, and this is something to watch against as it is impossible to ever stop.

These activities of helping poor people in towns and villages to earn some money, will be seen as being the same as the objective of Patunru and Resosudarmo (2024) of eradicating poverty.

Biomass is a clean, renewable energy source with CO_2 emission close to zero. Its use in Indonesia is already covered by existing government laws and regulations, so we can go directly to our distillation and production of charcoal for green steel, and a range of

chemicals for sale, and syngas that can also be used instead of natural gas for "green DRI" making.

There is a net zero emission, self-sustaining exothermic pyrolysis technology making high-grade green charcoal/biochar for metallurgical use, MetChar (2024) that would be just right for Indonesian conditions.

In making "green steel", charcoal will be used for: 1) making CO, 2) converting CO_2 to CO, 3) purifying recycled water for electrolysis, and 4) selling any excess to gold mines for CIP treatment.

Making CO with carbon of some sort is an old process of making town gas in so called "gas works". Converting CO_2 to CO, is the endothermic Boudouard reaction ie. $CO_2 + C = 2CO$. Purifying water is an everyday process in homes and towns and using charcoal for CIP (Carbon-In-Pulp) recovery of gold, is a lucrative business.

At first, before hydrogen making by electrolysis starts and its by-product oxygen becomes available to take care of heat deficiencies in the DRI reactor and converting CO_2 to CO, some CO_2 in the top gas will not be converted, but be sold, as is the current practice in PT Krakatau Steel.

The above processing steps take care of making "green DRI". Apart for the normal power use to operate pumps, blowers, pellet feeding equipment and process control equipment, this "green" step does not require any electric power for iron oxide reduction itself.

This is so very different to the next step of EAF melting, which is opposite, that is, it requires most of the power used for the main part of melting. In the steel making industry, EAFs are considered as one of the operations with the largest consumption of electrical energy, Logar and Shkrjank (2021).

For melting DRI in EAFs, the best that can be expected with all the energy saving additions and hot charging, is about 500 KWh/tls (ton of liquid steel). For its current production of about 18mty of steel, Indonesia will need to generate 9,000,000,000 KWh or have a power station of 1,000 MW capacity. For complete processing to steel bars, coils, plates, etc, add another 1,500KWh/t, making a total power generating capacity of 6,000 MW. As Indonesia is on track to reach 45mty of steel by 2035 this will require 135x1015KWh day and night, or a power station of 15,000 MW.

If all of the 135x1015KWh required is to be supplied by solar, wind and hydro and have power available at night and 24/7, the number of batteries to achieve it is astronomical. The sheer area required for solar panels, wind turbines and batteries is astronomical, too, and the total cost of all this is astronomical also. Then think of the projected 207mty of steel by 2060 – more panels, more batteries and more wind turbines – and much2 more of land to put them on. No people in any country would agree to this being done and pay for it – climate change, or not!

Current knowledge and experience suggest that nuclear energy can be the answer. In fact, as noted in the first paragraph of this paper, "At the G20 Summit in Brazil last year (2024), President Prabowo committed Indonesia to include 5 GW of nuclear power in achieving net zero emission." As noted above, to make Indonesian steel on track to reach

45 mty by 2035 “green” by using this nuclear energy, the 5GW will need to be trebled and increased to 70GW for the 207mty by 2060.

It should be pointed out that from a regulatory perspective, all relevant nuclear laws and procedures are already in place in Indonesia, and this, with President Prabowo’s commitment at the G20 Summit explains a sudden activity in nuclear power.

PT Thorcon Power Indonesia announced it had signed an agreement with Indonesia’s nuclear regulator to investigate building a 500 MW molten-salt reactor demonstration plant on Gelasa Island in Bangka-Belitung province.

In December 2024 Indonesia Energy Council has proposed 29 sites for nuclear power plants in a bid to secure reliable energy sources and reduce carbon emission. The sites stretch from North Sumatra, south-east across the archipelago to West Papua, Salim (2024).

In the latter case protesters have been immediately active with slogan of “Indonesia bukan Chernobyl”, which is simply normal ignorance of ordinary people world-wide about nuclear power, and consequently their fear of it. Yet nuclear waste has many uses and benefits that extend to many consumer products, like fire alarms, medical apparatus, printers, watches, etc.

In defence of this decision, Agus Puji Prasetyono, member of Indonesia National Energy Council said, "The earthquake fault line would have to be more than 5 kilometres away [from the plant] to minimise significant impact on construction." Defending building nuclear reactors in Indonesia in this way is counterproductive and causes more fear than decreases it – and must not be repeated!

The best response by government is as follows:

We totally agree. We are also Indonesians. That's why together we will build Mitsubishi gas reactors because there is absolutely no way they will melt down like the Chernobyl reactors.

Here, the reference is to the Mitsubishi Heavy Industries (MHI) High Temperature Gas Reactor (HTGR), which, unlike other common reactors, including the Chernobyl one, has a negative temperature coefficient. This means that with the increase in temperature caused by a greater number of nuclear reactions, the reactor automatically reduces the number of these reactions, returning to the previous and completely safe level. This is opposite to other reactors, and it also means that the maximum gas temperature leaving the reactor cannot be higher than 950^{o}C, which is still effective enough to generate power. Additionally, the gas used is helium, which cannot become radioactive, and this is opposite to other type of reactors currently used. And they can use spent fuel which means reducing its half-life further yet again and help with its eventual storage.

Additionally, using gas turbines to drive the alternators in a closed cycle, generating efficiency is higher than with steam as it uses Brayton cycle instead of the traditional Rankine cycle. Also, no water is necessary, which is very useful in arid areas and during times of drought.

There is a place in Japan called Takasago Hydrogen Park in the Hyogo Province and near its Capital City Kobe, where these HTG reactors are to produce tonnage hydrogen

for Japan's zero carbon by 2050 and many to be sold overseas – some already booked to Sarawak, Indonesia's Kalimantan neighbour.

To further allay the fears of local people of building HTG reactors in earthquake-prone Indonesia it is important to recall the catastrophic Kobe earthquake of January 1995, which caused more than 6,000 deaths and over 30,000 injuries and fires following the earthquake that incinerated half of the city.

The importance of Kobe earthquake is that the HTG reactors are being built and hydrogen produced in Tagasako, only a 50 km distance away from Kobe – confirming that HTG reactors are fully safe and impossible to melt-down in the "Ring of Fire" countries that includes Japan, Philippines and Indonesia.

4. CONCLUSIONS

Indonesia is one of the world's largest emitters of greenhouse gases (GHG). Most studies deal with major emissions and exclude steelmaking as such, which ranks fifth and emits 2.75t CO_2e/ton of steel. This paper focuses on GHG emissions of Indonesian iron and steel industry, now existing and under construction - and that projected to 2060.

It gives actual steps of how to start reducing the industry's GHG immediately using charcoal and employ ordinary people in environmental plantations and help poor people in towns and villages to earn some money by buying wood cuttings from them and processing it in distillation plants.

It considers Indonesian ways and culture. There is no modelling of any process and activity, so everything can be checked from first principles or by reference to the source.

One contentious conclusion is that to reach nett zero, it is imperative to use nuclear energy. Its use in Indonesia has been committed to by President Prabowo at the G20 Summit and its actual start with 29 reactors was announced in December 2024 and elicited immediate protests with a slogan of: "Indonesia is not Chernobyl. The best response by the government is as follows: We totally agree. We are also Indonesians. That's why together we will build the Mitsubishi gas reactor because it is absolutely impossible for it to melt down like the Chernobyl reactor.

APPENDIX: FUNDAMENTALS OF MAKING IRON

Making iron from iron ores is chemistry. People generally write chemical equations and use them, without ever thinking of what a chemical equation says. Let me write a simple chemical equation to make iron.

$$FeO + H_2 = Fe + H_2O$$

This equation asserts that to make iron, two requirements must be satisfied:

1. There must be iron oxide (FeO).

If there is no iron oxide, or if it is impure, iron will not be made, or it will be made inefficiently.

2. It and the reducing gas (H_2) must contact each other. This is shown by the plus (+) sign.

If there is no contact, or contact is poor, iron will not be made, or it will be made inefficiently.

Also, every chemical reaction is accompanied by a heat effect that can be small or large - and heat may be given up, or it may be absorbed.

Reactions that give heat up are called "exothermic" – a good example being $C + O_2 = CO_2$ + lots of heat given off, so temperature rises. It is, of course, the well-known combustion reaction.

Reactions that absorb heat are called "endothermic". An everyday example is reaction of baking soda with spirits of salt: $NaHCO_3 + HCl = NaCl + H_2O + CO_2$ + heat absorbed, so temperature drops.

What happens to the progress of the reaction follows Le Chatelier's Principle, namely:

If a dynamic equilibrium is disturbed by changing the conditions,
the position of equilibrium moves to counter the change.

For example, the reaction, $FeO + H_2 = Fe + H_2O$ is endothermic, that is, it absorbs heat, so as we increase the temperature, the reaction moves to the right, to produce more Fe.

On the other hand, the reaction, $FeO + CO = Fe + CO_2$ is exothermic, that is, it releases heat, so as we increase the temperature the reaction moves to the left, to produce less Fe.

Thermodynamics tells us what reaction is possible and under what conditions. It was invented by practical men to stop people wasting time on inventing perpetual motion machines. Fundamentals of thermodynamics of iron oxides reduction with CO and H_2 are presented in Figs 1 and 2 in which the Y-axis is, respectively, CO and H_2 concentration, and the X-axis in both is temperature.

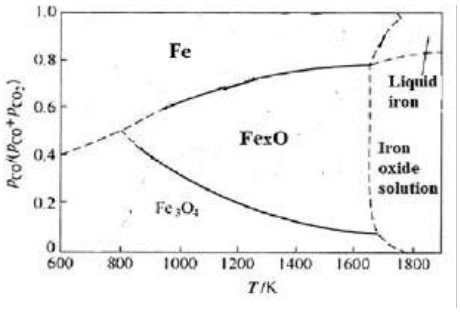

Figure 1. Reduction of iron oxides with CO.

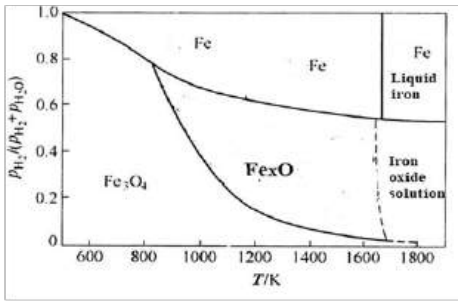

Figure 2. Reduction of iron oxides with H_2.

First, the figures do not show Fe_2O_3. It is not an omission. It is just that the Fe_2O_3 line almost coincides with the X-axis. Or, more colourfully, there is enough CO in a smoker 's breath to change Fe_2O_3 to Fe_3O_4.

In Figs 1 and 2, each line is an equilibrium line. Thus, with CO, to go from FeO to Fe at, say, 1200oK, CO concentration ratio is 0.70, and at 1400oK it is higher (= 0.75). But, with H_2, to go from FeO to Fe at 1200oK, H_2 concentration ratio is 0.65, and at1400oK it is lower (= 0.55). This result is just Le Chatelier's Principle in action!

The above thermodynamics tells us that to go from Fe_2O_3 to Fe is a stepwise process:

$$Fe_2O_3 \rightarrow Fe_3O_4 \rightarrow FeO \rightarrow Fe.$$

Let's look at the properties of each oxide. Table1, gives molecular weight, specific gravity, melting point, oxygen to iron ratio and crystal shape, of each, while Table 2 highlights what it all means in industrial practice.

Table 1. Physical Properties of Iron Oxides.

Compound	MW (-)	SG (-)	MP (°C)	O/Fe	Shape
Iron (Fe)	55.85	7.86	1535	0	Cubic
Hematite (Fe_2O_3)	159.70	5.24	1565	2/3	Trigonal
Magnetite (Fe_3O_4)	231.55	5.18	1538	4/3	Cubic
Wustite (FeO)*	71.84	5.71	1420	1/1	Cubic

*Actually, wustite is what is known as a non-stoichiometric compound, .
or ($Fe_{1-x}O$), where $0.833 < x < 0.957$.

Table 2. Properties of Iron Oxides Affecting Industrial Ironmaking.

Compound:	Fe_2O_3	Fe_3O_4	FeO	Fe
The O/Fe ratios are:	1.5	1.33	1.0	0
Oxygen to be removed:	0.17	0.33	1.0	
Or, as percentage:	11%	22%	67%	

It is clear from Table 2 that no matter whether we use CO or H_2 to do the reduction, 2/3 of oxygen has to be removed in the final step, AND that's a lot! In case of CO reduction at 1,000oC (1273K), for example, CO concentration, as can be seen in Fig 1 has to be very high (>0.70%) – so we need to really work hard to make sure that everything within our control is at its highest performance level.

In the case of H_2 reduction, as Fig 2 shows, it is easier (<0.70%) – as long as we make sure that our temperatures are maintained!

The stepwise reduction process, $Fe_2O_3 \rightarrow Fe_3O_4 \rightarrow FeO \rightarrow Fe$, is also followed by the kinetics of reduction – in other words, by the rate, or speed, of the reduction, which is so important in the economics of ironmaking.

The stepwise, or topochemical, to use the technical word, is an onion-like, reduction, illustrated for the CO case in Fig 3. It is exactly the same onion-like reduction for H_2, with H_2 diffusing in and gaseous H_2O diffusing out.

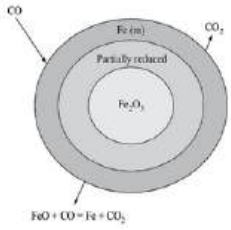

Figure 3. CO reduction of Fe_2O_3.

Hydrogen molecule and H_2O molecule are both smaller than CO molecule and CO_2 molecule, so diffusion-in of H_2 and counter-diffusion out of H_2O molecules are easier than CO molecules in and CO_2 molecules out, so H_2 reduction should be faster than CO reduction – this is true all other things being equal.

What does "all other things being equal" mean?

It means that the permeability structure of the starting oxide – and that of the other growing layers are the same. Because of different crystal structures, especially of hematite and magnetite, reduction of magnetite is much slower than that of hematite.

In fact, if the starting oxide is magnetite, it is standard industrial (economic) practice to heat it in air to convert magnetite to hematite and then use that product for reduction.

The reason is that the 16% of expansion in going from hematite (trigonal) to magnetite (cubic) creates cracks, as shown in Fig 4, that help gas diffusion.

(a)  (b) 

Figure 4. Insufficient cracking (a), and sufficient cracking (b).

Of course, if cracking is excessive and pellets disintegrate (They have high value of standard test for RDI – Reduction Degradation Index), then no matter how good their other properties, and price are, such pellets are simply, unacceptable.

At this stage we should make it absolutely clear that people talk about hydrogen and the "hydrogen economy" and lumping all hydrogens together. This must not be done, as it is not only not true, but it also interferes with talking about the economics of green steel production. We confirm that there are two principal kinds of hydrogen, namely: 1) energy hydrogen, and 2) chemical hydrogen.

For the reduction of iron oxides – and other metal oxides – we need chemical hydrogen, and for the production of energy for heating, melting, rolling, etc we need energy hydrogen – but only if its use for this, as such, or via electricity is economic . Of course, if it is advantageous or economic, we can use hydrogen for both at the same time.

By the way, there are three commonly distinguished hydrogen types: Green, Blue and Grey. Green is made with no CO_2 produced, Blue is made by steam reforming of natural gas with CO_2 capture, and Grey is produced in the same way, but without the CO_2 capture. Unit costs are the highest for the green hydrogen and lowest for the grey one.

The above principles of theory will help appreciate the overall view of iron oxide reduction, and any specific parts will be added at the time of need.

INDONESIA APPLICATION

Indonesian steel production in 2023 was 16mty, with about half from scrap melting in EAF (Electric Arc Furnace), and the other half from BF (Blast Furnace) and DRI (Direct Reduction Iron) plants.

The projected steel production by 2060 is 207 million tonnes per year (mty) with colossal GHG emission if nothing is done about it of 480,000,000 tonnes per year of CO_2-e!! So, it is obvious that all this has to be removed to reach zero carbon by 2060.

The EAF way of steel production is the green steel way, if – and only if, the electricity for melting, casting and rolling to make steel products like coils, sections and bars, comes from CO_2 -free sources.

It is clear that a green method of steel production has to be able to produce the same kind of amounts as a BF-BOF does. It also must be economic, safe and practical.

Current methods of mining iron ores produce many fines. In most cases these are of lower Fe content and usually preferred by the BF/BOF steel companies because they are cheaper and, in any case, feed to blast furnaces is usually agglomerated as sinter or sometimes as pellets.

Theory says that iron is produced by the contacting of molecules, such as illustrated by the equation $FeO + H_2 = Fe + H_2O$. In practical terms this means that the smaller are the iron oxide grains the faster is the reaction and more iron can be made. This points us to fluidized and semi-fluidized reactor types because they use only iron ore fines as feed.

Many fluidized and semi-fluidized reactors have come and gone. The one that has stayed and proven on an industrial basis is the Posco's Finex, with 2mty of DRI. Last year (2024) they announced development of HyRex, that extends Finex to use hydrogen. However, POSCO is demonstrating its HyRex process' performance in an ESF (Electric Smelting Furnace), mentioned on p 4, the molten iron from which is refined in BOF before casting. Just the same because of possible economic advantage of HyRex over Midrex, especially if Indonesia has to use its iron ore fines from various mines and those from its byproduct of nickel production from laterites and saprolites, we should follow its progress, in particular as it could then have potential to challenge Midrex.

To complete the overview of green steel processes, we should mention low temperature electrolysis of around 100oC. It uses ROM iron ore as feed. Fortescue is fully financing it. It is not known why.

Then there is BioIron – already at pilot plant scale of one tonne of DRI/hour. It uses biomass blended with iron ore reduced in a microwave furnace, followed by smelting in EAF to produce steel. Theory shows that bringing reactants FeO and C close together should really make the reaction proceed very fast, but it does not. The reason is that $2FeO + C = 2Fe + CO_2$, which then reacts with C as $CO_2 + C = 2CO$ – the most endothermic reaction in ironmaking known as Boudouard reaction in textbooks . The ironmakers call it a "solution – loss" reaction, meaning "solution" of carbon and "loss" of heat. The famous graph of Standish (1991) in Fig 5 shows the difference between the carbothermic reduction of iron oxides at 1000oC in a laboratory furnace and in a microwave oven. The reason is that in a laboratory furnace the heat travels to the centre of the pellet from outside by the slow process of conduction, whereas microwave being volumetric heating

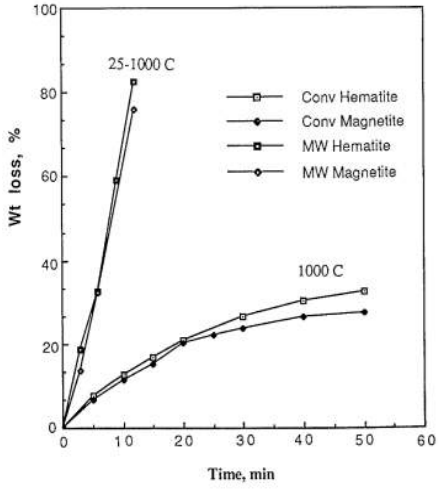

Figure 5. Conventional and microwave carbothermic reduction of Fe oxides.

the heat is available immediately in the centre, too, to cover the endothermic reaction. In other words, in laboratory furnace the pellets have "cold centres", and in a microwave oven they have not.

BioIron is funded ($215 million) by Rio Tinto. This is not understandable. My experience has been that apart from its niche application in drying, microwave processing of metals is only economic for high value metals.

Likewise, the low temperature electrolysis, funded by Fortescue, is not understandable also because it is impossible to have either process produce anywhere near the tonnages of steel required.

Needless to say, we don't talk about them for Indonesia at this time!

References

[1] Rocha, M.T., F.Carloni, S.Shaikh and C.Thorpe, Demystifying GHG emissions and removals from the AFOLU sector for states and regions: Prepared at Ricardo Energy & Environment as part of the Climate Footprint Project, June 2021.

[2] da Costa, G. Most Indonesia's steel industry highly emitting, competitiveness at stake: CREA (Centre for Research on Energy and Clean Air), 18 December 2024.

[3] IISAI, The Indonesian Iron and Steel Association, News Room, 16 November 2022.

Karim, S. Krakatau Steel Hentikan Operasiabrik Blast Furnace, Tempo, Rabu 29 Januari 2020.

[4] SAMATOR, PT Arohera, Indonesia International Hydrogen Summit, Hotel Mulia, Jakarta, 19-20 June 2024.

[5] AICN, Australia-Indonesia Centre News, 12 December 2024. Monash University Caulfield Campus, Melbourne 3145. Australia.

[6] World Economic Forum, Energy Transition: Four solutions to help reduce carbon emissions from industrial clusters. Accenture, in collaboration with the World Economic Forum, has developed a framework built around four key solutions to help reduce carbon emissions in industrial clusters: March 4, 2021.

[7] Santoso, S.D., S. Panda, E. Susanto, and A. Satrio, Indonesia's pathway to net zero 2060: Kearney Management Consultants, 27 August 2024.

[8] Bimo,E.S., China's Role in Indonesia's Coal-Powered Industry Poses Challenge to Prabowo's Green Goals: China Global South Project, 15 December 2024.

[9] Tachev, V., To Phase Out Coal by 2040, Indonesia Should Address Captive Coal and Scale Up Renewables: Energy Tracker Asia Newsletter, 18 December 2024.

[10] UNDP (United Nations Development Programmes), Global Climate Promise, Indonesia 2022.

[11] USDC, US Department of Commerce, International Trade Administration, Trade Data from S&P Global, Indonesia Exports of Steel Mill Products, 2023.

[12] Wijaya, A,. Decarbonization Starts with Accurate Data and Information, Institute for Essential Services Reform (IESR) at the Event for Demand Side Technology Catalog for Industry, Transportation, and Building Sector organized by the Embassy of Denmark in Jakarta, on Monday 16 December 2024.

[13] Triatmanto, B. and S. Bawono, The interplay of corruption, human capital, and unemployment in Indonesia: Implications for economic development, J Economic Criminology Volume 2, December 2023, 100031.

[14] Dokso, A., The Indonesian Ministry of Energy and Mineral Resources (ESDM) is moving towards establishing a regulatory framework to incentivize the development of green hydrogen: Energy News 21/06/2024.

[15] Patunru, A.A, and B, P. Resosudarmo, Climate Change Policies in Indonesia: Challenges and Economic Consequences, Chapter 6 in book: The Indonesian Economy and the Surrounding Regions in the 21st Century, pp.97-121, January 2024, Springer, Singapore.

[16] MetChar.com.au: Metallurgical Biochar, 2024.

[17] Kullman, J. Arizona State University News, October 05, 2023.

Logar, V and I. Shkrjank:The influence of electric arc furnace input feeds on its electrical energy consumption, J. Sustainable Metallurgy. 7 1013-26, 2021.

[18] Salim, N., T. Ardhya and S.Brooks, Earthquake-prone Indonesia considers nuclear power plan as 28 possible plant sites revealed, ABC News, Australia, 27 December, 2024.

RiESTech
Recent in Engineering Science and Technology

MBI

Article

Sugarcane Bagasse as Green Fuel and Reducing Agent for Lump Ore Reduction Process

Hendrik Nemers [1,*], Rianti Dewi Sulamet-Ariobimo [1], Johny Wahyuadi Soedarsono [2], Muh Fajar Ramadhan [3], Agus Paul Setiawan Kaban [3], Ahmad Maksum [4], Theo Thomas [5], Djoko Nirprawitno [6]

[1] Mechanical Engineering Department, Faculty of Industrial Technology, Universitas Trisakti, Jakarta 11440, Indonesia
[2] Laboratory of Prof. Johny Wahyuadi Soedarsono Department of Metallurgy & Material, Faculty of Engineering, Univesitas Indonesia, Depok 16424, Indonesia
[3] Department of Metallurgy & Material, Faculty of Engineering, Univesitas Indonesia, Depok 16424, Indonesia
[4] Research Center for eco-friendly Technology, Mechanical Engineering Department, Politeknik Negeri Jakarta, Depok 16425, Indonesia
[5] PT Refratech Mandala Perkasa, Bogor, Indonesia
[6] PT. Pertamina Geothermal Energy, Jakarta 10340, Indonesia
* Correspondence: nemmers68@gmail.com

Abstract: Carbon is an essential element in the iron reduction process. Cokes are used as a carbon source in the traditional reduction process in the beneficiary of iron. When the Ironmaking Technology Mark 3 (ITMk3) method is applied in the reduction process, many carbon sources are used, especially the sources with sustainable and eco-friendly such as coconut shells, palm kernel shells, rice husk, and sugar cane bagasse. Saccharum officinarum or sugarcane extraction produced bagasse as the by-product. Like coconut shells, this rich carbon by-product is not utilized. This work discussed the utilization of bagasse as a reducing agent in the iron reduction process. An analysis is made based on specific reduction temperature with the various ratio of iron to coal. The lump ore is originated from South Borneo. Unlike the coconut shell, in this work, the Baggasse was dried. The process temperature range between 700 and 1000OC. The ratios of ore to bagasse were 1 to 1, 1 to 2, 1 to 3, and 1 to 4. The reduction process was carried out in a muffle furnace. The result shows that the reduction process produced wustite (FeO). This work also compared sugarcane bagasse with other green reducing agents.

Keywords: Green-reducing agent; Sugarcane bagasse

Citation: Nemers, H., Sulamet-Ariobimo, R. D., Soedarsono, J. W., Ramadhan, M. F., Kaban, A. P. S., Maksum, A., Thomas, T., Nirprawitno, D. (2025). Sugarcane Bagasse as Green Fuel and Reducing Agent for Lump Ore Reduction Process. Recent in Engineering Science and Technology 3(03), 69–81. Retrieved from https://www.mbi-journals.com/index.php/riestech/article/view/98

Academic Editor: Iwan Susanto

Received: 27 February 2025
Accepted: 22 July 2025
Published: 31 July 2025

Publisher's Note: MBI stays neutral with regard to jurisdictional claims in published maps and institutional affiliations.

1. Introduction

The iron and steel industry remains fundamental to modern infrastructure and economic growth. However, it is also one of the most energy-intensive and carbon-emitting industrial sectors. The production of one metric ton of crude steel consumes approximately 800 kg of coal, contributing to nearly 7% of global industrial CO_2 emissions [1]. Additionally, this sector accounts for around 20% of total annual industrial energy consumption [2], primarily sourced from fossil fuels. Despite mounting environmental concerns, global steel demand is projected to grow steadily until at least 2050 [1], underscoring the urgent need for more sustainable production methods. In Indonesia, which possesses approximately 3.3 billion tons of iron resources—including primary ore, laterite ore, and iron sand—domestic production remains limited and insufficient to meet national

demand[3], [4], [5] . This situation presents both a challenge and an opportunity: to develop an independent iron and steel industry that leverages local resources while aligning with global sustainability goals.

In response to the growing environmental concerns surrounding the iron and steel industry, there has been increasing interest in the development of renewable and biomass-based reducing agents as sustainable alternatives to fossil fuels. Biomass is considered carbon-neutral, locally available, and capable of significantly reducing greenhouse gas emissions in metallurgical processes. Various biomass types such as sawdust [6], rice husk [7], rice bran, bamboo, coconut shell [8], and palm kernel shell [9] have been widely studied for their potential in replacing conventional carbon-based reducers like coal and coke. These studies have demonstrated that biomass materials possess sufficient fixed carbon content and thermal reactivity to participate effectively in reduction reactions, especially after undergoing processes such as carbonization, torrefaction, or briquetting.

Several researchers have specifically explored the efficacy of biomass in reducing different metal oxides. Torrefied biomass, for instance, has shown the ability to reduce hematite to metallic iron at lower temperatures than traditional reductants such as graphite [10]. Rath et al. [11] reported that vegetative biomass briquettes could effectively reduce iron ore slime, highlighting the importance of parameters such as particle size, temperature, time, and feed-to-reductant ratio. Similarly, Asmiani [12] found that blending biomass like canary shells with coal could enhance the calorific value and reactivity of briquettes. Research by Mansor [13] also suggests the potential commercialization of bio-coke derived from palm kernel shell due to its economic advantage, with production costs up to 31% lower than conventional biomass briquettes.

In addition to iron and nickel ores, biomass has also been applied in the reduction of other transition metal oxides. Notably, sugarcane bagasse has gained substantial attention not only as a biofuel but also as a reducing agent. Studies by Young et al. [14] revealed that sugarcane bagasse could effectively reduce pyrolusite (MnO_2), achieving manganese recovery rates exceeding 98% under optimal conditions (roasting temperature of 450 °C, 30-minute duration, and mass ratio of 0.9:10). Furthermore, research by Soedarsono et al.[15] confirmed the ability of sugarcane bagasse to reduce lump iron ore and produce wüstite (FeO), indicating its practical applicability in iron extraction. These findings underline a broader trend in green metallurgy that emphasizes the valorization of agricultural waste and by-products as low-cost, renewable inputs for industrial processes. However, further investigation is still needed to optimize the use of sugarcane bagasse—particularly in terms of reaction kinetics, phase transformation, and thermodynamic behavior during reduction—to ensure its scalability and consistency in industrial settings.

This study aims to address these gaps by investigating the effectiveness of sugarcane bagasse as a green reducing agent in the carbothermic reduction of lump iron ore using a muffle furnace. The research focuses on identifying optimum process parameters—such as temperature, time, and biomass-to-ore mass ratio—and evaluating the extent of reduc-

tion achieved. By comparing the performance of sugarcane bagasse to that of other biomass-based reducing agents, this work seeks to assess its practical applicability and economic potential in low-carbon iron-making processes. The findings are expected to contribute to the broader transition toward sustainable metallurgical practices, particularly in resource-rich, developing economies such as Indonesia.

2. Experimental Method

This study was conducted in two experimental stages to investigate the reduction behavior of lump iron ore using sugarcane bagasse as a biomass-based reducing agent. The first stage focused on determining the optimum mass ratio between the iron ore and the reducing agent, as well as identifying the most effective reduction temperature. The second stage evaluated the influence of reaction time on the reduction efficiency under selected temperature and ratio conditions.

2.1 Materials Preparation

The iron ore used in this experiment was lump ore sourced from Kalimantan, Indonesia, which was crushed to gravel-sized particles (approximately 1–2 cm). The reducing agent used was sugarcane bagasse (saccharum officinarum), collected from local sugar production residues. Prior to the reduction process, the bagasse was sun-dried under open-air conditions to reduce its moisture content, following the air-dried basis (adb) method. Both materials were used without further chemical treatment.

2.2 Experimental Setup and Procedure

All reduction experiments were carried out on a laboratory scale using a 10 kg capacity muffle furnace. The reduction process was performed in a closed ceramic crucible to ensure controlled reaction conditions. Inside each crucible, lump ore was embedded within a pile of dried bagasse to allow intimate contact between the ore and reducing agent during heating.

In the first stage, the objective was to assess the effects of ore-to-reductant mass ratio and temperature. Two mass ratios of lump ore to bagasse were investigated: 1:2 and 1:4. The crucibles containing the mixture were inserted into the furnace preheated to target temperatures of 700 °C, 800 °C, 900 °C, and 1000 °C. Each reduction run was maintained for a fixed holding time of 30 minutes.

In the second stage, the effect of reaction time was studied at selected temperatures of 700 °C and 1000 °C. For this step, the mass ratio of ore to bagasse was fixed at 1:2. Reduction durations of 45 and 60 minutes were applied to observe time-dependent behavior. After the heat treatment, the crucibles were allowed to cool inside the furnace to ambient temperature before further analysis.

2.3 Characterization and Analytical Methods

To evaluate the composition and properties of the raw materials and reduced products, several laboratory tests were conducted. Proximate and ultimate analyses of sugarcane bagasse were performed prior to the reduction process to determine its moisture, volatile

matter, fixed carbon, ash content, and elemental composition (C, H, N, S, O). These analyses were carried out at the Tekmira Coal Laboratory, Bandung, Indonesia.

The mineralogical phases of the lump ore before and after reduction were identified using X-ray Diffraction (XRD) analysis. This characterization aimed to determine the transformation of iron oxide phases (e.g., Fe_2O_3, Fe_3O_4, FeO) during the reduction process. XRD testing was conducted using standard powder diffraction methods with Cu-Kα radiation over a scanning range appropriate for iron-bearing minerals.

3. Result and Discussion

Table 1 presents the proximate and ultimate test result from sugarcane bagasse. Moisture content in bagasse is 6.75%. The calculated amount of moisture content in bagasse is a difference of 19% from the standard value. However, it remains within the limit for ideal moisturization content for a 5-15% reduction process and direct reduction process of less than 10%. The ash content is 1.77% which is a difference of 77% below the standard.

Moreover, the ideal ash content is 3%, within a variation between 0.5 to 5.0%. The ash content in bagasse is lower than the ideal content but still beyond the limit. Volatile matter (VM) of bagasse is 78.40%. It is 0.02% less than the standard value and 160% higher than the ideal value of 30%. Fixed carbon (FC) in bagasse is 13.08%. It is an extra 3% higher than the bagasse standard. Bagasse moisture content and ash are still within the limit compared to SNI 06-3730-1995 , with a maximum of 15% and 10%. FC is the most critical element among other components owing to its role in producing reduction gas. Results based on moisture, ash, and fixed carbon analysis showed that sugarcane bagasse is suitable as a reducing agent; however, with its high VM, the charcoal will quickly burn and disperse a lot of smoke.

Table 1. Result of Proximate and Ultimate Test of Sugarcane Bagasse

Parameters	Bagasse		Unit	Based
	Standard	Tested		
Proximate Test:				
Moisture in Air Dried Sample	8.35	6.75	%	adb
Ash	7.06	1.77	%	adb
Volatile Matter	72.95	78.40	%	adb
Fixed Carbon	12.70	13.08	%	adb
Ultimate Test				
Carbon	-	45.68	%	adb
Hydrogen	-	6.71	%	adb
Nitrogen	-	0.30	%	adb
Sulphur	-	0.24	%	adb
Oxygen	-	45.43	%	adb

Tabel 2. Result of Proximate and Ultimate Process of Several Green Reducing Agents

Parameters	Bagasse	Coconut Shells [16],[17]	Palm Kernel Shells [18], [19], [20]	Rice Husk [21]	Unit	Based
Proximate Test:						
Moisture in Air Dried Sample	6.75	7.98	3.70	8.70	%	adb
Ash	1.77	4.16	2.09	23.85	%	adb
Volatile Matter	78.40	9.02	74.04	54.10	%	adb
Fixed Carbon	13.08	78.84	20.17	13.35	%	adb
Ultimate Test						
Carbon	45.68	74.30	49.90	33.14	%	adb
Hydrogen	6.71	-	6.00	5.14	%	adb
Nitrogen	0.30	-	0.28	0.55	%	adb
Sulphur	0.24	0.50	-	0.12	%	adb
Oxygen	45.43	21.90	41.66	37.20	%	adb

Comparing the proximate and ultimate test result of sugarcane bagasse to other green reducing agents: coconut shells, palm kernel shells, and risk husk is presented in Table 2. It is possible to describe the advantage of bagasse compared to coconut shells and rice husk. The moisture content in bagasse is 15% below the moisture content of coconut shells and 22% below rice husk but 82% higher than palm kernel shells. It corresponds to the capability of bagasse to consume less energy and time in the drying process. Palm kernel shells have lower moisture than bagasse, but the moisture of palm kernel shells is below the standard of ideal moisture content for the reduction process. Lower moisturization might inhibit the formation of hydrogen and slower the reduction process.

Bagasse ash content is 58% below the coconut shell, 15% below palm kernel shells, and 93% below the risk husk. It indicates that bagasse is a better reducing agent than coconut shells, palm kernel shells, and rice husk since the ash formed is minor. VM in bagasse is 770% higher than coconut shell, 6% than palm kernel shells, and 45% than of rice husk. VM will affect the carbonization process. A high value of VM will form charcoal that is quickly burned but produces a lot of smoke, while the low value will result in hard burned charcoal but produces burned flammability. Sugarcane bagasse will be rapidly burned and make a lot of smoke compared to coconut shells, palm kernel shells, and rice husk. However, the bagasse VM contained CH_4 is used as reduction gas. The bagasse FC is 83% lower than coconut shells, 35% below the palm kernel shells, and 2% below the rice husk. Based on this finding, for the same condition, sugarcane bagasse will need more ratio in weight than coconut, palm kernel shells, and rice husk. In addition, the presence of CH_4 is consider as reducing gas to meet the process requirements.

Table 3. The Calculation for Carbon Requirement

Process [12]		**Reducing Agent Needed**			
CO for Hematite (Fe_2O_3) to Magnetite (Fe_3O_4)	mol	0.0145			
CO for Magnetite (Fe_3O_4) to Wustite (FeO)	mol	0,0292			
CO for Wustite (FeO) to Fe	mol	0,0876			
Total CO	mol	0,1313			
Total Carbon Required	mol	0.0656			
	gram	0.7872			
Total Carbon Required on 1000 ˚C (100%) [15]	gram	0.787			
Total Carbon Required on 700 ˚C (60%) [15]	gram	1.312			
Weight Ratio		**1:1**	**1:2**	**1:3**	**1:4**
Total Carbon Exsisted with 13.08% fixed Carbon	gram	1.44	2.09	2.75	2.88

Total carbon requirement based on calculation published by Soedarsono et. [17][17], as presented in Table 3, showed that the total required carbon at 700 ˚C and 1000 ˚C is 1.312 gram and 0.787 gram, respectively. The needs in weight ratio are presented in Table 2. Carbon content in 13.08% of fixed carbon for all weight ratios is greater than 10 to 265% of the needs. Based on this observation, the reduction will occur and be sufficient to complete the reaction.

Figure 1 depicts the result of the XRD analysis of the lump ore. The XRD spectrum shows that the ore contains hematite (Fe_2O_3) and magnetite (Fe_3O_4). In addition, other oxides appear as impurities, such as aluminum-iron oxide ($AlFeO_3$), nickel-titanium oxide $NiTiO_2$, and fayalite ($Fe_2(SiO_4)$). Magnetite and hematite have similar content of 26.32% based on their peak analysis.

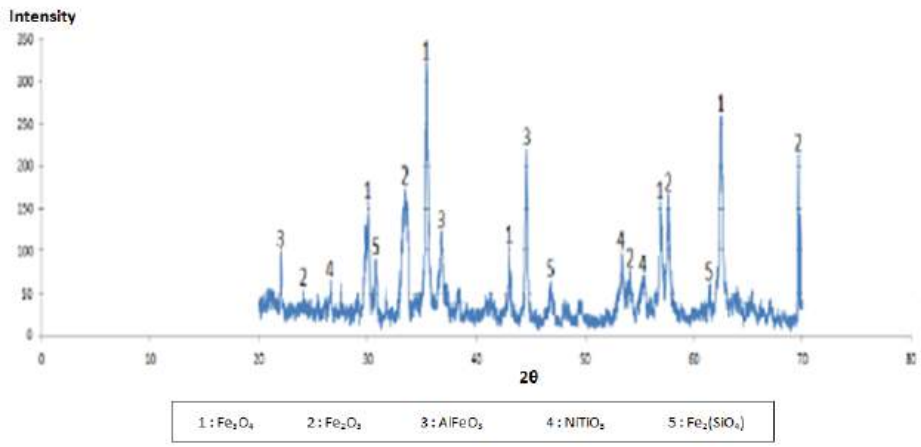

Figure 1. XRD Analysis for the Ores

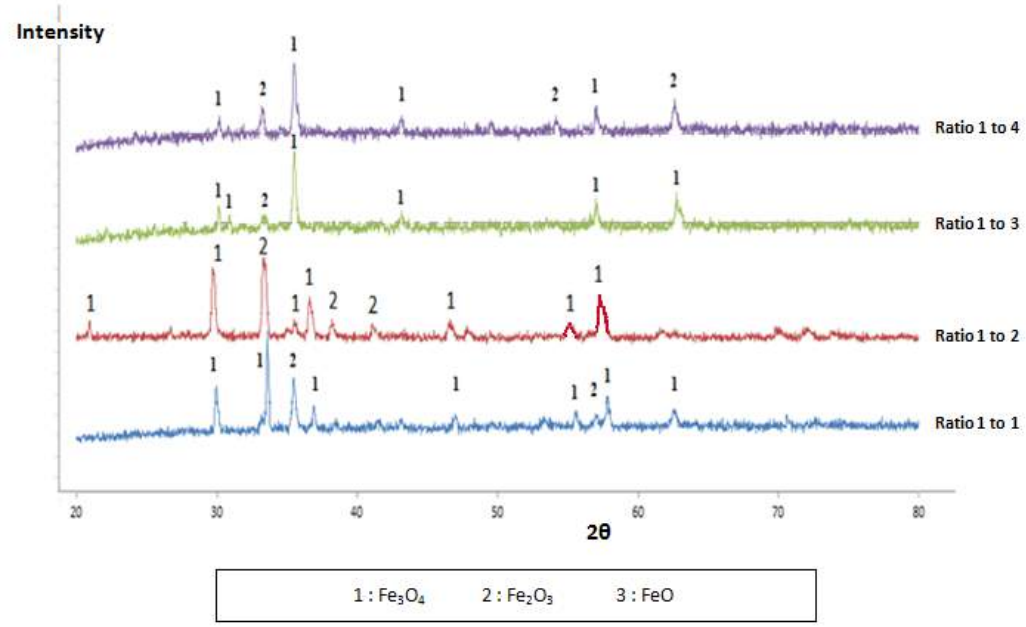

Figure 2. XRD Analysis in Reduction Process at 700OC for 30 minutes

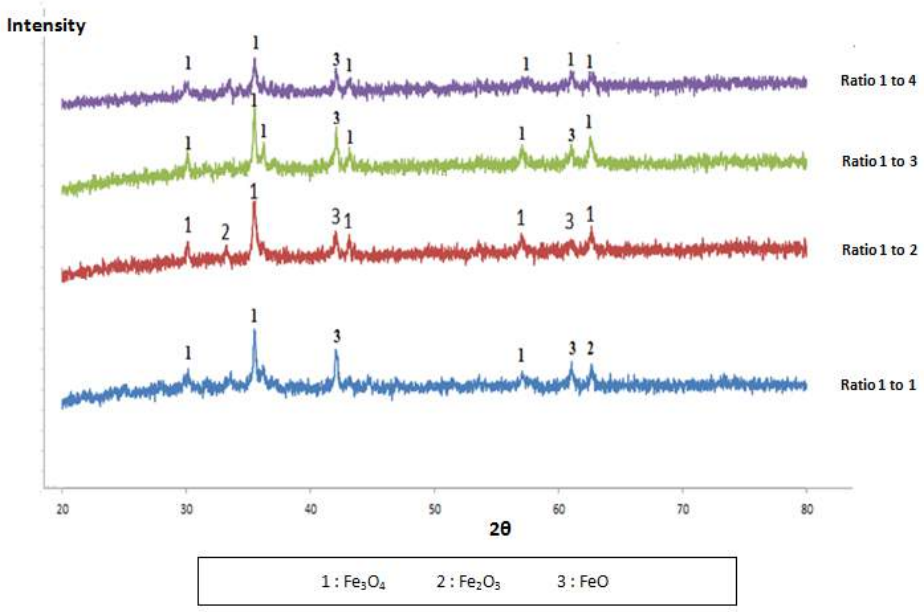

Figure 3. XRD Analysis in Reduction Process at 1000^{O}C for 30 minutes

Figure 2 shows the result of the XRD analysis during the reduction process at 700 ◦C. The weight ratios indicate the formation of hematite and magnetite. The formation of these compounds demonstrates that the reduction process has occurred. The level of intensity indicates the extent of the formation of the two phases. For magnetite, the highest intensity in the ore before the reduction process is 325 and after the process is 1800. In addition, hematite achieves the highest peak intensity before the process began is 225, whereas, after the process, the peak is slightly decreasing to 1400. The formation of magnetite indicates that the reduction process occurred and acted as a product in the first-stage process.

The number of peaks appearing in the XRD analysis represents the surface area. The greater the number, the larger the surface area. The larger the surface area has a pivotal correlation to the greater the amount of the formed magnetite phase. On this basis, the most significant magnetite formation, at 85%, occurred with a weight ratio of 1 to 3. Magnetite formation is given by the number of peaks for the other weight ratios. The resulting magnetite phase and their ratio are given in 78%, 70%, and 57% at 1:1, 1:2, and 1:4. Based on the result, the optimum ore of the bagasse weight ratio for the reduction process at 700 ˚C and 30 minutes is 1:3.

The results of the XRD analysis for the reduction process at 1000 ˚C indicate the presence of magnetite, wustite, and hematite, as shown in Fig. 3. Unlike the reduction process results at 700 ˚C, there is a difference in phases formation at each ratio. Magnetite, wustite, and hematite phases are formed at weight ratios of 1:1 and 1:2. For weight ratios of 1:3 and 1:4, however, only wustite and magnetite are formed. These results show that at weight ratios of 1:3 and 1:4, the second-stage reduction is completed. The highest intensities for wustite, magnetite, and hematite are 1700, 1700, and 1200. The highest wustite intensity is found at a weight ratio of 1:3. This pattern is the same as a result for the reduction process at 700 ˚C. Based on the number of peaks, wustite formation occurred to the extent of 33%, 25%, 37%, and 14% for weight ratios of 1:1, 1:2, 1:3, and 1:4, respectively. The corresponding values for magnetite are 50% for 1:1, 63% for 1:2, 63% for 1:3 and 86% for 1:4. As mentioned previously, hematite is only found at weight ratios of 1:1 and 1:2 with 17% and 12% content. Peak analysis compositions for weight ratios of 1:2 and 1:3 revealed that the weight of reduction required to complete the first-stage reduction at 1000 ˚C, three times the ore's weight required at 700 ˚C.

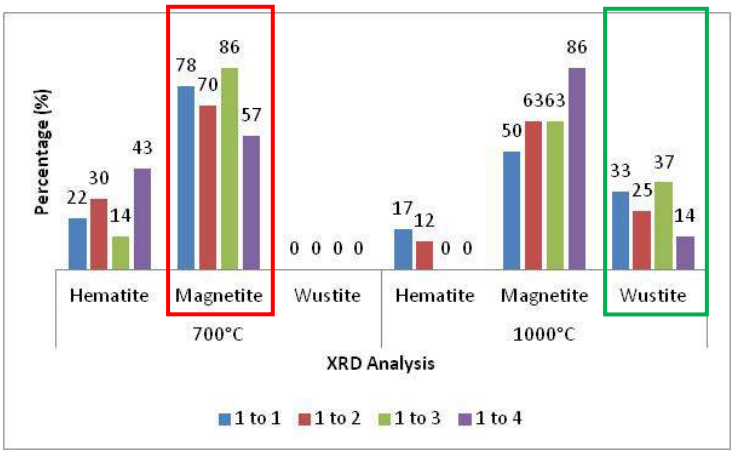

Figure 4. The percentage values for peak intensity in reduction process at 700 ˚C and 1000 ˚C

Figure 4 shows the pattern similarity by comparing the peak intensity values for the final product in each reduction process at their reduction temperature. Reductor weight gain is invariable with the final product of the reduction process. It confirms the presence of gases, which may have caused the reduction process to become an oxidation process. Hematite disappeared at the reduction temperature of 1000°C in a weight ratio of 1:3. In

this circumstance, the amount of reducing agent is sufficient to complete the first stage of the reduction process.

In contrast, the same result is different at a reduction temperature of 700°C. The Glaessner–Boudouard diagram (Fig. 5) shows the sequential reduction process at 5000C to promote the formation of magnetite from hematite. The most satisfactory result of this process is the production of wustite from magnetite and iron from wustite. The entire sequence will be completed when the supply of reducing agents is sufficient. The Glaessner – Boudouard diagram also displays the relationship between temperature and the reducing agent's formation. The graph shows that the reduction process at 700°C will require more reducing agents than at 1000°C since at 700°C, only 60% of the carbon reacted to form carbon monoxide, whereas, at 1000°C, all of the carbon created carbon monoxide.

Based on the Ellingham Diagram, magnetite formation began at 290°C and wustite at 700°C, as shown in Fig.6. The reduction temperatures used in this process are all in the range of metallic iron formation, which is more than 500°C. As shown in Tabel 3, the carbon supplied exceeded the calculation of the carbon requirement. The reaction should be completed based on this data, and metallic iron is present at 700°C and 1000°C. However, metallic iron is not formed at either temperature or with any of the weight ratios. It is now understood that the possibility of the incomplete formation of CO plays an essential role in the absence of metallic iron. Also, the stability of CO itself is an essential driving factor in the formation of metallic iron. Because of this temperature, carbon monoxide tends to react with oxygen and forms carbon dioxide.

Moreover, this case has shown that wustite (FeO) is not formed at 700°C due to the instability of carbon monoxide formation. Higher temperature facilitates metallic iron formation, as shown at 1000°C and supported by the Ellingham Diagram.

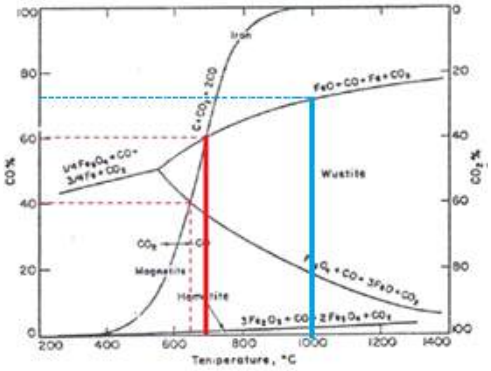

Figure 5. The Glaessner – Boudouard Diagram [22]

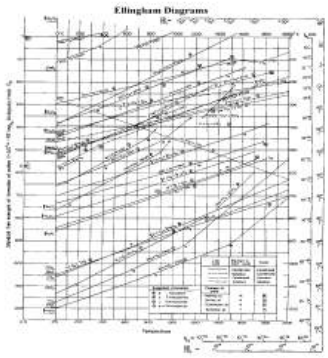

Figure 6. The Ellingham Diagram[23]

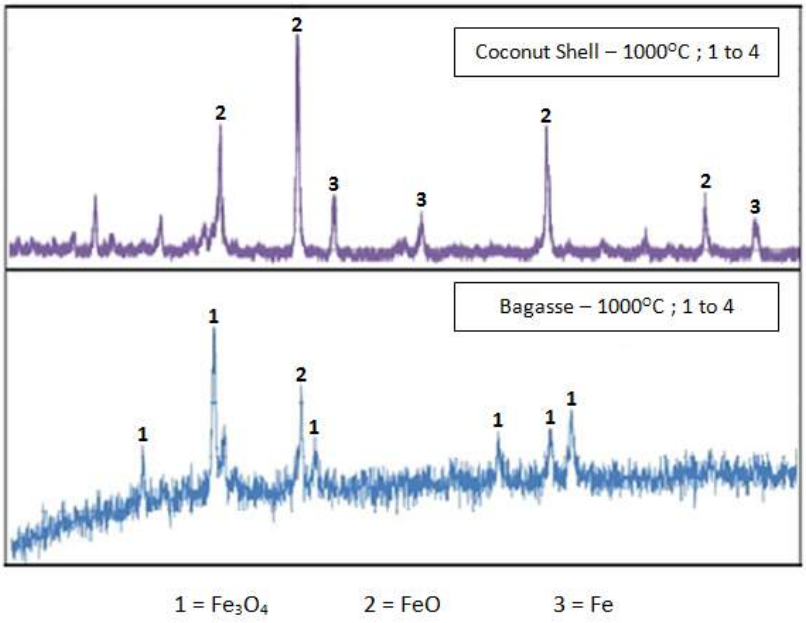

Figure 7. XRD analysis for reduction process with different reductors

The XRD result of the reduction process using coconut shell [16] showed the formation of metallic iron at a reduction temperature of 1000 ˚C with a 1:4 weight ratio. In contrast to earlier findings, however, a different result was obtained for bagasse. This fact is undoubtedly true in the case of a 1000 ˚C reduction temperature with a 1:4 weight ratio, the reaction gives magnetite and wustite formation. As mentioned previously, the process temperature and amount of carbon available fulfilled the requirements. Still, the reaction that occurred during the reduction process with bagasse was different from coconut shell. Bagasse supplied several types of gases that are essential sources of carbon monoxide. It also contained an amount of volatile matter that was 88% higher than for coconut shell, producing char. The XRD result showed that optimum wustite formation occurred at a weight ratio of 1:3. Based on all these data, the occurrence of oxidation was suspected to be the cause of the failure in the formation of metallic iron due to the excess of carbon from the oversupplied reducing agent.

Reduction of lump ore using sugarcane bagasse is different from lateritic nickel ore using palm kernel shell as a reducing agent at the same temperature and weight ratio parameter. The roasting temperature at 700 ˚C or 1000 ˚C gives the hematite of the lateritic nickel ore; however, the lump ore magnetite appears at 700 ˚C and wustite at 1000 ˚C [18], [19], [20]. Another advantage of this studies is to provide the optimum hematite content in lateritic nickel and lump ore. Based on our result, the weight proportion of 1:4 and 1:3 is suitable to meet the above requirement. These findings could be related to the effectiveness of sugarcane bagasse as a reducing agent compared to palm kernel shells.

In general view, the use of rice husk as a reducing agent for limonite ore [7] and iron sand [23] shows that the reduction process takes place until hematite is wholly trans-

formed to magnetite. Meanwhile, the reduction process using sugarcane bagasse progresses the transformation to wustite. Based on this general observation, it may conclude that sugarcane bagasse is more effective than rice husk. Extensive investigations are needed to verify this claim due to the difference in product targets.

4. Conclusion

Bagasse has demonstrated its ability to sustain a reduction process. It retains the double-acting features to supply carbon and several gasses such as hydrogen and methane to quicken the reduction process. Our findings show that the capability of sugarcane bagasse as a reducing agent is comparable to the coconut shells and husk rice. The rank of reducing agent is given as follows: Coconut shells > Bagasse Sugarcane > Husk Rice. However, it requires more profound attention and research to verify the claim.

The initial stage of the sugarcane bagasse reduction process shows the optimum roasting temperature is 700 °C and gives the magnetite state. Meanwhile, the subsequent stage gives wustite formed with the maximum roasting temperature at 1000 °C. Although the variation of roasting temperature and the product in each step may differ, the pattern of products based on their weight ratio is similar. The most significant degree of magnetite formation, as well as of wustite formation, occurred at a weight ratio of 1:3. The absence of metallic iron was suspected to be due to an oxidation process.

Acknowledgment

The authors wish to show their gratitude to The Government of Republic of Indonesia for the research funding and to all parties who have supported this research.

Declaration

The corresponding author, on behalf of all the authors, declare that there is no conflict of interest. The funders had no role in the design of the study; in the collection, analyses, or interpretation of data; in the writing of the manuscript, or in the decision to publish the results.

References

1. H. Mandova, WF. Gale, A. Williams, AL. Heyes, P. Hodgson and KH. Miah. Global assessment of biomass suitability of iron-making – Opportunities for co-location of sustainable biomass, iron and steel production and supportive policies. Sustain. Energy Technol. Assess., 2018; 27:23-39.
2. E. Mousa, C. Wang, J. Riesbeck and M. Larsson. Biomass application in iron and steel industry: An overview of challenges and opportunities. Renew Sust Energy Rev. 2016; 65:1247-1266.
3. DN. Usman. The Potensial of Deposits of Indonesia Iron Ore to Support the National Iron and Steel Industry (Ketersediaan Potensi Endapan Bijih Besi Indonesia dalam Mendukung Industri Besi dan Baja Nasional), 2010.
4. Ministry of Energy and Mineral Resources. Executive Summary of Recent Data and Balance of Mineral Resources, (Eksekutif Summary Pemuktakhiran Data dan Neraca Sumber Daya Mineral), 2015.

5. World Steel Association 2013, Steel Statical Year Book.
6. V. Strezov. Iron Ore Reduction using Sawdust: Experimental Analysis and Kinetic Modelling. Renew Energ, 2005; 31:1892-1905.
7. A. Maksum, MKE. Husein, S. Permana, A. Rustandi, JW. Soedarsonoa. A preliminary study on the reduction of limonite ore by using rice husk as a reducing agent. IOP Conf. Ser.: Mater. Sci. Eng. Vol. 316, 2018.
8. JX. Fu, C. Zhang, WS. Hwang, YT. Liau, and YT. Lin. Exploration of Biomass Char for CO2 Reduction in RHF Process for Steel Production. International Journal of Greenhouse Gas Control, 2012; 8:143-149.
9. RZA. Rashid, HM. Salleh, MH. Ani, NA. Yunus, T. Akiyama, and H. Purwanto. Reduction of Low Grade Iron Ore Pellet using Palm Kernel Shell. Renew Energ, 2014; 63: 617-623.
10. AT. Ubando, WH. Chen, HC. Ong. Iron oxide reduction by graphite and torrefied biomass analyzed by TG-FTIR for mitigating CO2 emissions. Energy, 2019; 180:968-977.
11. SS. Rath, DS. Rao, A. Tripathy, SK. Biswal. Biomass briquette as an alternative reductant for low grade iron ore. Biomass Bioenergy, 2018; 108:447-454.
12. N. Asmiani, A. Nawir, N. Jafar, AJ. Rinaldi, S. Widodo. Beneficiation of canary shell as a mixture of coal briquette. IOP Conf. Ser.: Earth Environ. Sci. Vol. 473, 2019.
13. AM. Mansor, LT. Wai, SL. Lim, FN. Ani, H. Hashim, SH. Wai. Potential commercialization of biocoke production in Malaysia – A best evidence review. Renew.Sust.Energ.Rev, 2018; 90:636-649.
14. KD. Yang, XJ. Ye, J. Su, HF. Su, YF. Long, XY. Lu, YX. Wen. Respon surface optimization of process parameters for reduction roasting of low-grade pyrolusite by bagasse. Trans.Nonferrous.Met.Soc.China, 2013; 23:548-555.
15. JW. Soedarsono, CE. Arifin, JS. Saragi, AA. Putra, A. Kawigraha, RD. Sulamet-Ariobimo, A. Rustandi. The Effect of Reduction Parameter in Processing Lump Ore with Gree Sugarcane Bagasse Reductor in Muffle Furnace. Mater.Sci.Forum, 2017; 893:195-201.
16. JW. Soedarsono, EM. Rajagukguk, LPP. Batubara, LJ. Romualdo, A. Kawigraha, RD. Sulamet-Ariobimo, A. Rustandi, S. Tjahyono and A. Zamri. Reduction Process of South Borneo Lump Ore using Renewable Coconut Shell Reductor in Rotary Kiln.
17. JW. Soedarsono, AM. Putra, A. Kawigraha, RD. Sulamet-Ariobimo, A. Rustandi and S. Tjahyono. Comparison of Lump Ore Reduction Process in Muffle Furnace and Rotary Kiln using Green Coconout Shell Reductor,
18. S. Adzhani, R. Hidayanti, A. Maksum, S. Permana, JW. Soedarsono. The influence of palm kernel shell mass ratio as a reducing agent in the lateritic nickel ore carbothermic reduction process. IOP Conf. Ser.: Earth Environ. Sci. Vol. 105, 2018.
19. D. Rahayu, A. Maksum, JW. Soedarsono. Effects of reduction time on carbothermic reduction of lateritic nickel ore using palm kernel shell as green reducing agent. IOP Conf. Ser.: Earth Environ. Sci. Vol. 105, 2018.
20. R. Hidayanti, S. Permana, A. Maksum, JW. Soedarsono. Study on the effects of temperature in carbothermic reduction laterite ore using palm kernel shell as reducing agent. IOP Conf. Ser.: Earth Environ. Sci. Vol. 105, 2018.

21. MF Ghiyats, A. Maksum, JW. Soedarsono. Preliminary study on the use of rice husk as a reducing agent in iron sand reduction. IOP Conf. Ser.: Earth Environ. Sci. Vol. 553, 2019.
22. RL. Stepershon. Direct Reduced Iron (Technology and Economics of Production and Use), USA Iron Steel Society of AIME.1980.
23. J. Russell and R. Cohn, Ellingham Diagram, Book on Demand Ltd., 2012

PT. Mencerdaskan Bangsa Indonesia

PT MENCERDASKAN BANGSA INDONESIA
(MBI), 4th Floor Gedung STC Senayan Room
31-34, Jl. Asia Afrika Pintu IX, Jakarta 10270,
Indonesia.